A Phase-Time Modulation Scheme for Peak-to-Average Power Mitigation in Multi-Carrier Wireless Transmission

David I Spalding

B.Sc.Eng. (Bristol)

A thesis submitted in partial fulfillment
of the requirements for the degree of

Master of Engineering

(Electrical and Electronic Engineering)

University of Canterbury
Christchurch, New Zealand
31 May 2006

Abstract

An explosive growth in demand for broadband mobile wireless services is currently being fuelled by cellular telephone users who, encouraged by service providers, are no longer content with voice transmission only but are demanding real-time video services, including multi-user, interactive games and 'movie' programmes. As these applications develop, expectations mount in other mobile user markets, especially the public safety arena, for comparable user features but with greater emphasis on reliability and robustness of the equipment and supporting network in adverse propagation conditions, remote locations and emergencies. These applications all have in common the requirements for efficient use of wireless bandwidth and of battery power, as well as seamless operation when moving, sometimes at high vehicle speeds, from one type of environment to another in a multi-user scenario. Orthogonal frequency-division multiplexed (OFDM) signals have been found to compare favourably with other modulation systems in these applications, the multi-carrier format being more tolerant of delay spread. It has been used in both code-division (MC-CDMA) and frequency-division (OFDMA) multi-user schemes, the latter having the advantage of maintaining orthogonality among users in fading-signal environments, with consequent simplification of signal processing.

The major drawback of OFDM has been the high peak-to-average power ratio (PAPR) that is characteristic of signals with multiple sub-carriers. A result of this is that the transmitter requires a linear power amplifier (PA) that generally has to be 'backed off' to accommodate the high PAPR. Additional back-off is required to achieve linearity, as well as sometimes-complex linearisation circuitry. The power usage and cost of such a transmitter is more acceptable in a base station, tending to limit the application of OFDM to downlinks. The potential application to hand-portable terminals has severe constraints of size, cost and battery life, exacerbated by the use of video-capable LCD displays, increasing motivation for the use of MIMO (multi-antenna) technology and the development of mobile ad-hoc networks, the latter being particularly applicable in the public safety arena. Previous efforts to ameliorate the PAPR problem have been principally directed at two areas, the reduction of signal PAPR, by block coding, clipping or other techniques, and methods of achieving PA linearisation with improved power efficiency. The first object of the present research was to establish, as far as practicable, the current state of the art in these areas, to set a performance baseline. The next step was to develop an improved transmitter modulation scheme that would not only be able to take advantage of any existing peak reduction methods but would transmit a signal that would be compatible with existing OFDM receivers.

A novel modulation technique is now presented, termed Quadrature Phase-Time Modulation (QPTM), that has been found to meet the requirements for linearity, simplicity and low cost, whilst being able to take advantage of constant-envelope PA technology, with its attendant power efficiency. After final amplification, the signal is restored by a passive narrow-band filter to standard OFDM form, having both phase and amplitude modulation. The QPTM system of modulation relies on a dual baseband pulse-width modulation process, performed at a substantially-higher rate than the upper baseband frequency, followed by direct quadrature modulation of a carrier signal. The work undertaken has been in the nature of a feasibility study, commencing with the theoretical basis of the technique, from which a behavioural system model was designed and simulated. After the system was simulated successfully, in several forms, a model was designed for realisation with available high-frequency integrated circuits. From this design, prototypes were constructed and tested. The prototype circuit boards also included an experimental UHF Class-D PA circuit, excluding the output filter, to facilitate ongoing development of the PA and filter subsystem as a separate project. This type of PA was seen as a potential complement to the QPTM modulator, although the technology was at an early stage of development. The prototype PA has a novel push-pull arrangement of GaAs FETs that employs a broadside-coupled tapered-stripline balun instead of the usual transformer. Preliminary measurements were made on the PA using both a spectrum analyser and a newly-available 8GHz-bandwidth digital oscilloscope to confirm basic operating characteristics. The performance of the QPTM technique at frequencies needed for broadband operation is dependent on its practical implementation, which has therefore been a major focus. The inherent difficulties in realising a highly-linear 40MHz triangle-wave reference generator, with a precise ultra-high-speed comparator and modulator system, have been overcome with the chosen design techniques and attention to several critical aspects. The result has been the successful demonstration of QPTM as an efficient PA modulation technique that is equally applicable to either narrow-band, high-capacity UHF or broadband OFDM microwave systems.

Acknowledgements

"If I have seen further it is by standing on the shoulders of Giants[1]"
- Sir Isaac Newton, 5th February 1675

This has been quite a journey for me and, to a large extent, an act of faith. What I have learned from the "giants" whom I have come upon in this research goes far beyond anything that I imagined at the start of the journey. For that I thank them all. With my feet more on the ground, I should like to express my thanks and enormous appreciation to those who helped and encouraged me at various times and, in doing so, helped me to build confidence in the many decisions that I had to make along the way.

I thank Doug McConnell and Adrian Busch of Tait Electronics Ltd, Group Research, for their interest in the work and making the whole project possible by arranging much of the support that was needed, as well as access to test equipment, CAD and prototyping facilities. Also at Tait, there have been several members of the Research and Development groups whom I cannot thank enough for their interest and enthusiastic support, including Keith Lewis, for challenging discussions, Ian Scott, for expert advice on microwave design, Sapna Sahi, for her help with PCB CAD, Fay Hutt, for library support, Mark Cotton, for facilitating access to a new microwave digital oscilloscope, Kishore Mehrotra, for help with math software, and Andrew Jones and Prabath Kamalasena for their assistance with RF models.

At the University of Canterbury my thanks go to my supervisors, Dr Lee Garth and Prof. Harsha Sirisena, for patiently encouraging me and providing assistance wherever needed, to Prof. Des Taylor, for stimulating my interest in communications issues at almost every encounter, and to the several other staff and postgraduate students who have shared their friendship with me through the Master's course and are forever to be part of my world.

Throughout this project, there has been one whose endless love and faith have made everything possible and to whom I shall be forever grateful. She is my dear wife, Carmen, whose support has been beyond measure. I should also like to thank my daughters, Sharmalee and Angela, for patiently waiting for the time when they would have a full-time father again.

[1] May be a reference to work of the Roman poet Marcus Annaeus Lucanus (AD 39-65): "*Pigmaiei gigantum humeris impositi plusquam ipsi gigantes vident"* (Pygmies placed on the shoulders of giants see further than the giants themselves).

CONTENTS

Chapter 1
PAPR in the Wireless System

Chapter 2
Quadrature Phase-Time Modulation

Chapter 3
QPTM System Simulation and Analysis

Chapter 4
An Experimental QPTM System

Chapter 5
Discussion, Conclusions and Further Work

LIST OF FIGURES

GLOSSARY OF TERMS

ACP	adjacent-channel power
ADC	analogue-to-digital converter
AM	amplitude modulation
Balun	balanced-to-unbalanced line transformer
BER	bit error rate
BPSK	binary phase-shift keying
Broadside-coupled	lines layered one-above-the-other in a printed-circuit stack
BTS	base transceiver station
Class-A	PA biased to operate entirely with a linear transfer function
Class-AB	PA operating in Class-A for small and Class-B for large signals
Class-B	PA amplifying linearly during one polarity only of input signal
Class-C	PA similar to Class-B but biased for reduced conduction angle
Class-D	efficient switch-mode PA with tuned output circuit
Class-F	efficient non-linear PA with harmonic-load tuning
Class-S	PA with switch-mode drain or collector envelope modulation
CDMA	code-division multiple access
CS Class-D	current-switching Class-D with parallel-tuned output
DAC	digital-to-analogue converter
DCL	digital Cartesian loop
DCT	discrete cosine transform
EER	envelope elimination and recovery
EDGE	Enhanced Data Rates for GSM Evolution
esr	equivalent series resistance
ETSI	European Telecommunications Standards Institute
EVM	error vector magnitude
FET	field-effect transistor
FFT	fast Fourier transform
FPGA	field-programmable gate array
GaAs	gallium-arsenide
GSM	Global System for Mobile communications, originally an abbreviation of Groupe Spéciale Mobile, a 2^{nd}-generation or 2G digital cellular radio system
IFFT	inverse fast Fourier transform
ISI	inter-symbol interference

Kahn technique	technique in which the phase and amplitude components of the modulating signal are applied separately to the PA stage
LDMOS	laterally-diffused metal-oxide semiconductor power transistor
Microstrip	transmission line on substrate surface with ground plane under
MIMO	multiple-input receiver with multiple-output transmitter
ML	maximum-likelihood
OFDM	orthogonal frequency-division multiplexing
OFDMA	orthogonal frequency-division multiple-access
OQPSK	offset QPSK
PA	power amplifier
PAPR	peak-to-average power ratio, defined as the ratio of the power of a sinusoid having the same peak waveform amplitude as the signal to the average power of the signal
PECL	positive emitter-coupled logic family
PER	packet error rate
PM	phase modulation
PMR	professional mobile radio
PRC	peak-reduction carrier in an OFDM signal
PSK	phase-shift keying
PWM	pulse-width modulation
QAM	quadrature amplitude modulation
QPSK	quadrature phase-shift keying
QPTM	quadrature phase-time modulation, a novel system that is the subject of the present thesis
RM	Reed-Muller
SLM	selective mapping of OFDM data
SPICE	Simulation Program with Integrated Circuit Emphasis, originating from the University of California, Berkeley, USA
SSB	single-sideband modulation
STBC	space-time block code
Stripline	buried transmission line, typically with ground above and below
TETRA	Terrestrial Trunked Radio, an ETSI-approved PMR standard
UHF	ultra-high-frequency band, nominally from above 300MHz to 3GHz
UMTS	Universal Mobile Telecommunication Services
VS Class-D	voltage-switching Class-D with series-tuned output
WCDMA	wideband CDMA, the radio interface for 3rd-generation (3G) UMTS

Chapter 1

PAPR in the Wireless System

1.1 Introduction

1.1.1 BACKGROUND

Increasing demand for wider bandwidth in hand-portable communications devices places pressure on designers to achieve more effective RF spectrum utilisation, requiring modulation schemes that use linear, less power-efficient, PA designs. Increased power needed for the transmitter, signal processing devices and video display all conflict with the need to minimise battery size and weight, whilst endeavouring to meet user demands for increased "talk time". The situation is exacerbated by multiple-input, multiple-output (MIMO) antenna schemes that substantially increase complexity, size and signal-processing power drain. These factors pose less of a problem for base stations or fixed links. Many of the latter operate in single-carrier narrowband UHF communication channels where MIMO could be used to achieve moderately-broadband data rates (with a high-order modulation such as 256-QAM) by taking advantage of the multipath propagation environment.

Multipath propagation can be harnessed in a MIMO system to mitigate fading effects and achieve high data rates. The technique is of particular advantage indoors, where there may be low delay spread and good multipath diversity. Outdoors, where the multipath propagation delay spread may be similar to or much greater than the symbol period, inter-symbol interference (ISI) becomes a greater issue for systems operating at high data rates. Doppler effects from moving vehicles add to this problem. Although the propagation models for indoor and outdoor environments are generally quite different, a mobile terminal is often required to operate reliably when moving freely from one such environment to the other.

Multiple antenna systems are more easily incorporated in broadband hand-portable transceivers that operate in microwave bands because of the physical dimensions required. However, the

modulation scheme has to be tolerant of the much lower signal-to-noise ratio (SNR) characteristic of a wider-bandwidth system.

The difficulties encountered in channel equalisation for MIMO may be alleviated by combining MIMO with OFDM. In the latter system, multiple, equally-spaced orthogonal subcarriers are each modulated using an *m*-PSK or *m*-QAM technique. This approach has been shown to have advantages in both indoor and outdoor environments [1]. For a given data capacity, an increased number of subcarriers increases the symbol period, allowing proportionately higher delay spreads to be accommodated. Thus, when OFDM is combined with MIMO, capacity may be maximised for a variety of indoor and outdoor scenarios.

The combination of MIMO with OFDM is considered to be an enabling technology that could fundamentally improve the spectral efficiency of a 4G mobile radio system. It is reported as having a significant advantage over CDMA for the implementation of MIMO technology [2].

The reduced complexity of equalisation associated with OFDM saves processor cost and power consumption. However, a disadvantage of OFDM is the need for the transmitter output stage in each channel to handle a wide range of peak-to-average power ratios, with consequent inefficiency.

Power consumption is a more significant problem for mobile terminals in high-bandwidth networks, particularly as many future systems will be configured as ad-hoc networks, in which any mobile terminal has to handle other network traffic on top of its own. Since OFDM is evidently emerging as a modulation system of choice for broadband networks, there is a need to address the matters of power amplifier efficiency and linearity when transmitting signals with high PAPR.

1.1.2 PROJECT OUTLINE

The project has taken a system approach to PAPR management, with a particular emphasis on the characteristics desirable for mobile equipment. Initially, PAPR reduction techniques have been examined, both coding and probabilistic, in order to determine practical PAPR handling requirements for the transmitter's RF modulator and power amplifier (PA) circuits. Alternative approaches for PA linearisation have been reviewed with respect to power efficiency, linearity and complexity or cost of implementation.

The bulk of the research effort has comprised an investigation into a proposed Quadrature Phase-Time Modulation (QPTM) technique as a means of achieving efficient and linear transmitter

output with characteristics similar to QAM-modulated OFDM. Based on modulation theory, a simulation model has been developed and analysed. This has been used to determine a suitable design configuration and estimate the performance to be expected. Design and construction of a prototype QPTM system incorporating a broadband pulse-width modulator has been undertaken. Its characteristics have been measured, using a spectrum analyser and a digital sampling oscilloscope, to evaluate the feasibility of the technique for practical applications. These characteristics have been verified against the simulation data.

The QPTM system appears to be suitable for use with virtually any PA, linear or non-linear. However, some performance limitations may be associated with the latter, particularly with reference to maximum carrier frequency and in-band intermodulation distortion. As an aid to future demonstration and evaluation of the potential efficiency of the QPTM technique in a practical wireless-OFDM system, we have included on the same prototype printed-circuit board as the QPTM modulator the active circuitry of an experimental Class-D switching PA circuit. In a novel arrangement, the latter has been combined with a broadside-coupled tapered-stripline output balun, considered to have potential performance benefits at UHF and microwave frequencies. Whilst development of this PA has yet to be completed to the stage where it would embody an output filter suitable for use in the QPTM system, we have been able, through the application of a newly-available microwave digital sampling oscilloscope, to demonstrate successful operation of the UHF switch-mode PA and arrive at an understanding of the fundamental design issues for this new technology.

1.2 PAPR as a System Parameter

1.2.1 RELATIONSHIP OF PAPR TO MODULATION

1.2.1.1 Single-Carrier Systems

High data bandwidth efficiency (in terms of b/s/Hz) may be achieved by using higher-order modulations based, for example, on QAM. This may be single-carrier or multi-carrier. In the single-carrier system, PAPR for an unfiltered baseband signal varies with the modulation order, as shown in the following table of examples:

Modulation	PAPR
m-PSK (reference)	0dB
16-QAM	2.55dB
64-QAM	3.68dB
256-QAM	4.23dB
256-QAM (modified)	2.85dB

Table 1.1 - PAPR for selected modulation formats

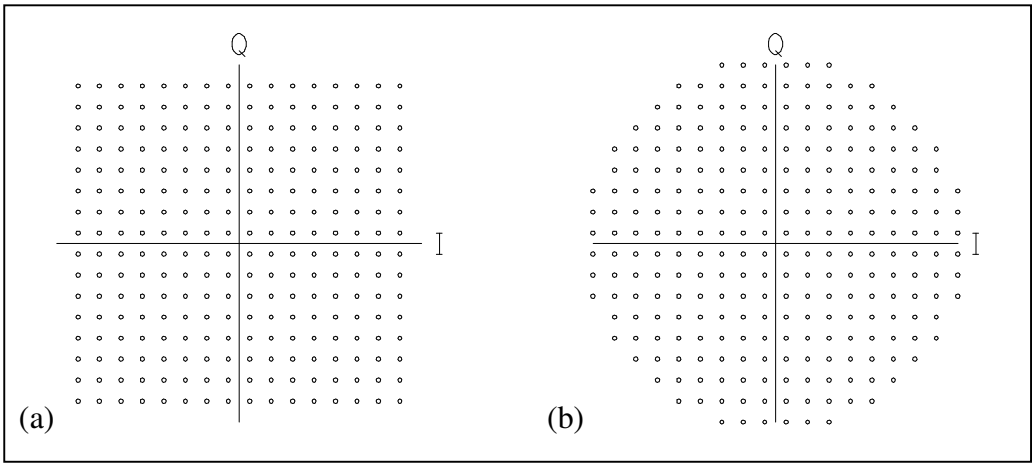

Figure 1.1 - 256-QAM constellations: (a) regular and (b) modified mapping to reduce PAPR

The last entry in Table 1.1 is for a constellation obtained by modifying 256-QAM to reduce PAPR. The modification is illustrated in Figure 1.1. It also improves the error vector threshold from 0.047 (-26.5dB) to 0.056 (-25.0dB), providing greater tolerance of noise and non-linear distortion. However, there is an additional processor load associated with encoding and decoding this constellation. In terrestrial communications it is common

to apply pulse shaping to the baseband signals, to reduce the bandwidth of the transmitted spectrum, but this causes overshoot and could, for example, increase the PAPR of the modulating signal by 4-5dB.

1.2.1.2 Multi-Carrier Systems

The complex baseband signal for one symbol in an OFDM system [1] may be expressed as:

$$x(t) = \frac{1}{\sqrt{N}} \sum_{n=1}^{N} a_n \exp(j\omega_n t) \tag{1.1}$$

where N is the number of subcarriers and a_n are the modulating symbols.

For moderately large numbers of m-PSK subcarriers the quadrature components of $x(t)$ each tend towards a Gaussian distribution (giving their sum a Rayleigh distribution). Consequently, whilst the peak value possible is N times the individual subcarrier peak, the probability of any value close to that peak occurring is very low. For example, with only 24 subcarriers, the probability of the PAPR exceeding 4dB is 10^{-2} and of exceeding 8dB is only 10^{-4} [1].

When the subcarrier modulation is a higher-order QAM type, as described in (1.2.1.1), the PAPR of the summed OFDM signal is increased by the PAPR of the QAM constellation used. However, the probability of these higher peaks occurring is correspondingly less. Moreover, since one of the advantages of OFDM is that subcarriers may have their modulation independently varied to adapt to channel conditions, the combined PAPR in any system using this technique may be difficult to predict and control, tending to limit the PAPR reduction options to those based on clipping of the signal prior to transmission.

1.2.2 SYSTEM PERFORMANCE TRADE-OFFS

PAPR management is a system problem, since it affects not only the dynamic range required of the transmitting power amplifier (PA) but also of the receiver and other components of the transmit and receive chains, particularly the analogue-to-digital and digital-to-analogue converters. Non-linearity in any of these may impact on the error rate for a given level and type of modulation. In a receiver, the PAPR at the ADC input may be even greater than that of the transmitted signal, owing to overshoot caused by filters in the receive chain. A further consideration is that non-linearity and clipping of the transmitter power amplifier causes spectrum

spreading with consequent adjacent-channel interference. This may be overcome by filtering and in some systems with a low probability of the PAPR exceeding the clipping threshold, for example, those with a low-order modulation like QPSK, the error rate from clipping may be acceptable.

When considering the most appropriate design solution for a hand-portable transceiver system, the issues of power consumption, size and cost are of major concern and have to be weighed against the potential gains in data bandwidth. In some schemes the signal processing needed for minimising PAPR may be sufficiently complex that even leading-edge technology gate arrays would not meet the speed requirements for broadband data transmission within acceptable battery power and cost constraints. Likewise, transmitter PA linearisation circuits may impose similar penalties. PAPR reduction may also incur an additional processor load in the receive path, for example, where a complex decoding or error-correction scheme is necessitated.

The availability of spectrum in the microwave bands provides opportunities to transmit data at high rates and statutory requirements for out-of band emissions are generally less stringent than in UHF bands. However, the optimum choice of modulation to maximise the data bandwidth efficiency is still constrained by the foregoing considerations of the signal processing and PA technologies, particularly as applied to high baseband data rates and microwave carrier frequencies.

1.3 PAPR Reduction Techniques

The following methods of reducing PAPR prior to modulation are dependent on the low rate of occurrence of large PAP ratios and include coding, clip-effect transformation and probabilistic methods.

1.3.1 BLOCK CODING

1.3.1.1 Golay Complementary Sequences

When the probability of exceeding a specified PAPR threshold is low, coding techniques may be considered as a means of controlling the maximum PAPR that may be generated and transmitted. In [1], van Nee and Prasad give as an example the case of 64-carrier QPSK in which approximately 10^{-6} of the possible symbols have less than 4.2dB PAPR. Thus, there would be 108 effective bits out of the 128 bits available. The problem has been in finding a suitable coding scheme.

Golay complementary sequences have been used as they have been found to make up a large number of the suitable code words. Moreover, a subset can give good forward error correction with suitable decoding. Golay codes maintain a low PAPR when *m*-PSK modulations are applied using similar rules to those for the code generator. For small numbers of subcarriers, it is possible to guarantee a PAPR of only 3dB for the signal to be transmitted.

Our research has uncovered some defining papers, particularly from the Hewlett-Packard Laboratories in Bristol. In [3], the relationship of Golay codes to Reed-Muller (RM) codes is identified. This leads to ways of structuring the codes. RM codes are easy to decode and fast Hadamard transforms are used. There are predicted performance tables for binary, quaternary and octary forms of modulation. In [4], the theme is developed, including the generation of Golay codes from Boolean functions. The application of maximum-likelihood (ML) and less complex iterative decoding approaches are also discussed.

Reference [5] relates to Rudin-Shapiro code constructions and discusses more cosets, of near-complementary pairs. The proposed application of PAPR techniques to 3G cellular systems is described in [6], where a Golay code is employed for the synchronisation preamble. Golay codes may be readily generated on demand or from look-up tables. However, maximum-likelihood decoding is non-trivial and [7] describes low-complexity decoding, with a near-ML approach. Another low-complexity approach is described in [8], while [9] compares simulated and practical results with Golay sequences.

Reference [10] is the definitive Lucent patent relating to an *m*-PSK OFDM system, which is identical to that described in the book [1] by van Nee and Prasad, where 8-PSK is used for the "Magic WAND" system.

1.3.2 CLIP EFFECT TRANSFORMATION

1.3.2.1 Peak Windowing and Clipping

Clipping of excessive signal peaks [1][11] is the simplest approach to PAPR reduction but has the disadvantages of generating in-band noise, which degrades bit error rate (BER), and out-of-band distortion, which may require filtering of the transmitter output signal. In-band noise may be minimised by clipping an over-sampled signal.

Peak-windowing may be used to control out-of band emissions. It involves multiplication of large signal peaks with a Gaussian or other non-rectangular window having good spectral properties. The window should be narrowband to control out-of-band emissions but fast enough in response to avoid affecting too many adjacent samples, as this would degrade the BER. In this case, the BER performance is not quite as good as for simple peak clipping.

1.3.2.2 Peak Cancellation

Peak cancellation [1] has been shown to be very similar to peak clipping followed by filtering and has a packet error rate (PER) performance nearly midway between peak clipping and peak windowing. The band spreading caused by peak clipping may be minimised by linear subtraction of a reference signal from each sample exceeding the allowable peak threshold.

A sinc function is suitable as a reference signal, provided that it is windowed to constrain its bandwidth to that of the OFDM signal. Typically this window has a raised-cosine form. This method would be applied after the cyclic prefix has been added and directly before the transmitter digital-to-analogue converter (DAC). Peak cancellation may alternatively be applied before addition of the cyclic prefix without using a stored reference function, but the method involves additional FFT and IFFT operations.

1.3.2.3 Receiver Reconstruction

According to Chen and Haimovich [12], the process of clipping and filtering described in (1.3.2.1) may be enhanced by an iterative reconstruction process in the receiver. Their method is claimed to be an improvement on previous methods that attempted to reconstruct “lost” time-domain signal samples by instead regenerating and cancelling clipping noise in the frequency domain.

In this method, the signal to be transmitted is clipped and out-of-band filtered in the digital domain, resulting in a transmitted signal PAPR that can be as low as 4dB for a 64-carrier OFDM transmission, for example. In the receiver, the clipping process is recreated using the detected symbols and the resulting data used to estimate and cancel the clipping noise in the frequency domain. The process is iterative but it was found that most of the benefit of the process was gained in the first two iterations. A plot of packet error rate (PER) versus the ratio of bit-energy to noise-density (E_b/N_0) showed performance within 1dB of an unclipped system for 64-carrier OFDM with the signal clipped to a 4dB PAPR.

1.3.3 PROBABILISTIC METHODS

1.3.3.1 Selective Mapping

Selective mapping [13] is a process in which the OFDM data is scrambled by a set number of sequences, an IFFT is performed and the sequence with the least PAPR is selected for transmission. As it depends on the probability of a random scrambling process generating a symbol code below a predetermined PAPR threshold, it is most effective when the threshold is set at, say, 7 or 8dB rather than about 4dB, where the probability of exceeding the threshold would be nearly unity.

A significant disadvantage is that side-information about the selected combination generally has to be sent to the receiver to enable the sequence to be decoded. This information not only consumes bandwidth but may itself be error-prone. A further disadvantage is that the repeated calculation of PAPR during each symbol period requires complex IFFT operations. We did consider whether aperiodic autocorrelation of the code input could be used to predict PAPR, as it would be much faster to compute than the complex IFFT operations currently needed. However, no reliable basis for this could be found and it was also shown by Ermolova and Vainikainen [14] that low autocorrelation coefficients are only a sufficient condition for low PAPR.

1.3.3.2 Partial Transmit Sequences

Like selected-mapping, partial transmit sequence [15][16] is a scrambling process. However, it differs from the former in that the OFDM subcarriers are divided into *m* clusters, an IFFT is performed on each and the *m* output sequences are then combined so as to minimize the PAPR.

1.3.3.3 Selective Mapping with Space-Time Block Codes

Selective mapping as described in (1.3.3.1) may be applied to each transmit channel in a space-time block-coded (STBC) system independently. However, this results in a system with high computational complexity. You *et al* [17] propose a simplified approach, in which the subcarrier vectors in each transmit channel are multiplied, subcarrier-wise, by a corresponding set of vectors that is the same for each channel. This set is determined such that the average PAPR is minimised over all transmit channels. The result is that only one common set of side information need be transmitted, regardless of the number of transmit channels. The PAPR performance is slightly degraded, by 0.25 to 0.5dB for clipping

probability in the 10^{-2} to 10^{-3} range, but the probability of erroneous detection of side information is significantly reduced because of the space-time diversity, compared to that of normal STBC selective mapping.

1.3.3.4 Peak Reduction Carriers

The method proposed by Lawrey and Kikkert [18], using peak reduction carriers (PRCs), is related to selective mapping. However, instead of scrambling the OFDM data with a set of sequences in order to find a sequence giving the least PAPR, an additional set of subcarriers is added to the data subcarriers. The magnitude and phase values of each of these additional subcarriers, or PRCs, are selected from predetermined sets so as to yield the least PAPR.

The technique is applicable to systems with a small number of subcarriers, 16 or less, because of the large number of combinations of subcarrier vectors that have to be evaluated. The authors found that, for BPSK, the number of PRCs required is about 40% of the number of data subcarriers. The additional power required by the PRCs detracts from the PAPR benefit provided. However, a net reduction in PAPR of 4.5dB is still claimed to be achievable with 10 data subcarriers and 4 PRCs. Whilst there is an indication that the system may be extended to higher-order modulations, the implications for complexity and performance were not discussed in the reference. One apparent advantage of the method, compared with selective mapping, is that no side information need be transmitted. A disadvantage is the loss of channel bandwidth.

1.4 Constant Envelope Modulations

Although there are currently several high-efficiency PA approaches, particularly variants of Classes D and F, all are non-linear types that require constant-envelope modulation. Class-D is a particularly efficient technique at lower frequencies, where it can approach the ideal of 100%. However, it has recently become of interest for UHF amplifiers because of advances in device technology and Raab *et al* [19] have pointed to its suitability for various pulse-width modulation schemes. As the operating frequency increases, the distinction between Class-D and Class-F becomes blurred because of practical component characteristics and at the higher UHF frequencies, a Class-F design approach [20][21][22] may be more applicable. Two previously-known modulation techniques have been found with promise for multi-carrier modulation.

1.4.1 CONTINUOUS-PHASE TRANSMISSION

In this method, by Tan and Stuber [23], the signal transmitted is phase-modulated, not conventional OFDM, and therefore requires a special receiver with a quite-complex phase demodulator. The authors propose to generate a multicarrier signal using the discrete cosine transform (DCT) and post-process this signal to phase-modulate the transmitter (Figure 1.2). The DCT is used because it is able to process frequency- and time-dependent data using real numbers.

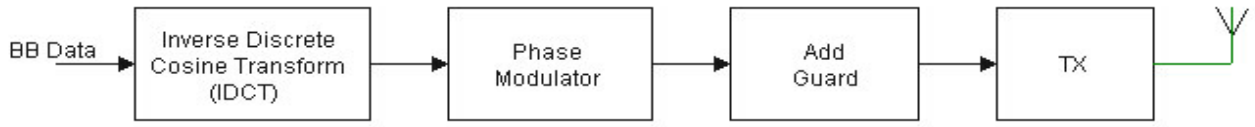

Figure 1.2 - Constant-envelope multi-carrier transmitter

The inverse process is performed in the receiver, after the channel estimation and equalisation steps (Figure 1.3). In the phase detection process, there is a requirement for adequate oversampling and an algorithm to manage "phase-wrapping".

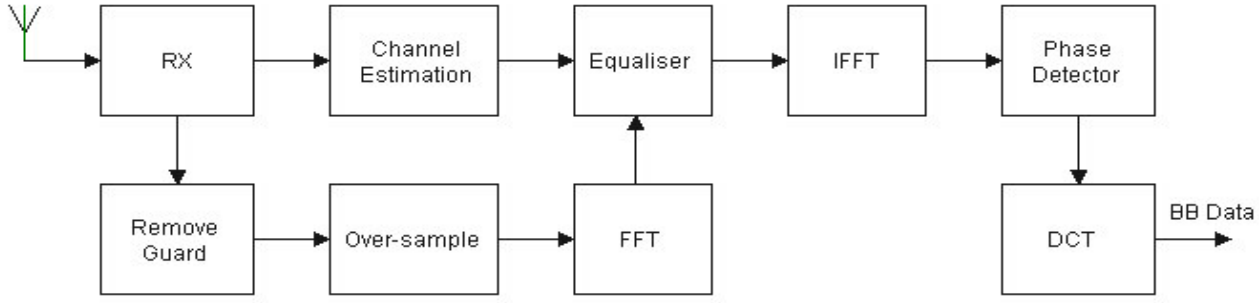

Figure 1.3 - Constant-envelope multi-carrier receiver

1.4.2 RF PULSE-WIDTH MODULATION

A method described by Keyzer *et al* [24] employs carrier pulse-width modulation, implemented with delta-sigma modulators. Its main drawback is that the digital circuits required to generate the modulation must operate at speeds considerably in excess of the carrier frequency.

The concept is illustrated in Figure 1.4, where waveform (a) is the desired microwave output and (b) represents a conventional analogue pulse-width and position modulated signal that would generate (a) after bandpass filtering. Normally it would be extremely difficult to generate such a pulse waveform accurately at UHF or microwave frequencies. Waveform (c) is the output of a proposed delta-sigma modulator, clocked at 8 times the desired RF output frequency. In this waveform, the pulse width, representing amplitude, may have any of the values 0, 1 or 3 clock periods and the pulse position, representing phase, may have any one of the eight clock periods. The noise generated by these approximations is filtered by the PA output bandpass filter.

Figures 1.4 to 1.7 below are reproduced from [24].

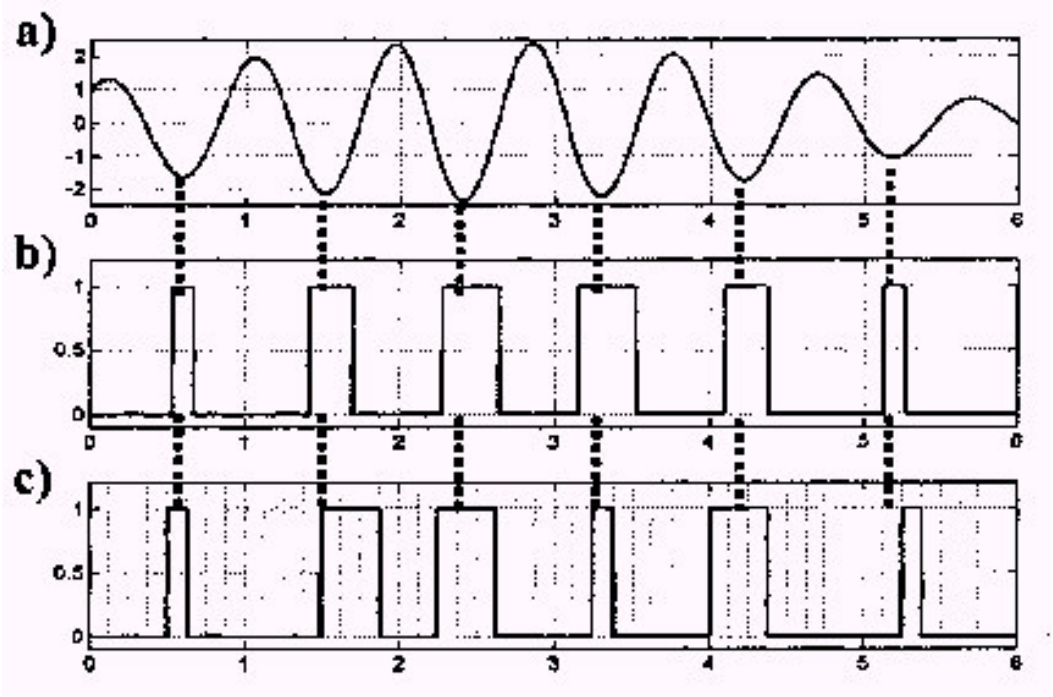

Figure 1.4 - RF delta-sigma modulation [24]
(a) Desired RF signal output; (b) pulse-modulated RF waveform;
(c) delta-sigma RF pulse-modulated output ©2002 IEEE

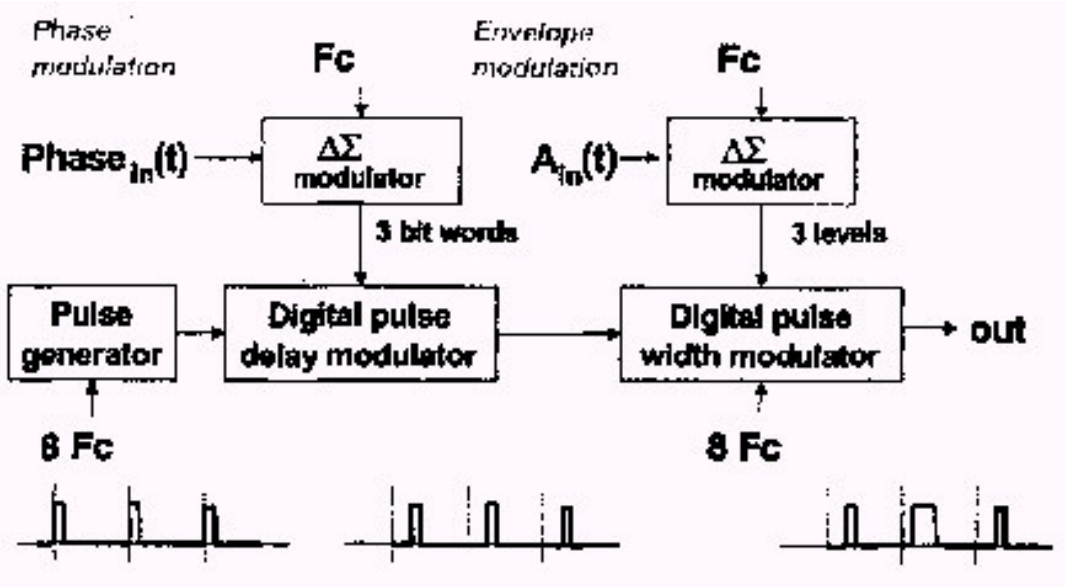

Figure 1.5 - Block diagram of delta-sigma modulation system [24]
Representative output signals are shown ©2002 IEEE

In Figure 1.5 is shown a block diagram of a system capable of encoding the required RF modulation. For cellular systems, the required clock rate for the modulator is about 7GHz.

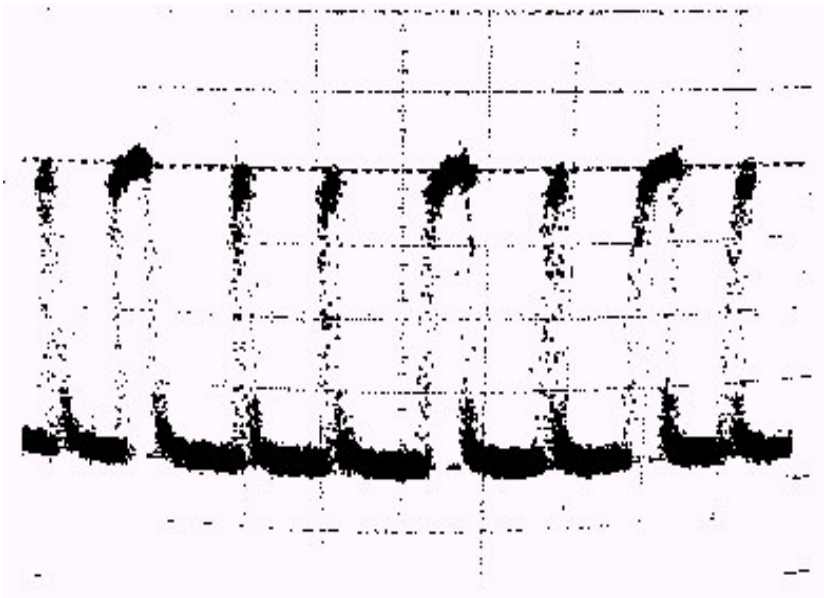

Figure 1.6 - Delta-sigma RF PWM measured digital output data stream [24] (scale: 2ns/div, 200mV/div) ©2002 IEEE

The authors present both simulated and measured performance plots. The time-domain measured data is clearly difficult to measure, as evidenced by the plot of the digital output data stream in Figure 1.6. The test frequency was also limited for this reason. In practice, there may be a linearity issue for higher-order modulation formats, owing to the potential non-linearity of the pulse-width translation. The authors' system was apparently intended for OQPSK.

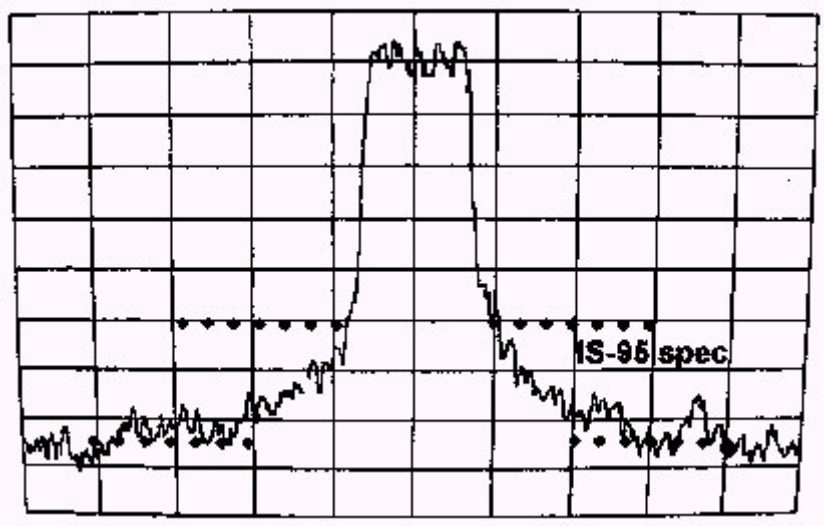

Figure 1.7 - Delta-sigma RF PWM measured output spectrum for OQPSK [24] (span 5MHz, centre frequency 400MHz, vertical scale 5dB/div) IS-95 specification limits shown for adjacent- and alternate-channel power ©2002 IEEE

The output spectrum for OQPSK in Figure 1.7 shows that the system could potentially meet the requirements for a CDMA system provided additional out-of band filtering is included and that digital and mixed-signal circuitry can be satisfactorily scaled up to the required 7GHz clock rate.

1.5 Amplifier Linearisation Techniques

Currently, linear amplifiers are used for OFDM. However, these are typically characterised by an increasing non-linearity at high signal amplitudes and the usual method of achieving the required linearity in a transmitter is to "back off" the PA so that only the more linear portion of its amplitude range is used. Additional "back-off" must be applied to allow for the PAPR, resulting in a most inefficient PA. Clearly, there is a trade-off between processing overhead to achieve low PAPR and the cost, complexity and power efficiency of the PA [25].

Some improvements have resulted from variations of the Kahn technique that employ switch-mode technology in the amplitude-modulation branch of the PA modulation [26]. Considerable research has gone into the design of PA's that can be efficiently modulated and achieve linearity, most using a variant of the Kahn technique and may have feed-forward or feedback linearisation applied. Some current amplifier linearisation techniques include the following.

1.5.1 DYNAMIC BIAS

In the dynamic bias technique [25] the envelope of the signal is detected and used to control both the PA supply voltage, via an efficient switch-mode dc-dc converter, and the PA gate bias, to maintain the amplifier in a linear region. The method gives up to a factor of 2 increase in efficiency at mid-range but results in a slight loss of efficiency at full power because of the loss in the dc-dc converter.

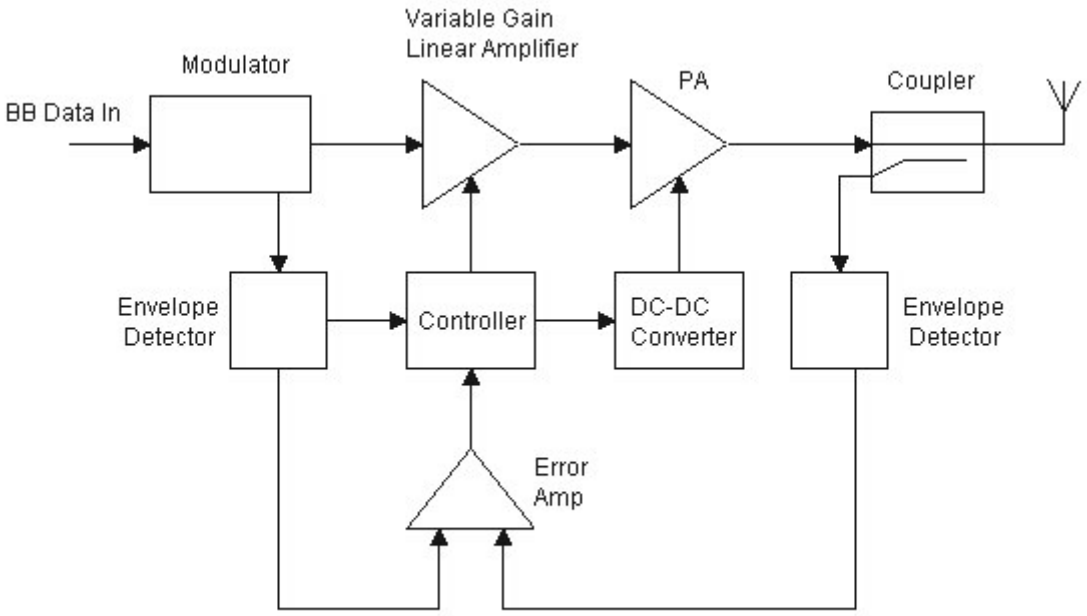

Figure 1.8 - Dynamic bias with envelope feedback

Figure 1.8 shows an improved version of this technique [27], in which envelope feedback is applied to control the gain of the PA driver stage. This has the effect of further lowering adjacent channel power (ACP). Bandwidth limitations would be imposed by delay in this feedback control loop as well as in the response time of the dc-dc converter for the PA supply voltage. In this reference example, a 400kHz dc-dc converter switching frequency was chosen for a modulating signal bandwidth of 30kHz. The PA is designed to operate as a linear amplifier for very low signal levels, to minimise AM/PM distortion.

1.5.2 ENVELOPE ELIMINATION AND RECOVERY (EER)

In the Kahn EER technique, the signal is split into amplitude and phase components, using an envelope detector and limiter respectively. The envelope detector modulates the PA supply voltage and the limiter phase modulates the gate. However, it needs delay lines to compensate for path delays. The effect of differential delays and envelope modulator bandwidth on distortion have been investigated by Raab [26]. Envelope feedback may be applied to reduce distortion and allow an efficient class of PA to be used [28][29]. This is shown in simplified form in Figure 1.9. Efficiency in excess of 50% was claimed for an output power of 5W at 835MHz using QAM modulation. Third-order intermodulation products in a two-tone test at 5W average output were given as –30dBc.

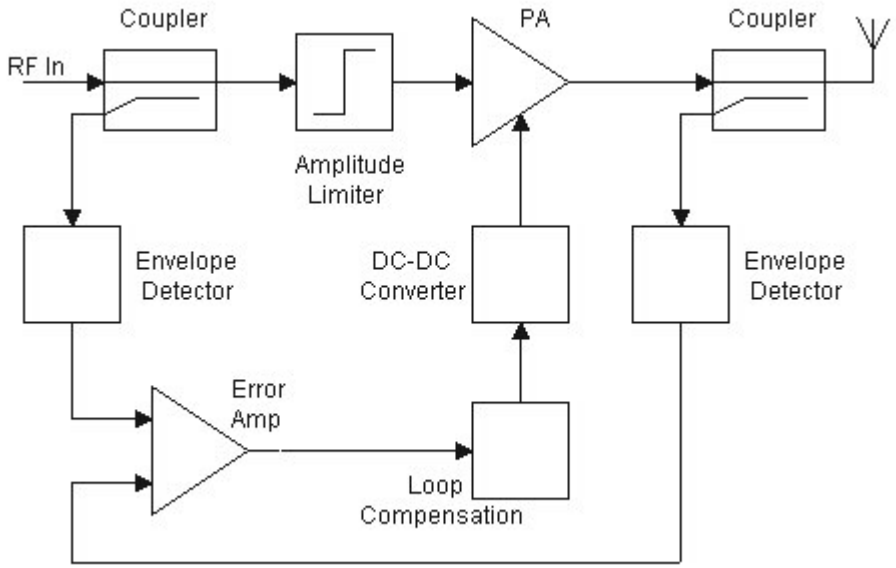

Figure 1.9 - Envelope elimination and recovery

1.5.3 ENVELOPE TRACKING

The problem of achieving precise supply modulation in the Kahn EER technique is reduced by using an envelope tracking approach, although the architecture is substantially the same (Figure 1.9). The principal difference is that the PA is a linear type, Class-A or Class-B, for example, that has the fully-modulated signal applied to its input. Envelope information is used only to control the PA supply voltage via a switch-mode up- or down-converter, the former being more common in battery-operated portables as the higher supply voltage can improve efficiency. A small back-off, typically 10%, avoids distortion from power supply timing and amplitude errors but still allows efficiency enhancement of 50-100% over a linear fixed-supply system [20].

Two main approaches to envelope tracking have been found, suiting different applications. The first of these [31] avoids the problem of high-rate supply modulation by responding only to the average power of the RF input signal and is particularly suitable for CDMA application, where there is system control of transmitted power. However, interest has been growing in the technique of wide-bandwidth envelope tracking, which may be suitable for high-bandwidth OFDM applications like the IEEE 802.11g WLAN standard [32]. This specifies a channel bandwidth of 16.25MHz in a 2.4GHz frequency band, a PAPR of up to 10dB and EVM of 5.6% for a 54Mb/s data rate. The major challenge in this technique is the achievement of accurate time alignment, although it has been shown to be less critical than for the Kahn EER technique. In the reference [32], Wang *et al* claim an improvement in efficiency of more than 100% compared with a

conventional linear Class-AB PA, making use of high-speed FPGA hardware for signal processing.

1.5.4 POLAR FEEDBACK LOOP

The polar feedback technique [30], was developed to enhance the PA efficiency of the base transceiver system (BTS) in wideband code-division multiple access (WCDMA) mobile wireless networks. The system, shown in Figure 1.10, compares the amplitude and phase of the PA output signal with the RF drive signal and uses the derived error signals to apply corrections prior to the PA stage. Practical gains in power output and efficiency of 1.1dB and 4% respectively have been obtained for an experimental GaAs FET output stage operating at 1.91GHz, for an error vector magnitude (EVM) of 2.5%. The resulting efficiency of 18.1% compared with 15% for the more linear LDMOS transistor type normally used in a BTS without polar feedback. The efficiency could be further enhanced, perhaps at the expense of linearity, by employing switched-mode, Class-S amplitude modulation of the PA, as in the preceding methods (1.5.1) and (1.5.2).

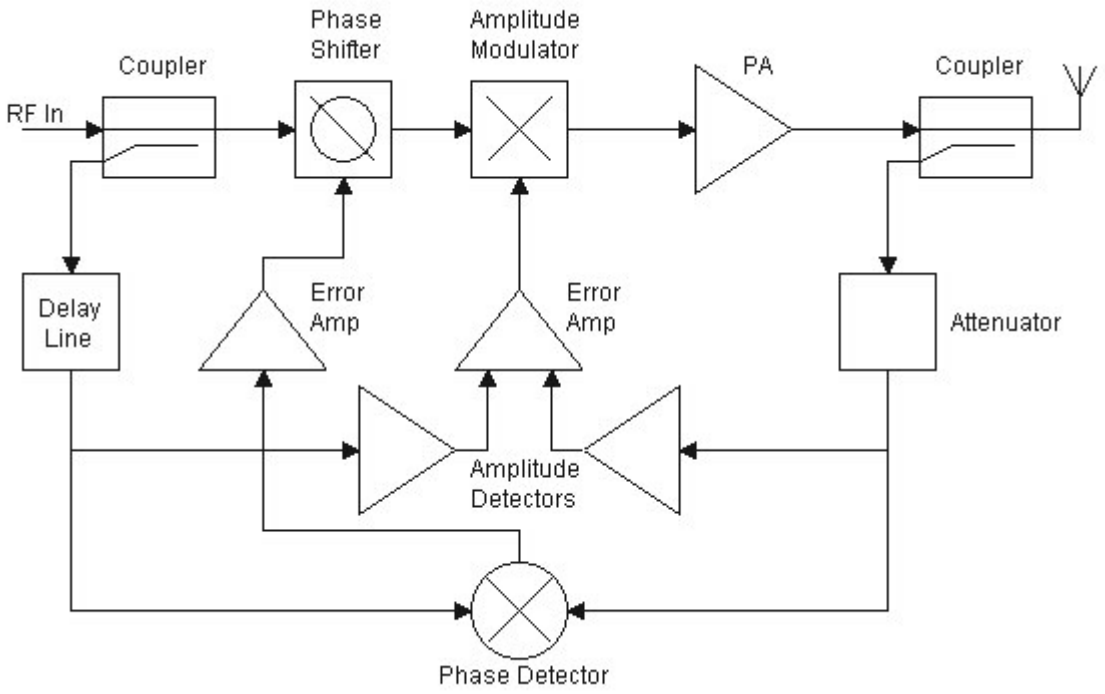

Figure 1.10 - Polar feedback loop

A major limitation of this technique is in the correction bandwidth, resulting from the signal path delay. The delay line in the input signal reference path compensates for the main signal path delay, so that precise error values may be obtained. However the amplitude and phase corrections

are being applied to the input signal after this same delay, limiting the loop bandwidth. The latter is generally required to be at least 5 times the bandwidth of the modulating signal.

1.5.5 CARTESIAN FEEDBACK LOOP

A Cartesian feedback loop system [25] is shown in Figure 1.11. The output of the transmitter is sampled using a directional coupler and the samples are demodulated to Cartesian coordinates. These components are subtracted from the input to generate error signals that are used to cancel the distortion in the output. There are significant design issues relating to noise and distortion in the feedback components, as well as loop gain and stability considerations. As the requisite loop gain depends on the uncorrected linearity of the PA, which in turn depends on the degree of back-off in the PA, there is a design trade-off to be made between efficiency, linearity and stability.

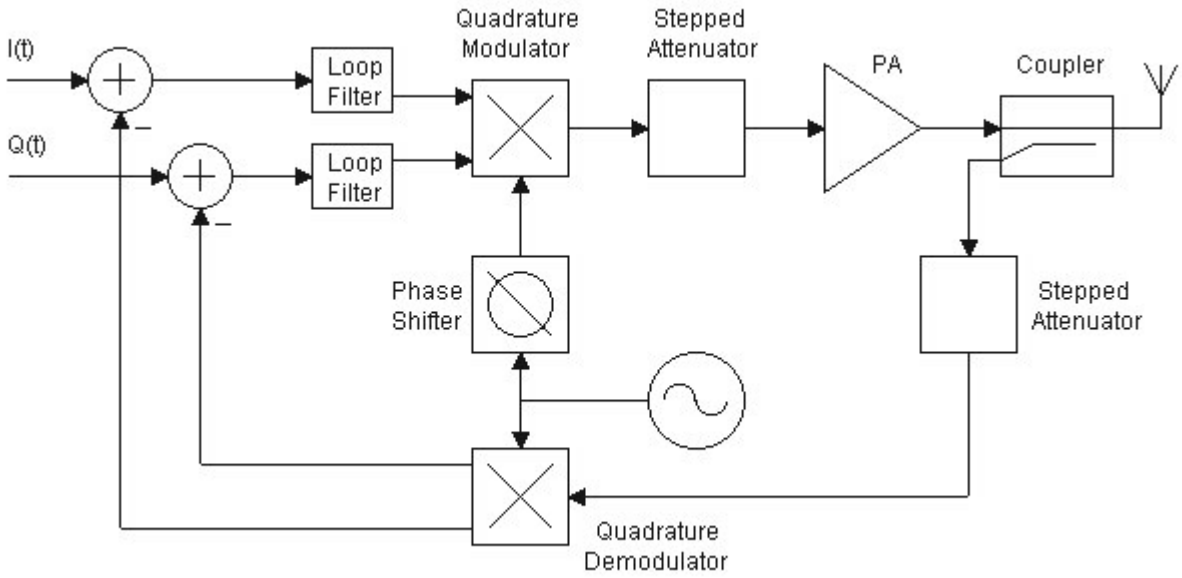

Figure 1.11 - Cartesian feedback loop

Design of a digital Cartesian feedback loop (DCL) is described in [25] as well as a hybrid technique that combines it with EER. Figure 1.12 shows the elements of an experimental DCL configuration that was implemented in [25]. Up to 23dB of linearity correction was achieved for a 20kHz loop filter and TETRA modulation.

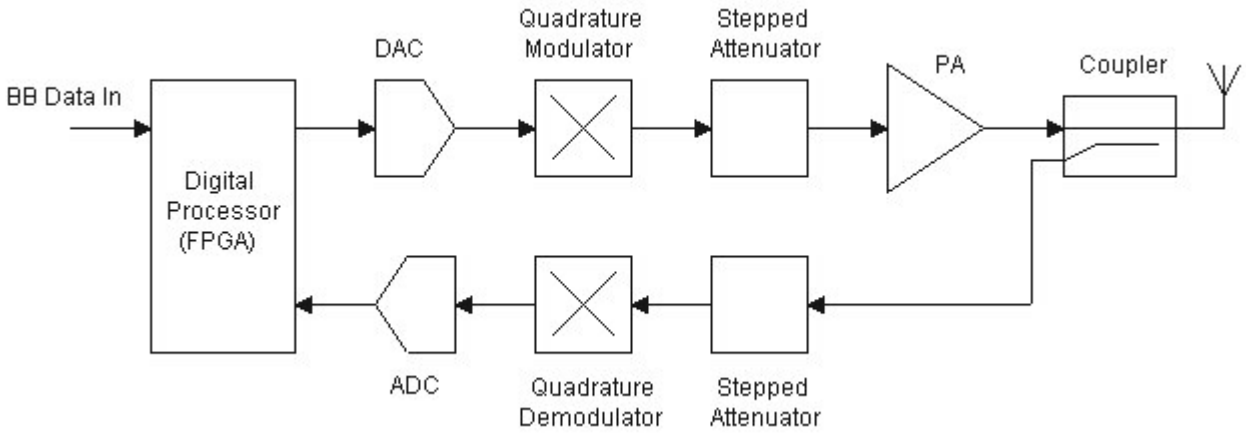

Figure 1.12 - Digital Cartesian feedback loop

1.5.6 DIGITAL ADAPTIVE PREDISTORTION

Complex gain mapping is a form of digital adaptive predistortion that has achieved success because of its small look-up table and fast response time [25]. In this system, shown in Figure 1.13, the squared signal amplitude is used to address gain and phase lookup tables to generate predistortion. An advantage of this technique is that the adaptation process takes place at a low rate compared with the modulation frequencies and is therefore not subject to stability trade-offs. However, it does not correct for quadrature modulator errors, although another form of predistortion, known as Cartesian mapping, is able to correct for these errors.

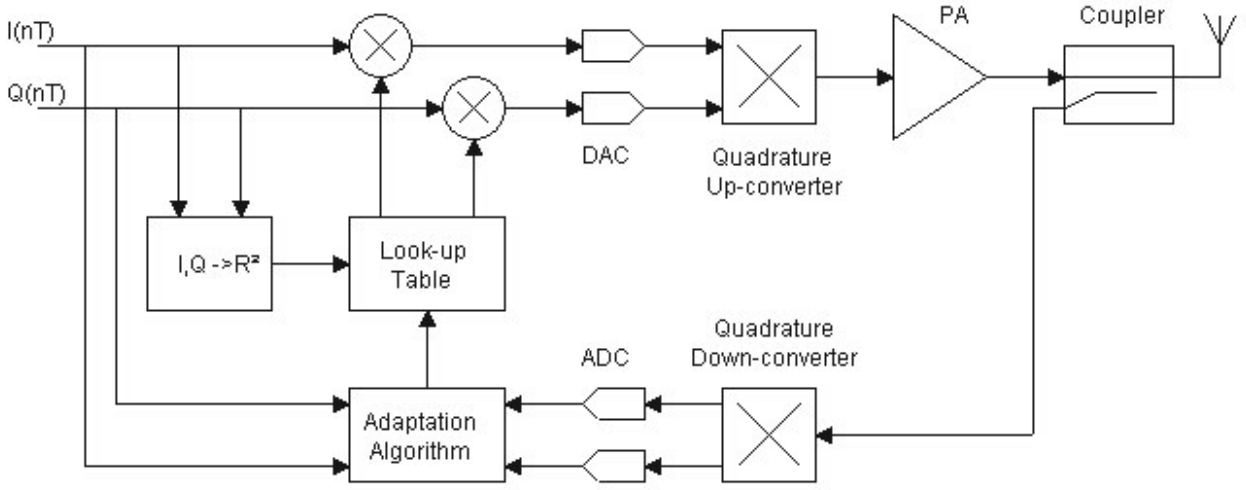

Figure 1.13 - Digital adaptive predistortion

1.5.7 THE DOHERTY AMPLIFIER

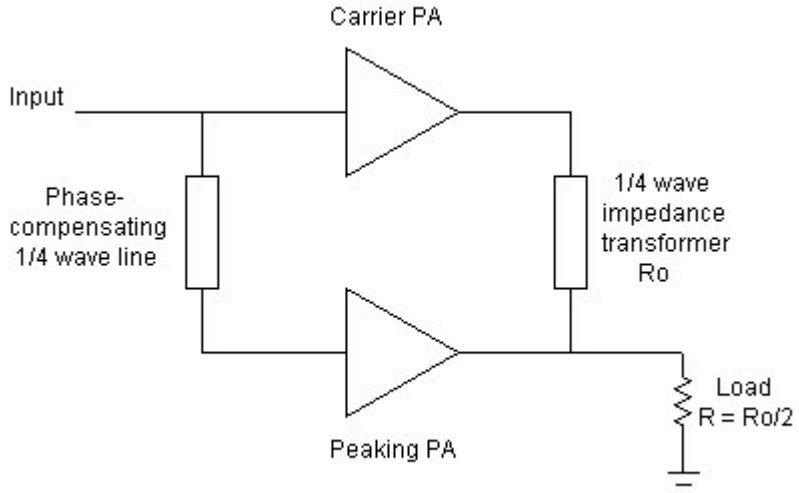

Figure 1.14 - Doherty amplifier system

In 1936 Doherty introduced a new linear PA system [33] that was developed at Bell Telephone Laboratories for the Western Electric Company. The system was capable of delivering over 60% efficiency and an audio distortion level of 1%, with feedback Subsequently, it was used in all Western Electric 1, 5 and 50kW transmitters [34]. Figure 1.14 shows the basic configuration, in which there are two, originally identical, amplifiers driving a common load. The first, termed 'carrier PA', is biased in Class-B and driven continuously with an input level such that, at the average value of the signal, about half the value of the peak voltage for an AM transmitter, the stage is just entering the saturated state where the Class-B amplifier is most efficient. The impedance transformer presents the amplifier with a load of $2R_0$ at this stage. The second amplifier, termed 'peaking PA', is biased off up to this point but begins to conduct in Class-C mode above this level. As it does so, it raises the apparent load impedance and this is converted by the impedance transformer to a lower value at the output of the carrier PA, allowing the latter to deliver more power whilst staying close to the saturated state. At maximum signal input, the peaking amplifier has enough drive to be close to Class-B operation and the two amplifiers deliver approximately the same power, each driving an effective impedance of R_0. In order to achieve the correct phase relationship between the outputs, the 90^o phase shift of the output impedance transformer has to be corrected by an equivalent phase-shifting element at the input. The sum of the two outputs has an approximately linear relationship to the input signal and, at the AM broadcast frequencies, could be easily improved by applying feedback. For other modulation formats, such as applications with high PAPR, it is possible to have different power-sharing

ratios. These may be achieved by feeding the two PA units with different supply voltages and changing the load impedances.

In recent years there has been a resurgence of interest in the Doherty technique for microwave applications [35]. The use of feedback for linearisation tends to be impracticable at these frequencies, necessitating the use of alternative techniques. A 2GHz, 1W PA that uses Class-F amplification with feed-forward linearisation is described in [36] and achieves –50dB distortion with an efficiency of 52%. A method is presented in [37] of improving gain and phase response of the Doherty amplifier using a DSP for gate bias control in combination with digital predistortion. In a CDMA application, adjacent channel power was shown to be lowered by 10dB using the DSP approach.

1.6 Summary of PAPR in the Wireless System

1.6.1 PAPR REDUCTION TECHNIQUES

PAPR reduction using complementary codes is only applicable to *m*-PSK systems. An objective of current MIMO research is very high bandwidth and a prime candidate for achieving this is higher-level *m*-QAM modulation, using at least 64 subcarriers. For this, other techniques such as clipping or SLM are probable choices. Clipping has been found to be the most practical scheme, probably including filtering to limit out-of-band distortion components, since SLM has two major disadvantages, computational load and the need to transmit explicit side information, although it has the advantage of fewer bit errors. There is also a significant problem of maintaining subcarrier phase relationships from the digital processor through to the final transmitter PA. This may be hard when several stages of up-conversion are used indicating that direct carrier modulation may be preferable to give greater accuracy. The technology of suitable direct quadrature modulator components has been steadily advancing and the precision of such parts may now be sufficiently high to warrant consideration of the approach.

1.6.2 CONSTANT ENVELOPE SUMMARY

The constant-envelope modulation techniques have been found to fall into two basic categories, exemplified by those described above. The continuous-phase technique reqires the OFDM signal to be converted to a phase-modulated signal and is transmitted in that form, requiring the receiver to demodulate the phase as well as the OFDM signal. It is therefore adding complexity at both the base station and terminal, as well as being incompatible with current equipment. In contrast, carrier pulse-width modulation is typically filtered after the PA and may be received and

demodulated by a conventional receiver. Filtering is unlikely to be a major difficulty in such a system, although it may constrain operation to a selected frequency band, but switching circuits associated with broadband UHF systems may present considerable design challenges.

1.6.3 PA LINEARISATION SUMMARY

In order to achieve the highest efficiency, non-linear PA stages may be required, indicating the use of EER systems. However, Mann [25] has shown that the linearity obtainable from EER is not sufficient to meet the specifications of mobile radio systems like TETRA unless it is combined with, for example, a digital Cartesian feedback loop. For a wideband system such as EDGE, with 200kHz channel spacing, there could still be significant difficulty in achieving loop stability. Linearisation methods that do not rely on "real-time" feedback loops, such as digital adaptive predistortion, thus appear to be more suitable candidates for broadband OFDM systems. However, as the correction available would then be limited, the choice of PA class and envelope modulator converter technology (for example, PWM or sigma-delta) may have a significant impact on the results that would be achievable. Both the wide-bandwidth envelope tracking technique and the Doherty amplifier in combination with DSP have emerged as potential options.

1.6.4 PROPOSED SOLUTION

In order to achieve the PA efficiency associated with constant-envelope operation, as well as compatibility with existing equipment, we have focussed on pulse modulation techniques. A system has been proposed that enables quadrature components of an OFDM baseband signal to be separately pulse-width modulated and used to directly modulate an RF carrier in a way that results in a constant-envelope signal. This may be amplified and filtered to yield a transmitter output signal that is virtually indistinguishable from a conventional OFDM transmission.

Chapter 2

Quadrature Phase-Time Modulation

2.1 Introduction to QPTM

In this research we propose a novel technique that could simultaneously achieve linear modulation and high power efficiency. The technique is suitable for implementation in either the analogue or the digital domain. Unlike the constant-envelope approaches described earlier, this technique also enables the transmitted signal to be made compatible with existing OFDM receivers.

2.1.1 CONCEPT

The requirement for amplitude linearity in a PA may be obviated by employing signals that have constant-envelope characteristics. We have found that one may generate a constant-envelope signal by quadrature-modulating a carrier signal at the transmitter frequency with two pulse-width modulation (PWM) signals $p_I(t)$ and $p_Q(t)$. These PWM signals are generated respectively by modulation of the baseband quadrature signals $x_I(t)$ and $x_Q(t)$ on a suitable reference signal. A QAM signal may be recovered by filtering the PA output before transmission (Figure 2.1).

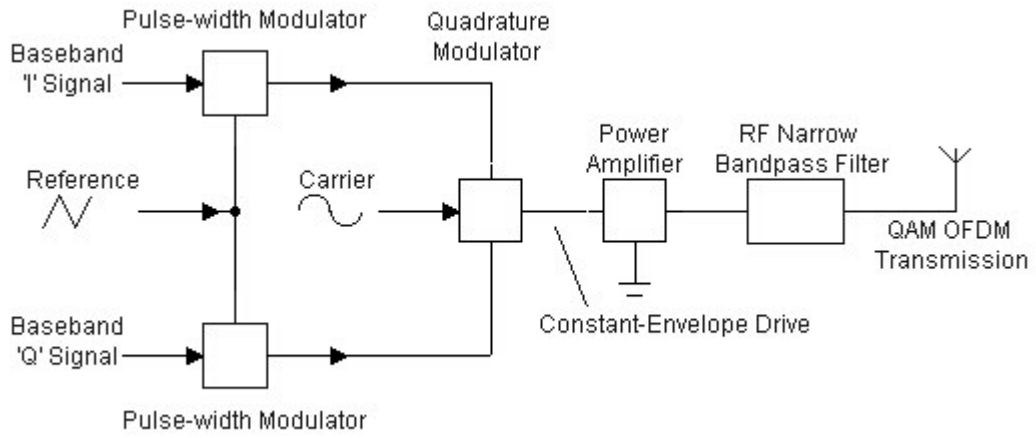

Figure 2.1 - QPTM System Concept

2.1.2 THEORY

From expression (1.1),

$$x(t) = x_I(t) + jx_Q(t) \tag{2.2}$$

Then we generate the PWM signals using

$$p_I(t) = \text{sgn}\,(x_I(t) + r(t)) \tag{2.3}$$

and

$$p_Q(t) = \text{sgn}\,(x_Q(t) + r(t)), \tag{2.4}$$

where $r(t)$ is the reference triangle or saw-tooth wave.

The output of the quadrature modulator is thus

$$m(t) = p_I(t)\cos\omega_c t + p_Q(t)\sin\omega_c t \tag{2.5}$$

The resulting modulated carrier $m(t)$ is similar to QPSK but with a non-uniform period in any state and, in general, only a 90-degree phase shift occurs at any transition (simultaneous transitions of I and Q PWM signals are possible but have very low probability).

A procedure for analysing the spectrum of PWM signals using the double Fourier series method was presented by Black [38]. This is a lengthy procedure and not easily applied to complex modulating waveforms. However, since we are interested in the characteristics of the modulated signal spectrum we prefer to use another procedure described in [38] (originally by J.G. Kreer), that is applicable to any form of pulse modulation and arbitrary modulating signals. The method is reproduced in Appendix 1 for convenience. It may also be applied to both uniform and natural sampling.

In uniform sampling, samples of a signal are acquired at uniformly-spaced time intervals and the samples then compared at the same uniform rate with the instantaneous values of a reference signal. With natural sampling, the instant of sampling varies within a time window for each sample depending on the time of coincidence of the signal and reference values. In pulse-width modulation, natural sampling may be used to modulate the phase of either or both edges of the pulse. For practical reasons, natural sampling has been used throughout the current project, along with symmetrical, double-edge modulation.

From Kreer's method (Equation A.7), the spectra of symmetrical, double-edge modulated, naturally-sampled PWM signals may be represented as:

$$p_{(I,Q)}(t) = \frac{2k}{T} x_{(I,Q)}(t_n) + \sum_{m=1}^{\infty} \left[\frac{4}{m\pi} \right] \sin m\pi \left[\frac{1}{2} + \frac{k}{T} x_{(I,Q)}(t_n) \right] \cos m\omega_r t \qquad (2.6)$$

where t_n denotes the time in the nth period that $x_I(t)$ and $x_Q(t)$ were sampled. ω_r is the fundamental angular frequency $2\pi/T$ corresponding to the cyclic pulse frequency f_r of $1/T$. The simplifying assumption has been made here that the sample rate is high enough for both pulse edges to be considered as modulated by the same sample value $x_{(I)}(t_n)$ or $x_{(Q)}(t_n)$. Here we have cancelled the DC component and multiplied the spectrum by 2 to give a pulse magnitude of ±1 for each of the quadrature modulator inputs $p_I(t)$ and $p_Q(t)$.

Only the first term on the right-hand side of (2.6) is wanted as a component of the transmitted output spectrum, the other spectral components being removed after final RF amplification by a narrow bandpass filter. However, we are particularly interested in examining the sideband orders to determine the significance of any harmonic components that may overlap the wanted signal band. Each of the spectra $p_{(I,Q)}(t)$ of the PWM signals contains, respectively, samples of the original baseband signal $x_I(t_n)$ or $x_Q(t_n)$, represented by the first term in (2.6), and a series of spectral components grouped around, and resulting from amplitude modulation of, each harmonic of the reference ω_r, represented by the second term in (2.6). The latter are scaled in amplitude inversely with reference harmonic order m. In the amplitude-modulating component of the second term, $\sin m\pi \left[\frac{1}{2} + \frac{k}{T} x_{(I,Q)}(t_n) \right]$, the signal is an angle, that has a different effect depending on the value of m. This term becomes $\sin \left[\frac{m\pi}{2} + \frac{m\pi}{2} x_{(I,Q)}(t_n) \right]$ if we make $k = T/2$. We now can see that when $m = 1$, the amplitude of the term is sin $\pi/2$, or 1, when $x(t_n)$ is zero, and otherwise varies from sin 0 through sin $\pi/2$ to sin π as $x(t_n)$ varies from –1 to +1. This is a frequency-doubling effect (as well as having the non-linearity associated with the sine function). There is also an average positive value so that the $f = f_r$ spectral line will have a significant amplitude, depending on the input signal.

When $m = 2$, the amplitude of the modulating term is zero when there is no signal and varies from sin $-\pi$ through 0 to sin π with an input signal varying from –1 to +1. Thus there is no spectral line

at $f = 2f_r$ and double sidebands occur at spacings from $2f_r$ equal to the signal input frequency and odd harmonics of this frequency.

When $m = 3$, the amplitude of the modulating term is sin $3\pi/2$, or –1, when there is no signal, and varies from sin 0 through sin $3\pi/2$ to sin $6\pi/2$, as the input varies from –1 to +1. Since it is possible for the amplitude value to spend more time in the positive sectors from 0 to π and 2π to 3π than in the negative sector, partial cancellation of the $3\pi/2$ offset can occur, significantly reducing the $f = 3f_r$ spectral line. However, the amplitude characteristic for this order is highly distorted, with both even and odd components.

There is no need to examine the components associated with higher values of m as they are low enough in level and far enough removed from the baseband to have no real impact on filtering requirements or linearity performance.

One factor that has a bearing on the quality of the recovered signal is that the functions $x_{(I,Q)}(t_n)$ in Equation (2.6) are not continuous but a series of samples of the input I and Q signals. Consequently, the second term of (2.6) generates infinite spectra centred on each harmonic m that overlap the baseband signal spectrum. As they are within the wanted signal range they cannot be filtered out. Accordingly, an oversampling rate for the reference frequency will be selected that is well above the Nyquist rate, so that the interfering components are sufficiently reduced in value, depending on the requirements of the selected baseband modulation scheme.

In audio and other low-frequency applications, the original signal is normally recovered by low-pass filtering to eliminate all but the wanted signal. In this application, however, the quadrature modulator output signal is centred at the RF carrier frequency and so a bandpass reconstruction filter may be used to reject out-of-band products after amplification by the PA. By this means, a signal may be transmitted that is substantially identical to an OFDM signal that has been transmitted in the usual manner via a linear PA.

2.1.3 PTM SPECTRAL ANALYSIS USING MATLAB®

The general expression for the basic PWM process, used for Equations (2.3) and (2.4), is

$$p(t) = \text{sgn}\,(x(t) + r(t)) \tag{2.7}$$

We have used this as a basis for a MATLAB® [39] program for generating plots of simulated PWM signals. These have been generated for single- and two-tone inputs for one channel, with frequencies chosen principally for clarity of illustration. In a QPTM system the two channels, I and Q, will be separately pulse-width modulated and the resulting PWM signals then used to

product-modulate cosine and sine components respectively of a carrier, the outputs being linearly summed. The output spectrum would have similar characteristics to that of a single PWM channel modulated onto a carrier and so we only need to simulate one channel here.

The following parameters were used for the simulations:

RF carrier frequency: 500MHz

Frequency of modulating baseband signal, single and two-tone tests: 5MHz

Frequency of modulating baseband signal, two-tone test: 2MHz

Sample rate: 4096MSa/s (binary value)

Number of data samples in FFT: 4096

Reference over-sample rate: 100 (even number)

Reference triangle wave frequency: 40.96MHz (> 2 x baseband frequency – chosen as high as practicable to minimise subsequent filtering complexity)

Reference triangle amplitude: +/-1

Peak amplitude of modulating signal: 0.99 (must be < reference amplitude)

The approach taken has been to generate first a PWM spectral plot with a single-tone baseband input and then show this modulated onto an RF carrier. This permits a comparison to be made with the theoretical observations in (2.1.2). The baseband frequency of 5MHz is relevant to broadband microwave applications but the carrier frequency of 500MHz is typical of UHF mobile radio. However, this frequency ratio allows clear distinction of spectral lines in the plots and the UHF band has been chosen for prototyping an actual system because of measurement convenience and availability of parts and equipment. There has also been some interest in the possible application of this technique to high-data rate UHF systems operating in commercial 25kHz channels.

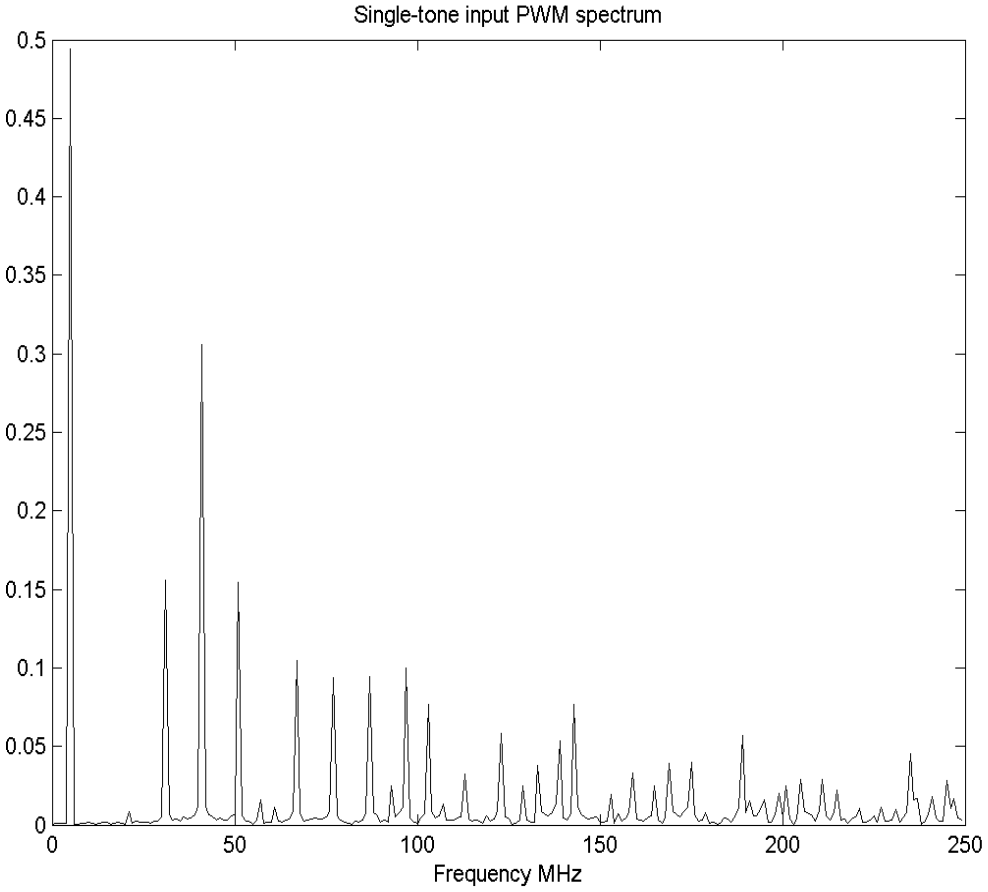

Figure 2.2 - 5MHz input, 40MHz reference, PWM magnitude spectrum

The spectrum in Figure 2.2 shows the baseband signal at 5MHz and the prominent reference line at 40MHz. Also clear is the frequency doubling effect in the displacement of sidebands centred on the reference. As was predicted, there is no reference harmonic line at 80MHz and there are almost equal 1st and 3rd harmonic sidebands in the 80MHz band. The reference 3rd harmonic is well-suppressed at 120MHz.

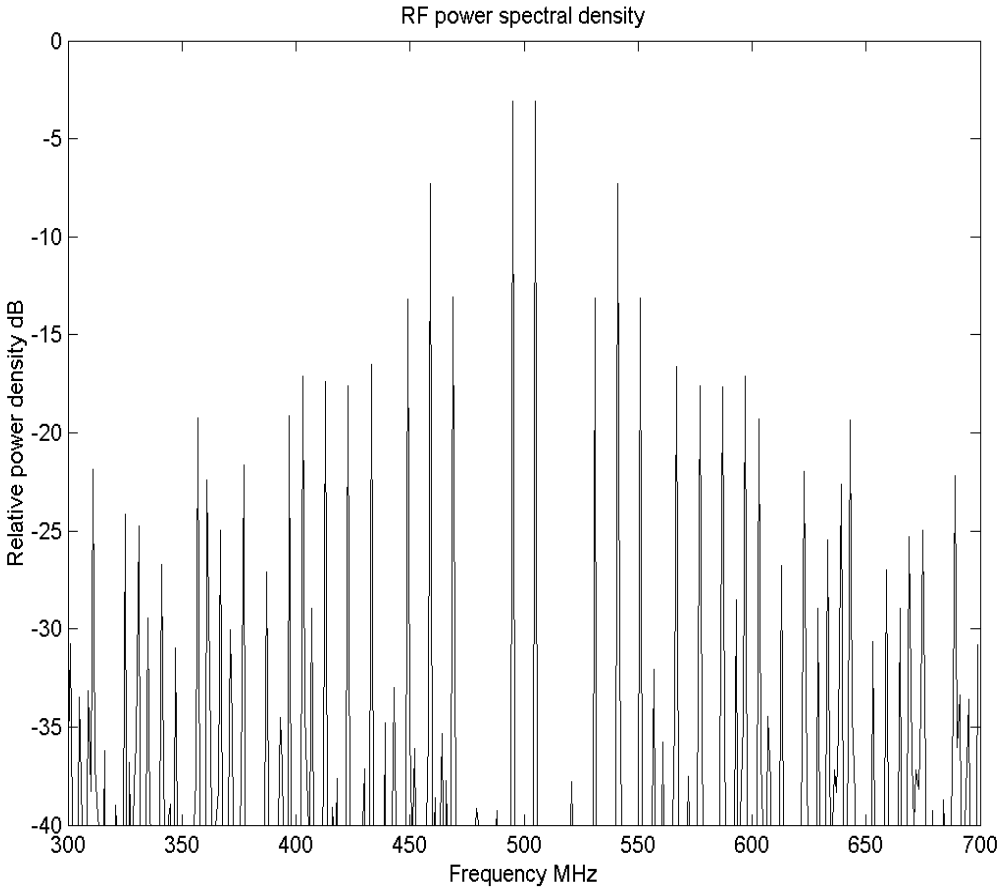

Figure 2.3 - Spectrum of 5MHz tone, 40MHz reference on 500MHz carrier

The spectrum of Figure 2.3 has been displayed on a decibel vertical scale to show a wider dynamic range and to allow easy comparison with later RF spectrum analyser plots. The plot appears to correspond well with Figure 2.2, with no apparent anomalies. In order to recover the amplitude-modulated carrier after amplification by a PA, the plot shows that a bandpass filter with passband extending beyond ±5MHz from the 500MHz carrier and with stopband edges at around 475MHz and 525MHz would be suitable. A stopband rejection of 40-70dB would most likely be required depending on the application and relevant wireless regulations.

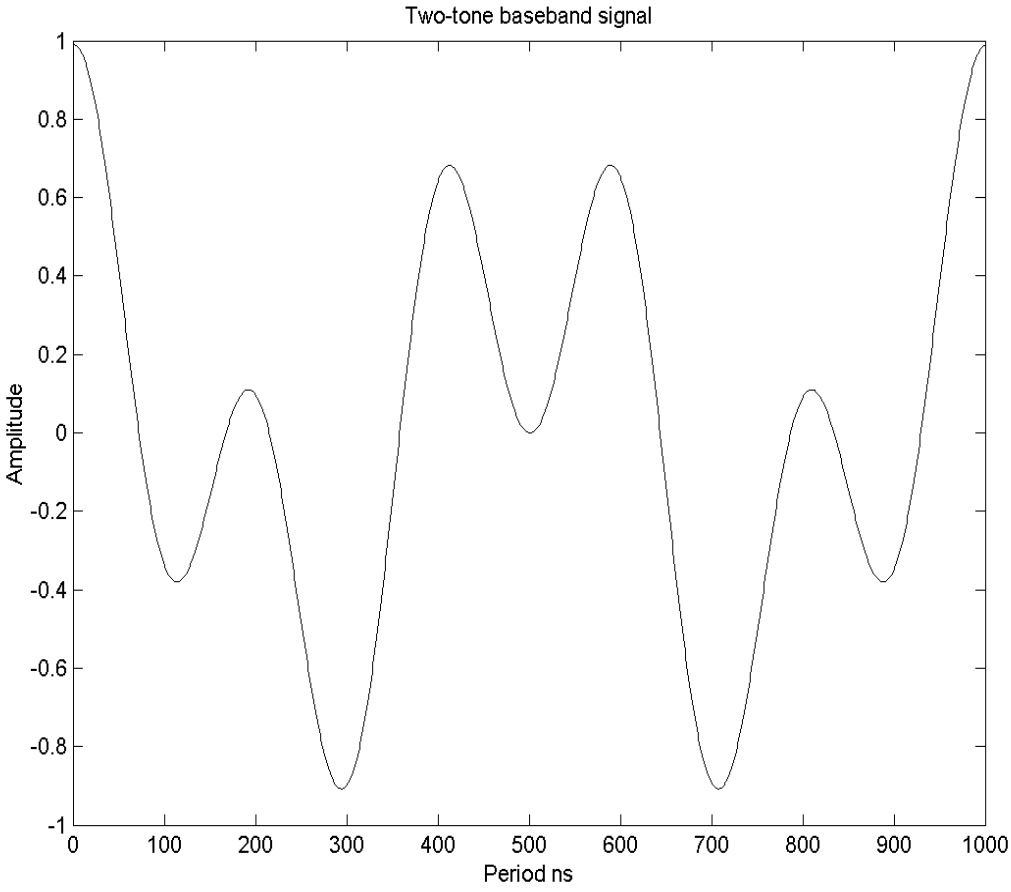

Figure 2.4 - 2MHz and 5MHz two-tone baseband signal

A time-domain plot of the two-tone test signal used for the next simulation is shown in Figure 2.4. Note that the amplitude of each tone has been backed off to avoid clipping, resulting in reduced power levels in the subsequent spectral plots.

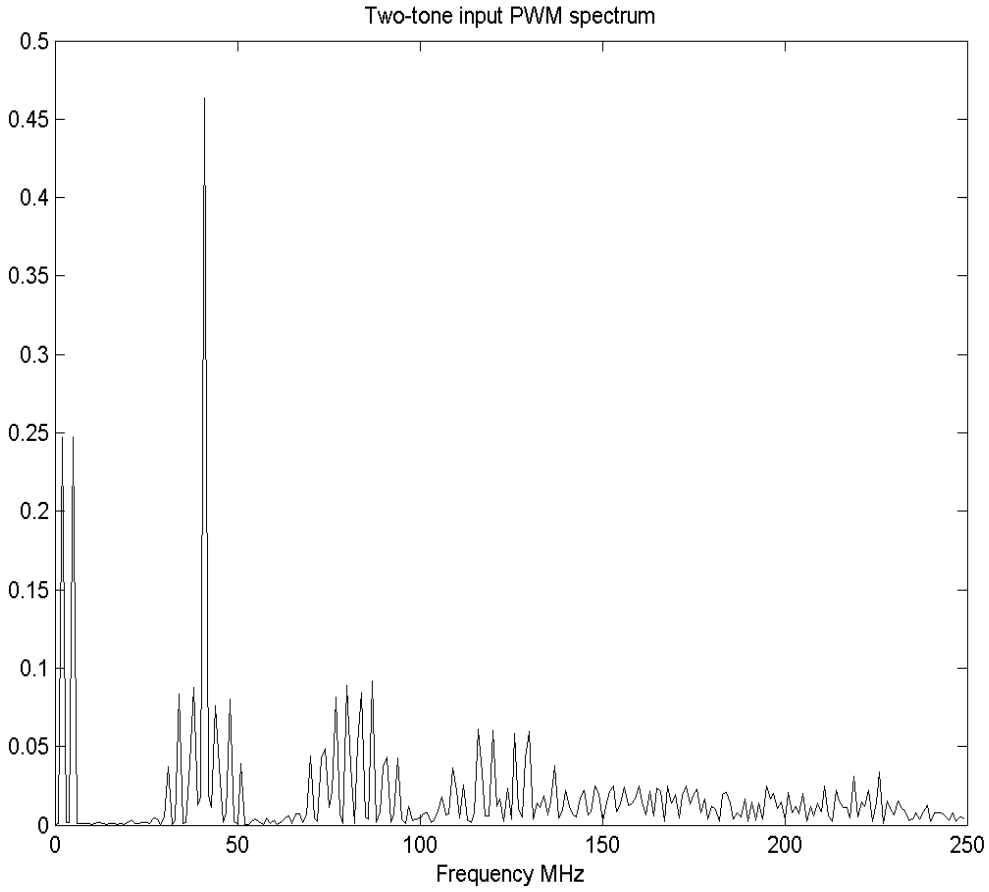

Figure 2.5 - PWM magnitude spectrum for 2MHz and 5MHz inputs with 40MHz reference

The spectrum in Figure 2.5 shows the spectrum for two equal tones, reduced in power to avoid clipping, with the result that the reference line at 40MHz is now dominant. There appear to be intermodulation products in the sidebands of the 40MHz band, in addition to the expected frequency-doubled sideband offsets.

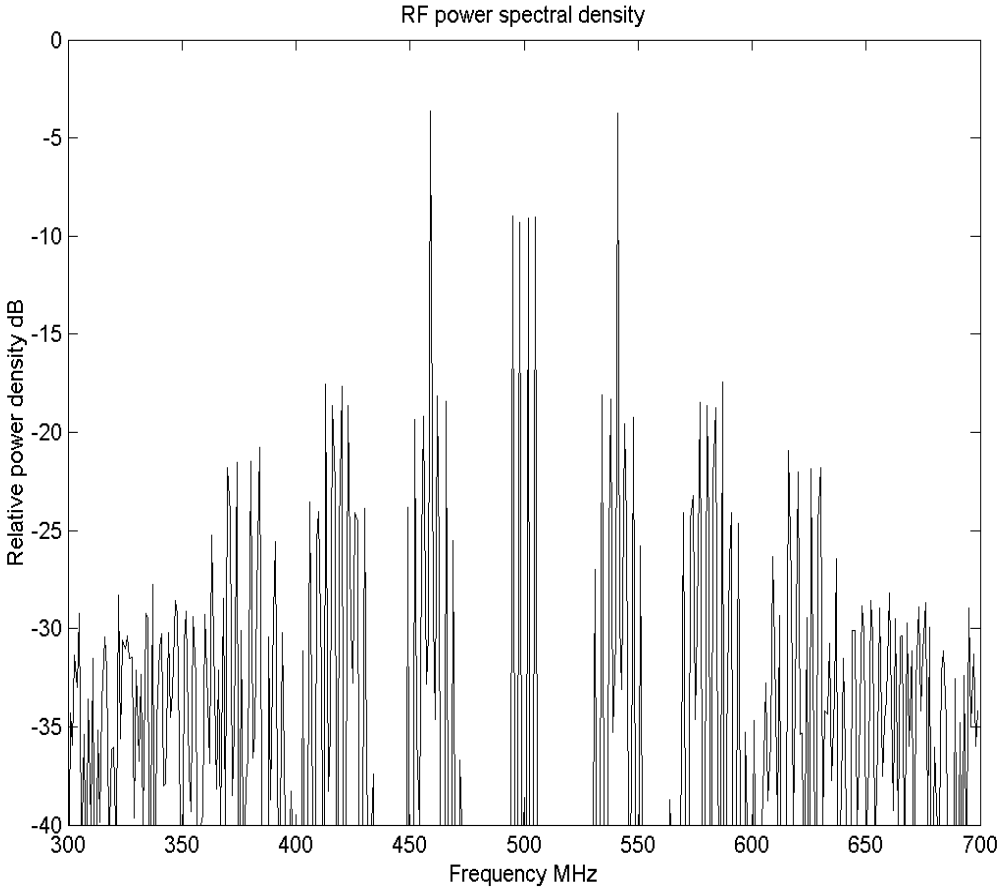

Figure 2.6 - Spectrum for two-tone PWM, 40MHz reference, 500MHz carrier

The spectrum for RF carrier amplitude modulation by a two-tone PWM signal is shown in Figure 2.6. There is no evidence of intermodulation or harmonic distortion in the wanted channel around 500MHz. The remainder of the spectrum appears to follow expectations, based on the previous spectral plot in Figure 2.5.

2.2 QPTM System Description

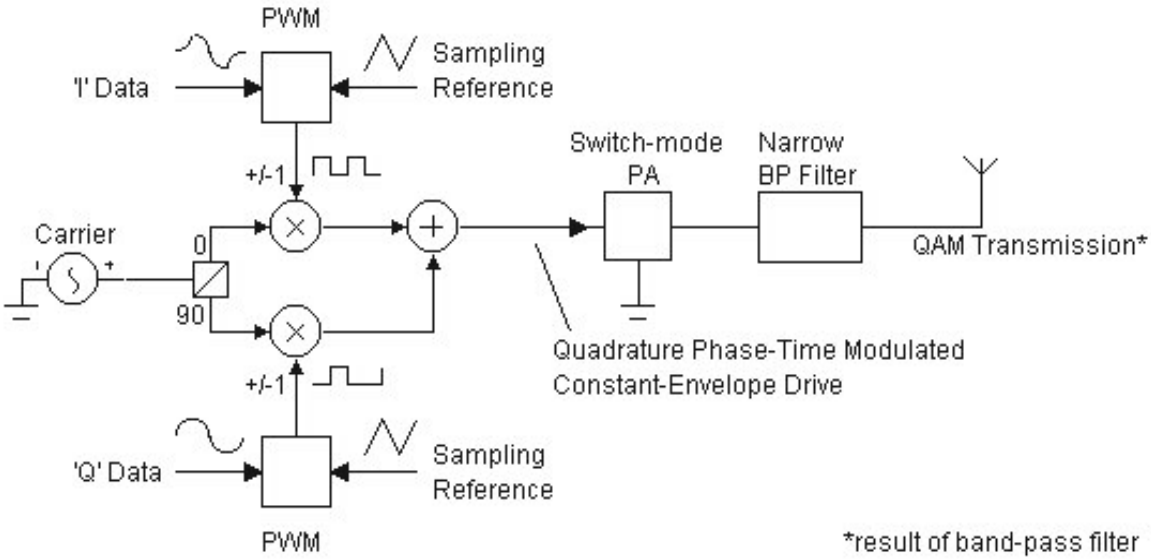

Figure 2.7 – QPTM system with switch-mode PA

The system as shown in Figure 2.7 comprises two pulse-width modulators for I and Q baseband signals, a direct-quadrature modulator subsystem, non-linear (e.g. switching) PA and a narrow-band output filter. (The direct quadrature modulator is available as a real component that incorporates the functions of carrier phase-shifter, two product modulators and a summer in a single integrated circuit. The availability of such high-performance and wide-bandwidth parts adds considerably to the attractiveness and feasibility of the proposed solution.)

It is envisaged that ultimately this process would be accomplished in an OFDM digital processing subsystem but conceptually the process may be represented by the configuration in Figure 2.7. This diagram also shows an ensuing switch-mode PA (it could alternatively be linear) and output narrowband filter that would be required to transform the phase-time modulated output to a QAM transmission, for compatibility with linear OFDM systems.

The I and Q baseband signals (that is, the IFFT output symbols containing a number of *m*-QAM modulated OFDM sub-carriers) are each fed via the corresponding pulse-width modulator to the modulating inputs of a direct carrier modulator. These inputs to the multiplying elements of the modulator are bipolar (e.g. +/-1), the duration of, for example, the + phase corresponding to a number (not necessarily an integer) of carrier signal periods proportional to the corresponding I or

Q baseband signal amplitude at a sample instant. It is assumed that the IFFT outputs are anti-alias filtered prior to sampling by the pulse-width modulator.

The other multiplier inputs are unmodulated sine and cosine carrier signals. The sum of the modulated carriers is a quadrature-modulated constant-amplitude signal that drives the PA input. The PA output is fed to the antenna via a bandpass filter, resulting in an output to the antenna that is modulated in both amplitude and phase. A significant advantage of this proposed technique is that a normal OFDM receiver may be used with it. However, the PA and bandpass filter combination are designed to meet the specific requirements for QPTM signals.

2.3 Summary of QPTM

In this chapter we have examined the basic characteristics of a QPTM signal and the manner in which it is constructed. A basic theory was presented and followed by Matlab simulation of example PWM signals, the component parts of a QPTM signal, that have been chosen to reveal the characteristics to be expected in an ideal system. The transmitter output spectrum prior to filtering was also simulated. A model system was then presented that demonstrated how the QPTM system might be realised with conventional wireless components. In the next chapter, the simulation of such a system is performed in detail to provide the basis for a practical system design and construction.

Chapter 3

QPTM System Simulation and Analysis

3.1 Analysis of QPTM Simulation Models

Simulation of the QPTM system was performed using the program MicroCap 6™ [40], a comprehensive SPICE-based schematic-entry simulator capable of both systems- and circuit-level simulation, as well as any combination of the two. The simulator has been found useful not only for design but also for investigation of observed characteristics when testing a prototype.

3.1.1 BEHAVIOURAL MACROMODELS

Macromodels (macros) have been used to describe the behaviour of many of the functional blocks in the system. They have generally been defined by internal functions or circuitry, or a combination of these, and have also been nested where required. In several instances, use has been made of the facility to pass parameters to the macro from a higher level in the system. A description of the special macros created for the QPTM system is given in Appendix 2.

3.1.2 QPTM ANALYSIS FOR LINEAR PA

The QPTM system shown diagrammatically in Figure 2.6 was developed as a system model with appropriate behaviour assigned to each functional block. The resulting schematic diagram is shown in Figure 3.1. In this figure, a reference triangle wave 'Ref' of 250mV amplitude and 40MHz repetition frequency is fed to one input of each of two comparators 'Comp', the other inputs of which are respectively supplied with I and Q baseband signals that are represented by 'Fsin' and 'Fcos'. The corresponding signal sources, 'BBI' and 'BBQ' are, for convenience, similar to those used in the Matlab simulations of Chapter 2 and are, respectively, 2MHz and 5MHz sinusoidal waves of 240mV amplitude. This is just under the triangle-wave amplitude to avoid saturation of the conversion process. The requirement for the reference frequency to be more than twice the modulating frequency also meets the slope constraint for a symmetrical triangle wave. The comparators are modelled, in simplified form, on the actual high-speed devices intended to be used for prototyping (see par. A2.2). The comparator outputs 'I_in' and 'Q_in' are rectangular pulses at the reference frequency and of widths proportional to the

instantaneous magnitudes of the baseband signals. These PWM signals are fed to the I and Q modulation inputs of the 'Q-Mod' block, whilst the 'LO' input of this block is fed with a carrier-frequency sine-wave, typically 500MHz. The 'Q-Mod' block is modelled on a direct-quadrature modulator integrated circuit (see par. A2.4). The output 'Qm' of the modulator is amplified linearly by a simple scalar to a representative transmitter signal level. The resulting signal 'Pa' is passed through a narrowband Chebyshev filter '500M-Chb' (see par. A2.8) and appears as the signal 'Tx' across the 50 ohm dummy load, in place of an antenna.

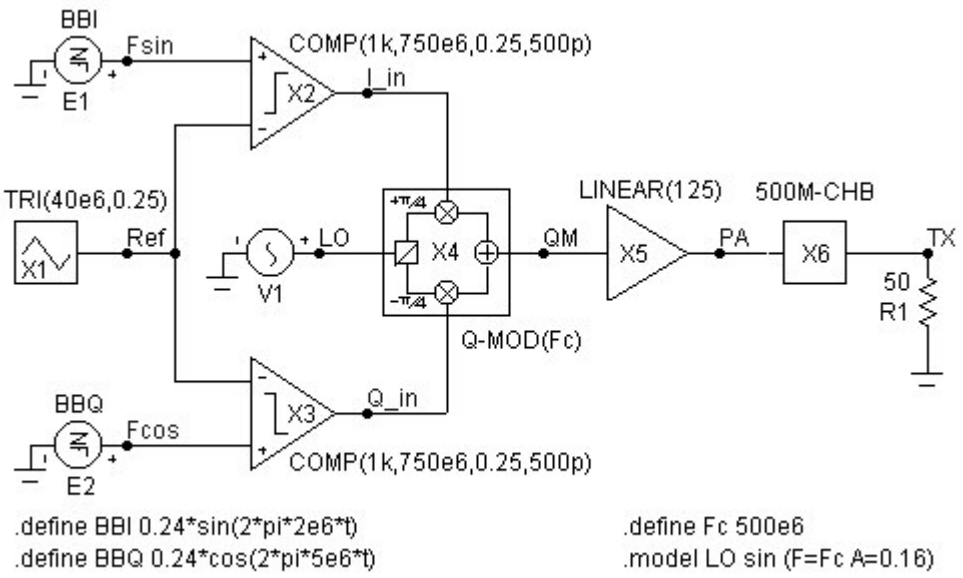

Figure 3.1 - QPTM-Lin.cir - linear QPTM system with I and Q baseband

A transient analysis plot of the system in Figure 3.1 is shown in Figure 3.2. The PWM process for the I and Q channels is clearly shown by superposition of the corresponding input signals and the reference triangle wave. The lower trace shows the envelope of the transmitted signal 'TX' after passing through the narrowband filter.

Figure 3.3 shows the spectrum of the signal 'PA' prior to the narrowband filtering and this matches very closely the spectral plot in Figure 2.5. The 2MHz and 5MHz tones appear as double-sideband modulation around 500MHz, with the carrier being completely suppressed. The first reference frequency components appear 40MHz either side of the 500MHz carrier frequency, each with double sidebands corresponding to second harmonics of the baseband signals. The virtually clear bands between these components and the pass-band signals each have a width equal to the reference frequency minus three times the highest modulating baseband frequency. These define the transition bands for specification of the ensuing bandpass filter, although the

amplitude of the reference-frequency components, generally almost equal to, or greater than, that of the wanted passband signals, is a major determining factor in any such specification.

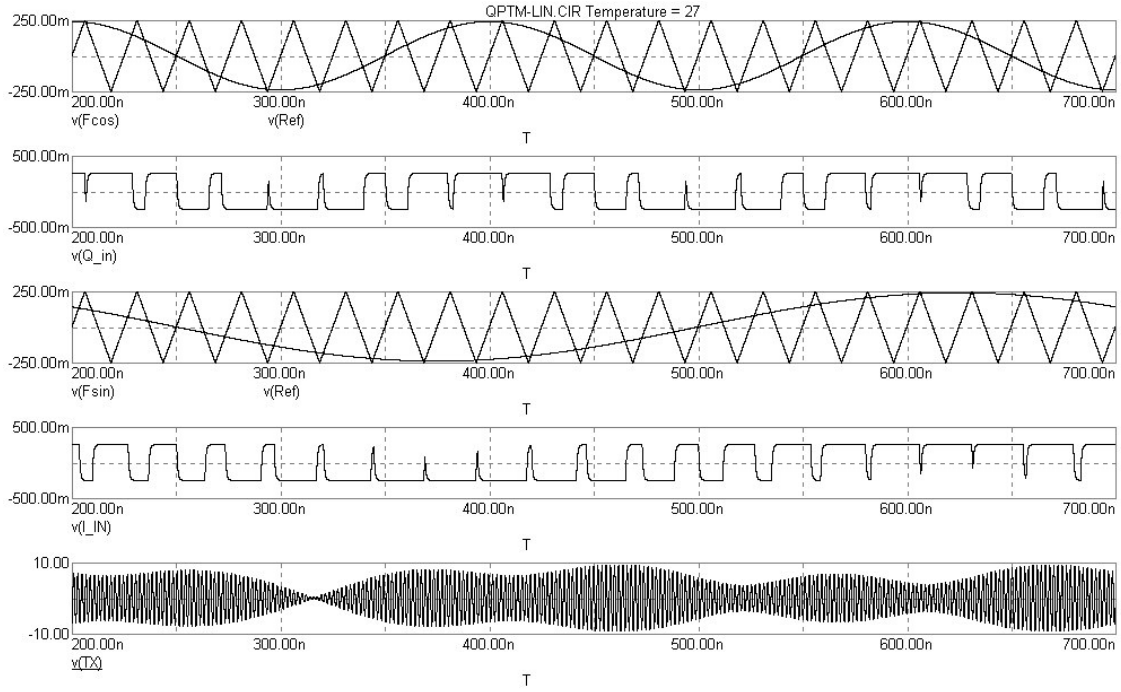

Figure 3.2 - Transient analysis of QPTM-Lin.cir with 2MHz and 5MHz inputs

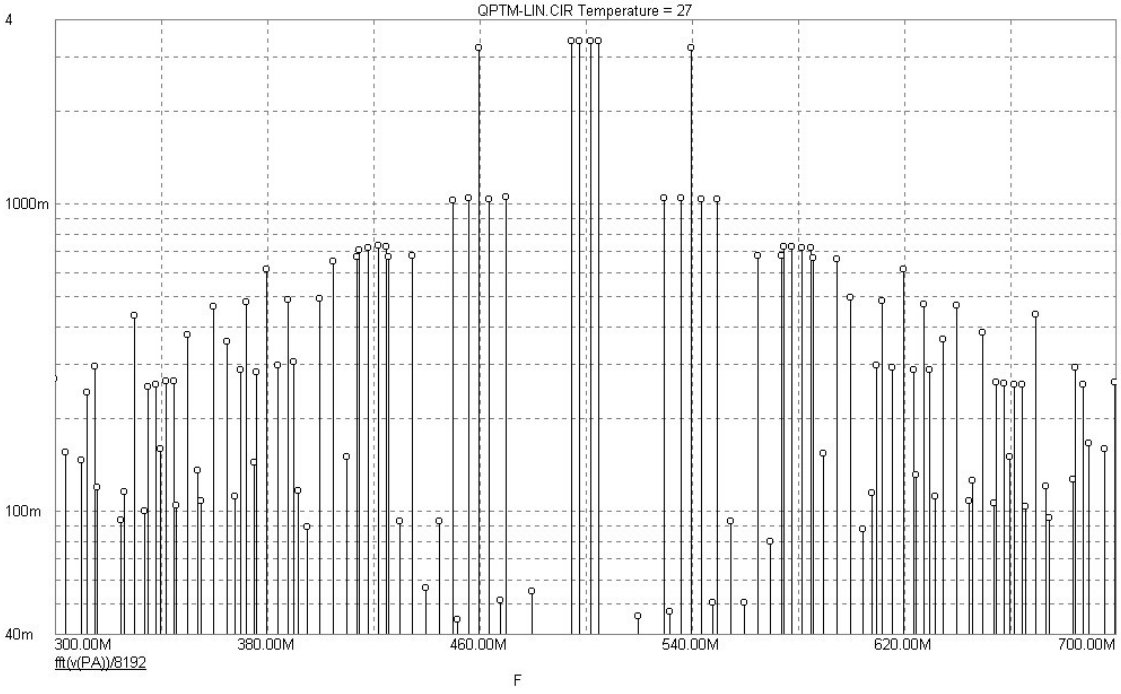

Figure 3.3 - PA output spectrum of QPTM-Lin.cir with 2MHz and 5MHz inputs

Figure 3.4 shows the transmitted spectrum, after passing through the 10th-order Chebyshev filter '500M-Chb'. The passband response appears flat to within a small fraction of a dB, whilst out-of-band components are below about –40dBc.

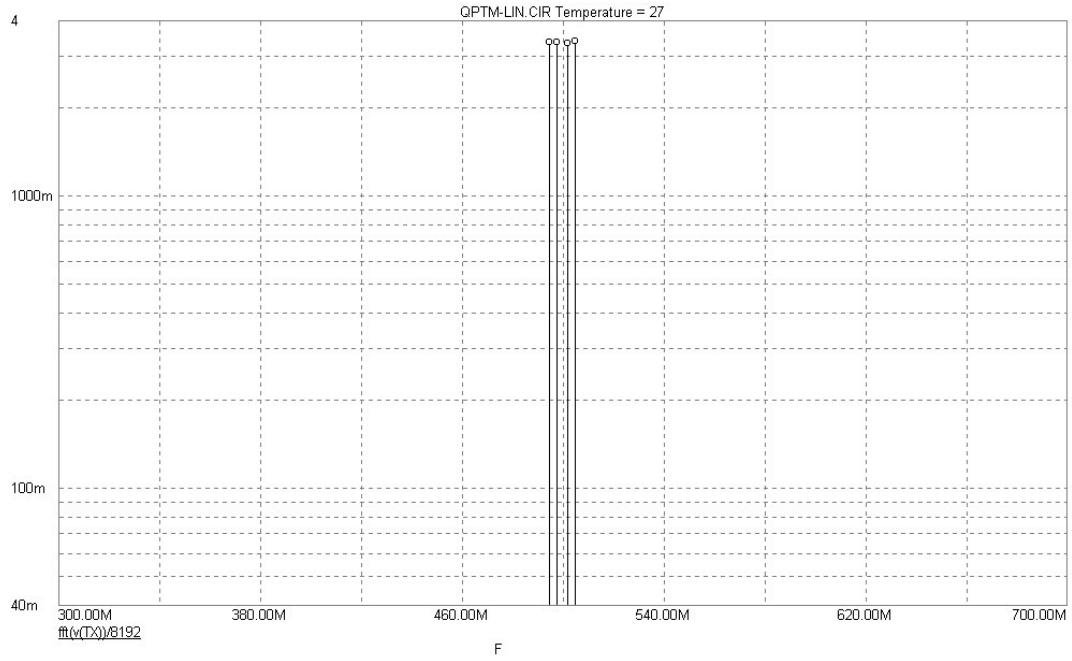

Figure 3.4 - Filtered TX spectrum of QPTM-Lin.cir with 2MHz and 5MHz inputs

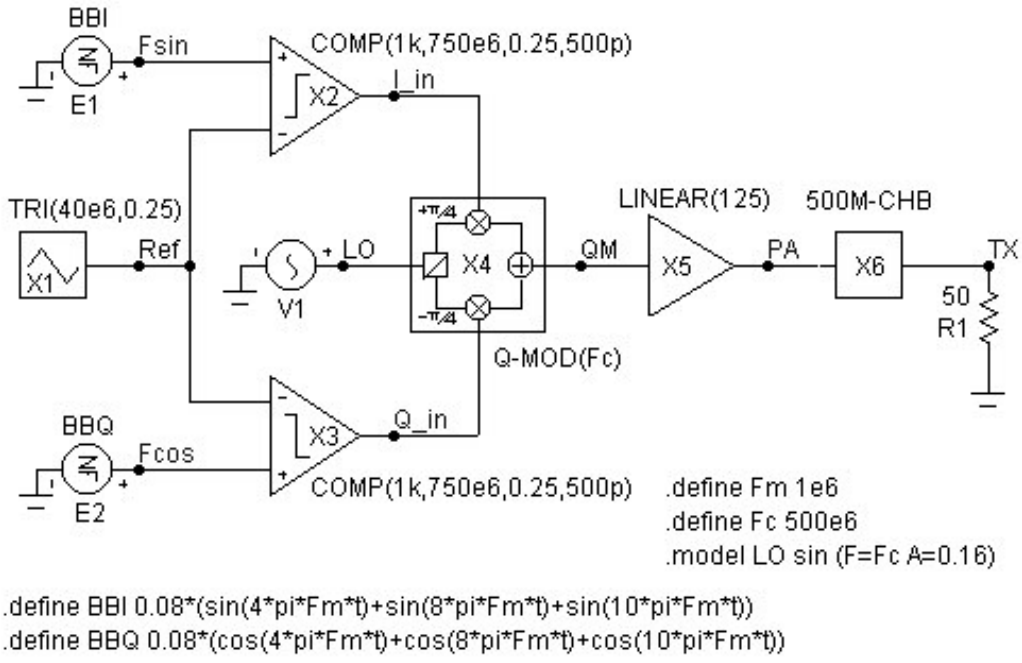

Figure 3.5 - QPTM-SSB.cir - linear QPTM system with SSB modulation

One way of testing both phase and amplitude distortion of the baseband signals by the QPTM process is the use of single-sideband modulation. The result of any such distortion would be the presence of baseband frequency components in the alternate sideband of the carrier. Figure 3.5 shows the composite simulation signal inputs used, comprising the sine and cosine components of 2, 4 and 5MHz frequencies. These were chosen so that any intermodulation components would also be clearly evident. However, the spectral plot in Figure 3.6 shows that any such distortion components would be low, at least 46dB below the wanted signals, in an ideal system.

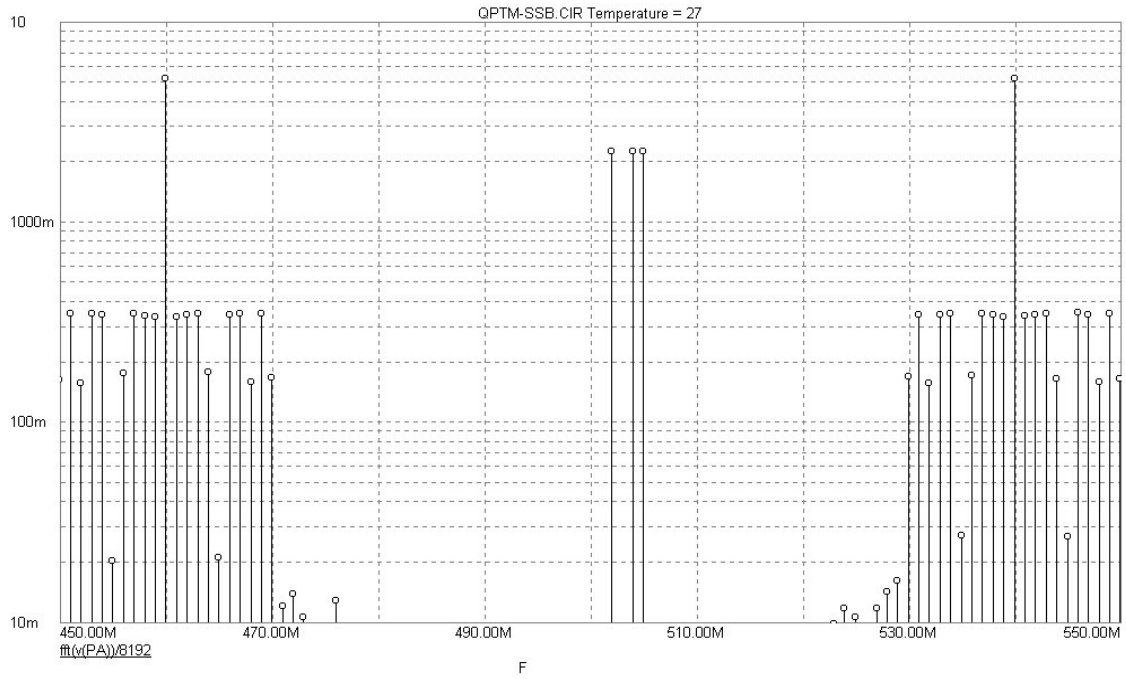

Figure 3.6 - PA output spectrum of linear QPTM system with SSB modulation

3.1.3 QPTM ANALYSIS FOR CLASS-D PA

All of the analyses in the preceding sections of this chapter have dealt with linear outputs of the modulation process. One of the objects of the present investigation is to examine the possibility of using non-linear, or switching, PA technology. Because of the wide bandwidth occupied by the unfiltered QPTM signal, there is the potential for significant interfering frequency components to be generated by a non-linear amplifier. The effect of this has been examined by simply substituting a Class-D macro in place of the linear PA block in the circuit of Figure 3.5. The spectral plot so obtained is shown in Figure 3.7(a) and this does display some baseband components in the alternate, lower, sideband, the largest being about 25dB below the wanted upper-sideband signals. A 3MHz intermodulation component at about –30dB is also evident. These spurious harmonics are attributed to the fact that, although the ideal QPTM signal is constant-envelope, it is not strictly so when the risetime of the PWM switching device or the

quadrature modulator input stage is limited. This presents no problem when followed by linear amplification and filtering but the "infinite clipping" of an ideal Class-D stage behaves as a distortion process. A much faster, but impractical, risetime results in the plot of Figure 3.7(b).

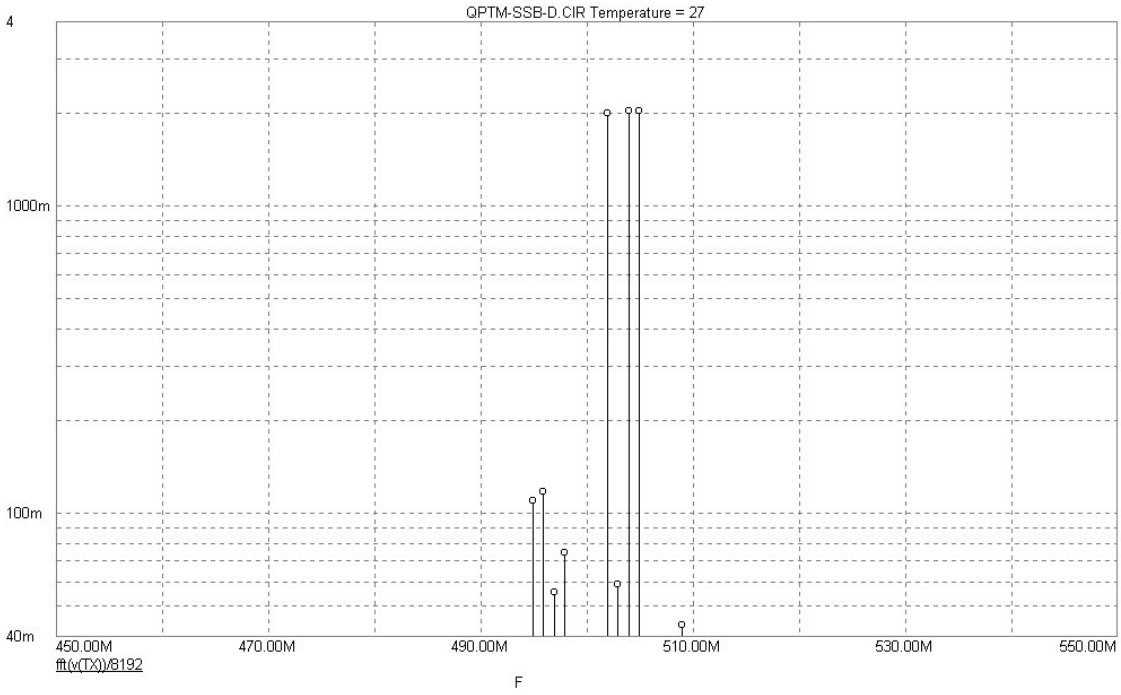

(a) Pulse-width modulator bandwidth limited to 400MHz

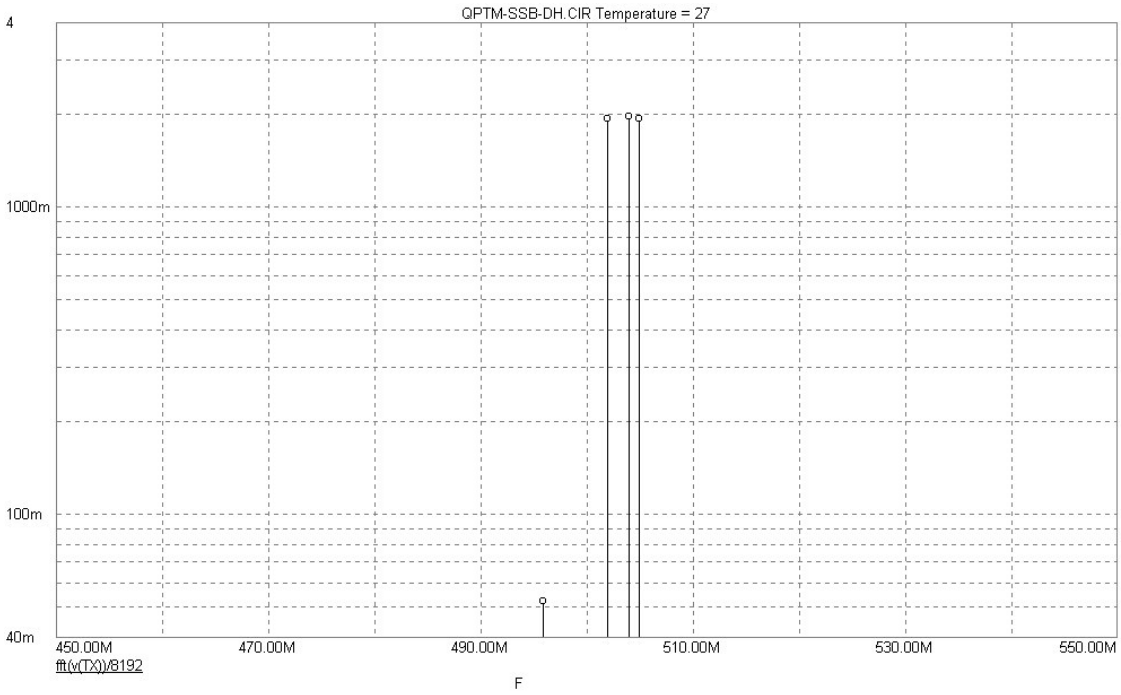

(b) Pulse-width modulator bandwidth extended to 8GHz

Figure 3.7 - Filtered TX spectrum of Class-D QPTM system with SSB modulation

3.1.4 SUPPRESSED-CARRIER QPTM

The presence of strong reference-frequency components in the QPTM signal is presenting as a limiting factor in the system dynamic range and power efficiency. Moreover, it is a determining factor in the required output filter complexity. Consequently, we have conducted a preliminary investigation of a variation of the process, which we call Suppressed-Carrier QPTM. This employs a three-state modulation signal at the quadrature modulator input to eliminate reference-frequency components from the output signal, although outer sidebands are still present in the spectrum. A drawback is that if the QPTM output of the modulator is linearly summed, a three-level signal results, rather than constant-envelope. This could be dealt with using a linear amplifier or an efficient Class-S technique [26], for example, or by combining the I- and Q-modulated carriers after amplification by separate PA stages. Alternatively, the I- and Q-modulated carriers may be generated in alternate time slots and combined by time division multiplexing. The PA would then have only a two-level signal to handle. Although there is no indicated preference at this stage, the separate-PA approach has been simulated, as an example system, and shown in Figure 3.8. A modified form of the Chebyshev bandpass filter macro is employed as a combiner, with linear PA stages, for system simulation purposes only. Due regard would have to be paid to the quadrature signal phasing, particularly switching currents, in a practical system that used non-linear power amplifiers.

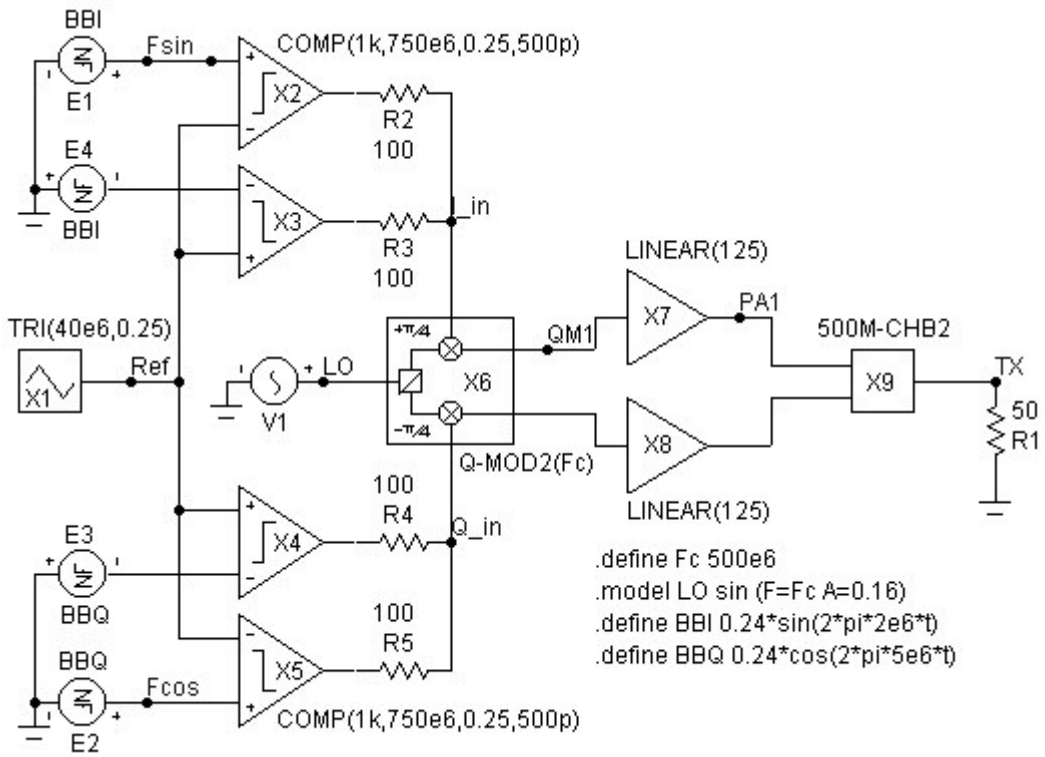

Figure 3.8 - Suppressed-carrier QPTM system

Figure 3.9 shows the characteristic I and Q PWM waveforms applied to the quadrature modulator, for the respective 2MHz and 5MHz baseband inputs. The pulse risetimes shown are realistic for the type of comparator being used for this function in the subsequent prototyping (see Chapter 4).

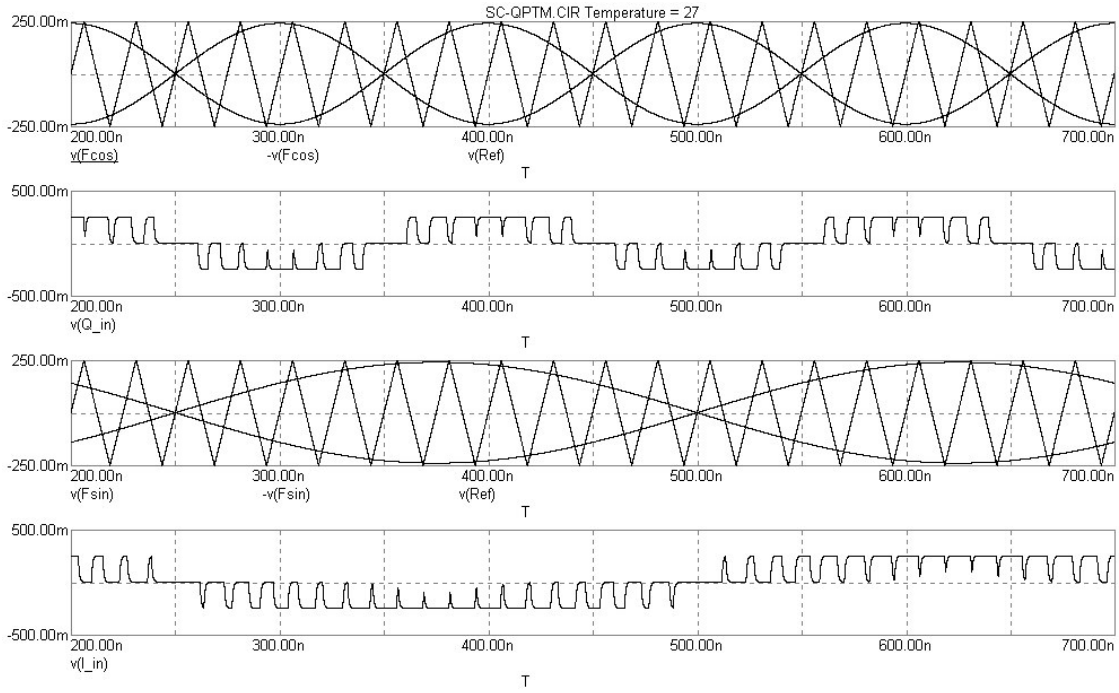

Figure 3.9 - Suppressed-carrier PWM waveforms relating to Figure 3.8

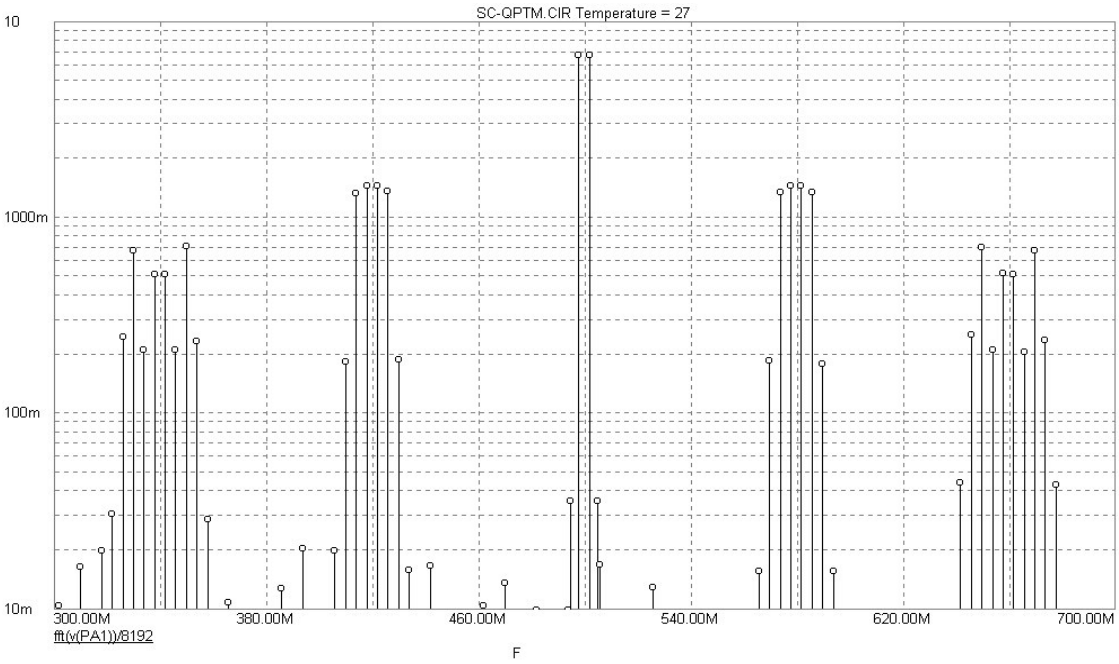

Figure 3.10 - Channel 1 PA output spectrum for suppressed-carrier QPTM

Figure 3.10 shows the I-channel PA output spectrum, with 2MHz modulating tones. The low-level 5MHz components result from currents cross-coupled through the combiner from the Q channel. The important feature of this plot is the absence of sidebands around the reference frequency offset of ±40MHz from carrier. Figure 3.11 shows the composite transmitter signal after filtering. The close-in harmonics are below –40dB with respect to the wanted signals and result from PWM spectral images referenced to twice the carrier frequency (Figure 3.12).

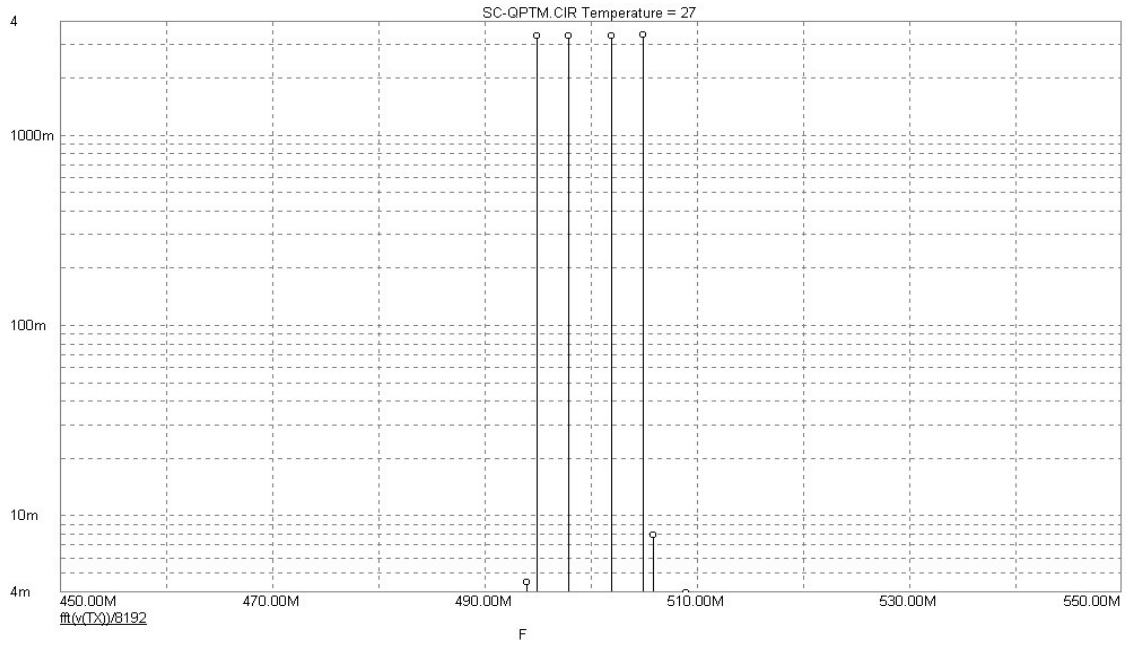

Figure 3.11 - Filtered TX spectrum for suppressed-carrier QPTM

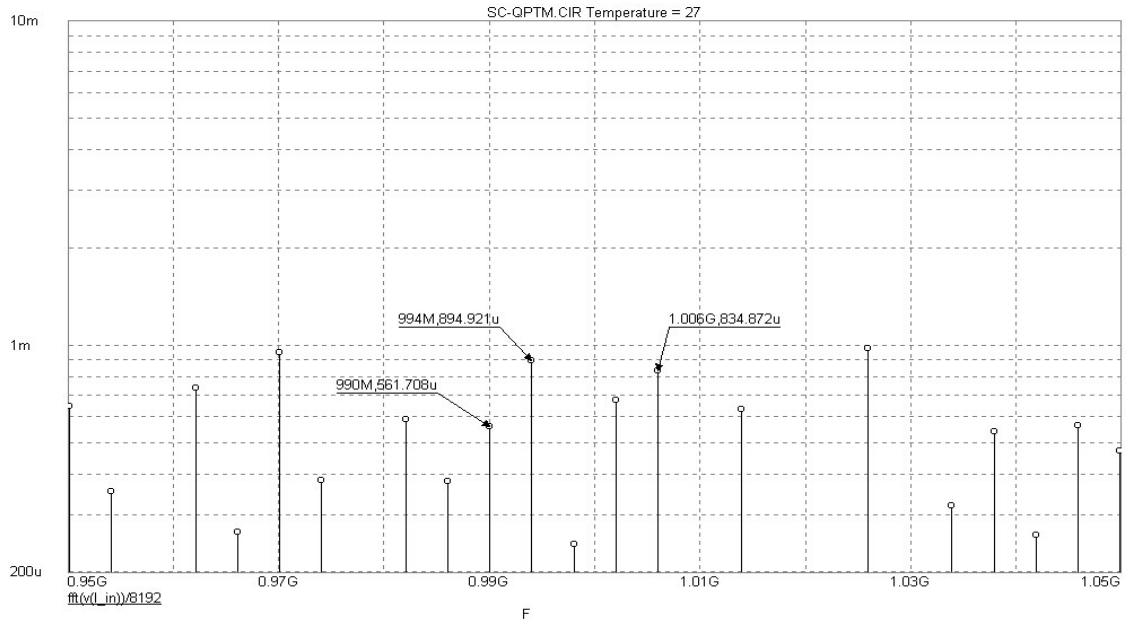

Figure 3.12 - SC-QPTM PWM image frequencies for 2MHz baseband input

3.2 Discussion of Analysis Results

Good agreement has been obtained between the MicroCap and earlier Matlab simulation plots. The two-tone QPTM modulation spectrum for the MicroCap system model with linear PA, shown in Figure 3.3, exhibits pactically the same characteristics as the Matlab plot of Figure 2.5, using similar test signals. There are no apparent spurious components within the wanted passband. A more critical test for distortion, using SSB modulation, reveals no anomalies in the spectral plot of Figure 3.6. The most significant distortion products are below –46dB with respect to the wanted passband signal components.

When a Class-D PA model was substituted in the system, some baseband components were generated in the alternate, lower, sideband, as shown in the narrowband-filtered spectral plot of Figure 3.7(a). The largest component is about 25dB below the wanted upper-sideband signals. A 3MHz intermodulation component at about –30dB is also evident. The principal cause of the distortion was found to be the limited PWM bandwidth. The plot of Figure 3.7(b), with much wider bandwidth, confirms the reduction in harmonics. However, a difficult custom modulator integrated circuit design would have to be undertaken to achieve such bandwidth.

The most significant problem identified with the QPTM technique has been the presence of dominating sidebands related to the reference triangle-wave frequency. A possible solution to the reference spectrum problem, Suppressed-Carrier QPTM, has been modelled and simulated. In this model, the I- and Q-channel modulation outputs have been kept separate to allow for combination after the PA stage, since the combined signal has three levels, including zero, instead of being constant envelope. The modulated carrier signals could still be combined linearly as before if an efficient PA is used with linearity correction at the two non-zero levels. This would be easier to design than one required to handle an infinitely-variable level amplitude-modulated signal. Alternatively, time division multiplexing could be used for combining the I- and Q-modulated carriers to generate just a two-level signal. This method requires two quadrature-phased reference signals but the design of these circuits and the PA may be less difficult.

Figure 3.10 shows the output of the I channel (2MHz baseband signal). The most significant spurious components are seen to be about 45dB below the wanted sideband signals. Figure 3.11 shows the composite transmitted signal after filtering.

3.3 Summary of QPTM System Simulation and Analysis

This chapter has described the simulation and analysis of a model QPTM system that had parameters chosen to represent those to be used in a practical, experimental prototype that would

be reasonably representative of some real-life applications. The sampling reference frequency of 40MHz and carrier frequency of 500MHz are consistent with this and present a significant challenge for a practical design task. Thus, the data obtained from the simulation analyses is of great value in generating expected performance indications for the prototype design following.

Chapter 4

An Experimental QPTM System

4.1 QPTM Prototype Design

The prototype system comprises two distinct signal-path sections and a power supply section. For the power supplies, standard integrated circuit voltage regulators have been used for the positive supplies and a switched-capacitor voltage inverter for a negative bias supply, required particularly for the GaAs FETs in the PA. A policy was adopted for the prototype of providing separate regulation for each part of the system, both to avoid interaction and to facilitate the separate testing of individual circuit blocks. The signal circuits are divided into the modulator and the Class-D PA subsystems.

4.1.1 MODULATOR

The modulator section comprises the reference triangle-wave generator, two identical high-speed differential comparators and the direct quadrature modulator. Only the first of these requires transistor-level design as the other functions can be substantially implemented with off-the-shelf parts, albeit they are parts with state-of-the-art performance.

4.1.1.1 Reference Generator Design and Simulation

Two essential performance requirements may be stated for the reference generator. The first is that the linearity of the triangle-wave slopes shall be sufficiently good to satisfy the baseband distortion requirements of the host system, since this defines the actual transfer characteristic of the modulator, and the second is that the waveform repetition frequency shall be high enough to permit bandpass filtering of the PA output to be accomplished by a low-complexity filter, with associated low insertion loss. Typically, these requirements are in mutual conflict as precision linear, or even digital, circuit techniques that may be applied to low-frequency signals are generally not easily usable at very high frequencies because of the effects of circuit parasitics. Many OFDM applications have channel bandwidths in the 1-20MHz range, so that, to determine feasibility, a useful target for the

reference generator frequency may be 40MHz. A linearity of ±1% would be compatible with 256-QAM single-carrier applications. Sufficient dynamic range is required to handle signals with over 4dB peak-to-average power ratio (see Chapter 1) and preferably at least 8-10dB for wider application. A circuit technology that has been found to deliver both good linearity and high frequency of operation is the emitter-coupled oscillator, or multivibrator. As usually implemented at lower frequencies, this circuit only needs one cross-coupled collector-base feedback path but, to achieve symmetry at high frequency we have designed a balanced feedback and biasing arrangement. The circuit, as simulated, is shown in Figure 4.1. Here, transistors Q1 and Q2 are the switching devices whilst Q3 and Q4 are matched current sources. The frequency is a function of the RC time-constant of C1 with R1 and R2, modified slightly by the bias dividers formed by R4, R7 and R5, R6, as well as a number of parasitics. C2 and C3 are 'speed-up' capacitors to neutralise the effective base input capacitance of Q1 and Q2. For these, and the timing capacitor C1, parasitic series inductance and equivalent series resistance (esr) have been included in the model.

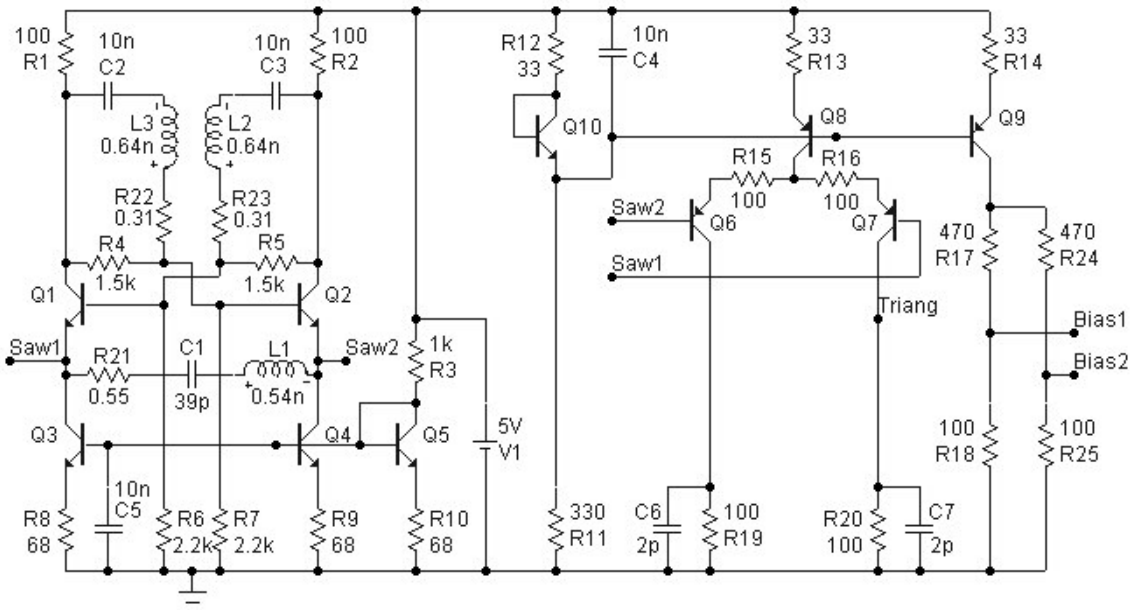

Figure 4.1 - Reference triangle-wave generator simulation circuit

The emitter-coupled oscillator is normally used to generate square waves and does not have a triangle-wave output. It does, however, have two sawtooth waveforms accessible at the emitters of Q1 and Q2 which, when differenced, yield a good triangle waveform, with cancellation of most of the switching aberrations present on the individual sawtooth signals. This action is performed by the differential amplifier comprising Q6 and Q7, the

collector outputs of which are terminated in 100Ω resistors R19 and R20 and feed the two PWM comparators that follow. Two dc outputs 'Bias1' and 'Bias2' track the dc levels of the triangle-wave outputs and are used to bias the baseband signal inputs of the comparators. The simplicity of this circuit, combined with the use of 6-8GHz f_T transistor arrays, has resulted in good linearity at the design frequency of approximately 40MHz. The integral non-linearity between 10 and 90% of the triangular waveform shown in Figure 4.2 is shown by cursor measurements to be 0.29%. (The deviation from a "best-fit" straight line would be half of this).

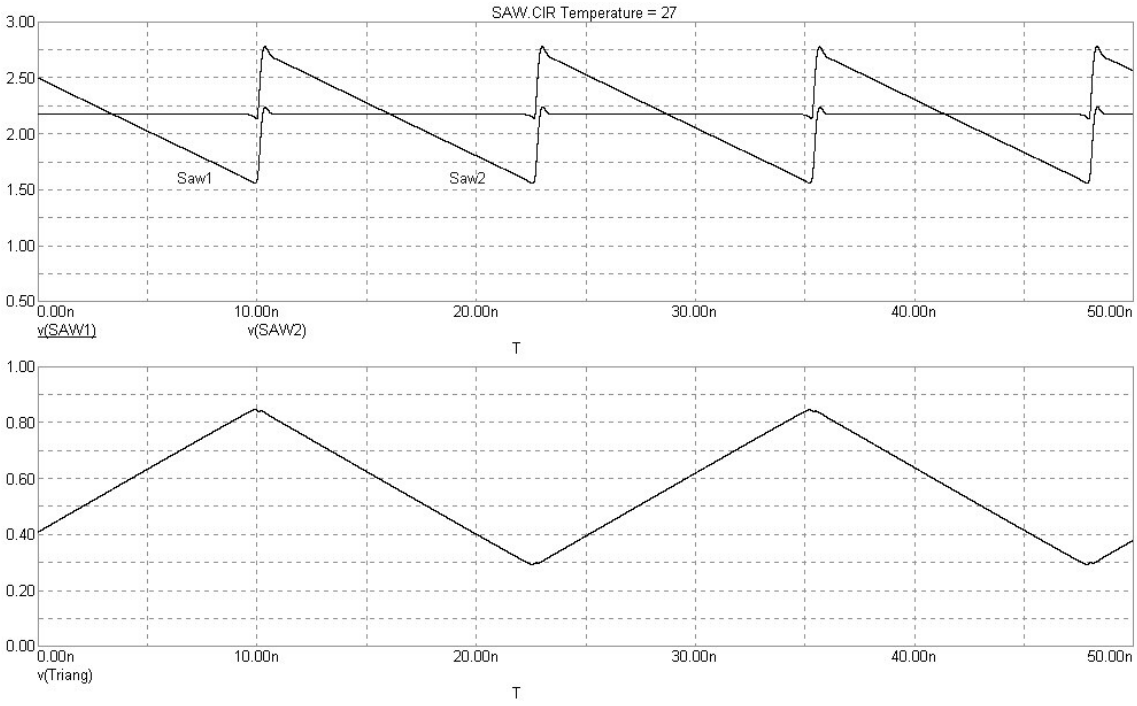

Figure 4.2 - Transient analysis of reference triangle-wave generator

4.1.1.2 PWM Comparators and Quadrature Modulator

The arrangement of the reference generator, dual comparators and quadrature modulator is shown in Figure 4.3. I and Q baseband signals are fed in via 50Ω microstrip lines and the comparator outputs are of the differential PECL type, fed via doubly-terminated differential 100Ω striplines to the 'BBI' and 'BBQ' inputs of the direct quadrature modulator to ensure the preservation of accurate rectangular waveforms. A single-ended carrier signal is injected at the 'LO_IN' port, where it is transformed by a balun to drive the 'LO' input of the quadrature modulator via a differential stripline. The use of differential lines is helpful in reducing cross-coupling, particularly of switching signals.

Similarly, a differential microstrip line transports the modulated carrier output to the following PA subsystem.

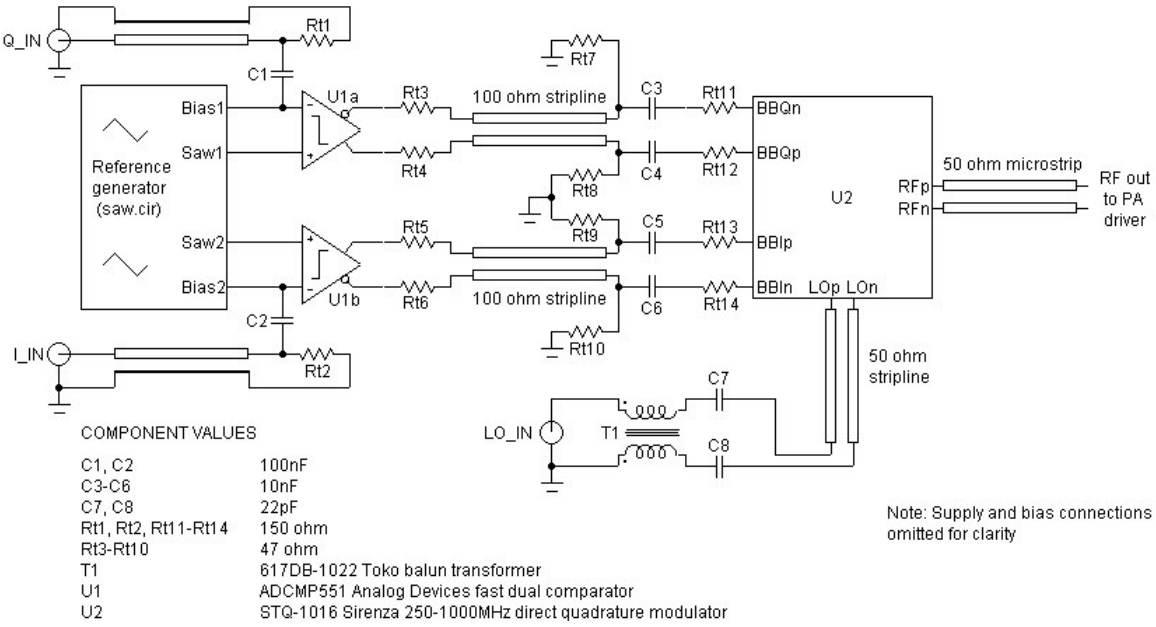

Figure 4.3 - Simplified diagram of quadrature modulation circuit

4.1.2 CLASS-D POWER AMPLIFIER

A Class-D switching amplifier potentially offers the highest efficiency among the various PA topologies [19][39]. In an ideal, loss-less switching circuit the efficiency is 100% and a figure of over 90% is readily achievable with real components at audio frequencies. A two-switch totem-pole or four-switch bridge arrangement is common for audio solutions. However, at UHF the losses are much higher, mainly because of switching times, and a balanced push-pull topology is likely to be more suitable because of the problems that would be encountered in attempting to provide a suitable drive signal for the high-side switch in a totem-pole arrangement. A further switching-mode option is the choice between voltage-mode and current-mode switching. The former is tuned to give a sinusoidal output current and the latter a sinusoidal output voltage. We have modelled both types.

4.1.2.1 Transient Simulation of Output and Driver System

For the prototype it was decided to target an output power level of approximately 1W, providing a convenient measurement level and reasonably simple construction without the need for heatsinks on any power devices. The output switching device chosen was the MicroWave Technology MWT-17 GaAs FET, for which a SPICE (Triquint) model was available although, because of availability, the prototype was eventually constructed using

the virtually identical Mitsubishi Semiconductor MGF 0913A device. The GaAs FET is a microwave amplifier with very low feedback capacitance, essential for high switching speeds. The 'on' resistance is also important in the switch and is characteristically around two ohms, although it is not specified by the manufacturers as the device is intended for linear applications. The gate drive presents the greatest difficulty as, ideally, a square-wave of about 3V peak-to-peak is required, at the lowest practicable impedance so that the effect of feedback capacitance is minimised. In this prototype the emphasis has been placed on obtaining predictable drive waveforms and being able to probe these easily and make accurate measurements. To this end, the FET gates are fed via doubly-terminated transmission lines from broadband amplifiers, although this consumes extra power.

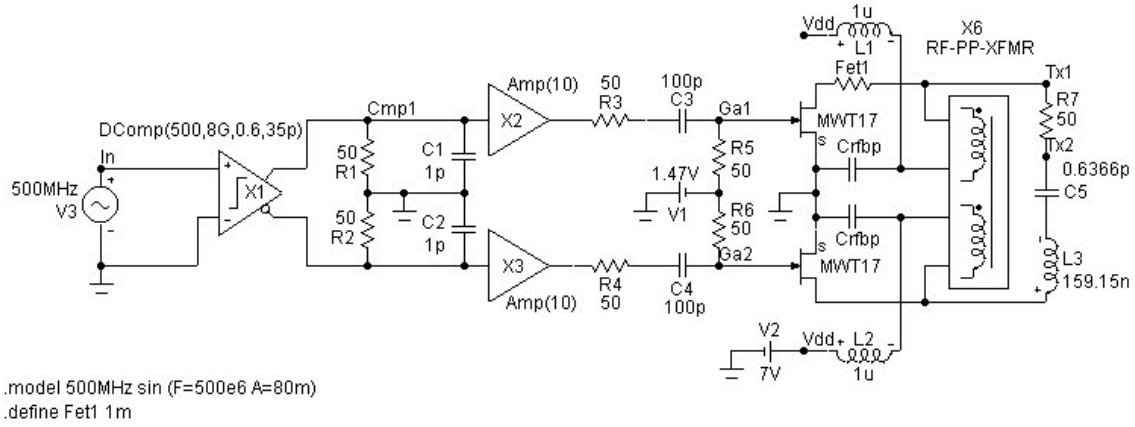

Figure 4.4 - Simulation model for voltage-switching Class-D PA

The circuit arrangement chosen for the voltage-switching (VS) model is shown in Figure 4.4, in a simplified form for simulation. For the gate drive, a square wave is generated by the ultra-fast comparator model X1, which is programmed with input bandwidth and output risetime parameters from the datasheet of the Analog Devices ADCMP573, followed by another band limiter, R1-C1, representing the 5GHz bandwidth of a pair of Sirenza SBB-5089 amplifiers that, in the prototype, feed the approximately-square waveform differentially to the gates of the two GaAs FETs. 50Ω lines at the latter interface present a 25Ω source to each FET gate and dc gate bias is set at -1.47V, the nominal gate cut-off voltage. This may not be optimal in terms of output switching losses but is considered to be a good starting point. Coupling between the two FET drains is provided by the push-pull transformer macro X6. The usual third winding, to give a single-ended output, has been omitted to avoid complicating the interpretation of results and the 50Ω load R7 is applied differentially. As a result, a conventional 1:1 balun may be used in an experimental circuit. The element Crfbp comprises a set of three chip

capacitors in parallel, chosen with regard to self-resonant frequency and esr to maintain a low series impedance across the frequency band of interest [40]. Components L3-C5 tune the load (with Q of 10) to the carrier frequency. Usually the VS topology is shown with a single bias inductor feeding the center tap of the output transformer primary but we have used two inductors, L1 and L2, to supply the centre connections of a split primary, as this reflects our practical prototype and allows for individual current-limiting feedback to be applied around each FET, primarily as a safety measure during experimentation. The RF-PP-XFMR macro, although lossless, is realistic in terms of parasitic capacitance and leakage inductance. The effects of these parasitics are evident in the transient plots of Figures 4.5 and 4.6.

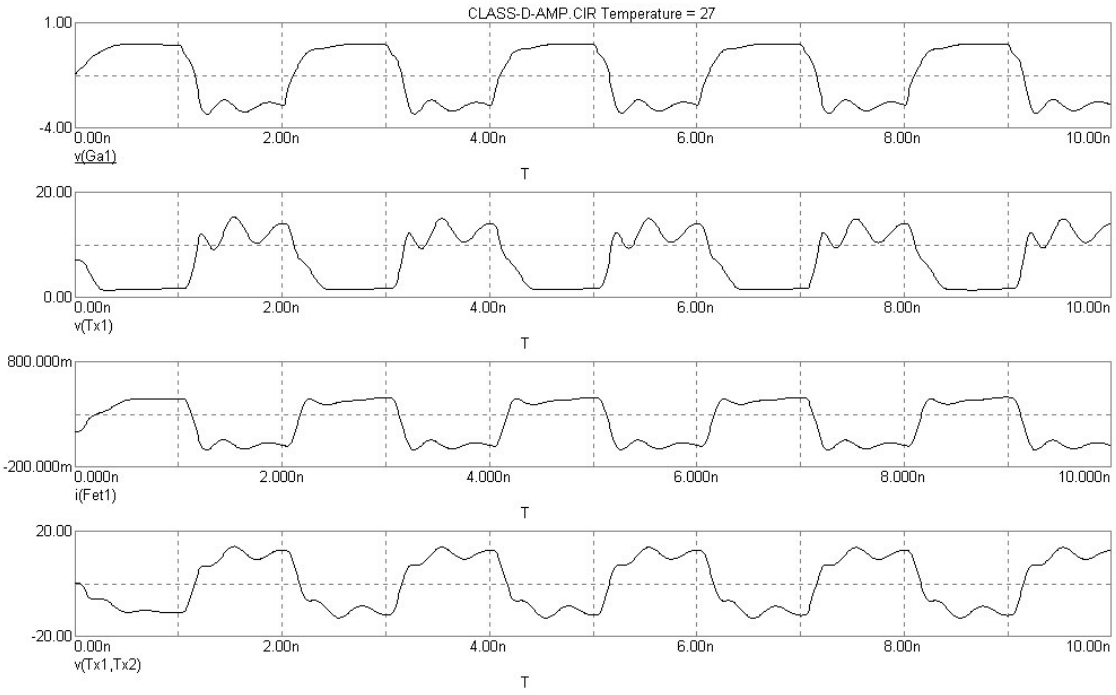

Figure 4.5 - Transient waveforms for voltage-switching Class-D PA of Figure 4.4 (untuned load, L3 and C4 shorted)

Two configurations of this model have been simulated, one with the load untuned and the other with it tuned. In the first case, which is not a practical one, the load provides damping of all harmonics, as shown in Figure 4.5. The ringing is caused by the transformer parasitics. One may clearly see that the gate voltage risetime (top trace) is responsible for slow turn-on of the FET (2^{nd} trace) and this, in turn results in FET heat dissipation during the drain-current rise and fall times (3^{rd} trace).

In the second configuration, with L3 and C4 in circuit, the harmonic currents encounter a high, inductive load impedance, resulting in the waveforms of Figure 4.6. The lightly-

damped harmonic peaks are high enough to cause damage to the output FETs if they occurred in real life. Also of interest is the magnitude of the harmonic feedback to the gate (trace 1). However the efficiency of this stage, relating load power to dc input, and remembering that the transformer model is lossless, is still quite high at 78.8%. Output power is 1.44W.

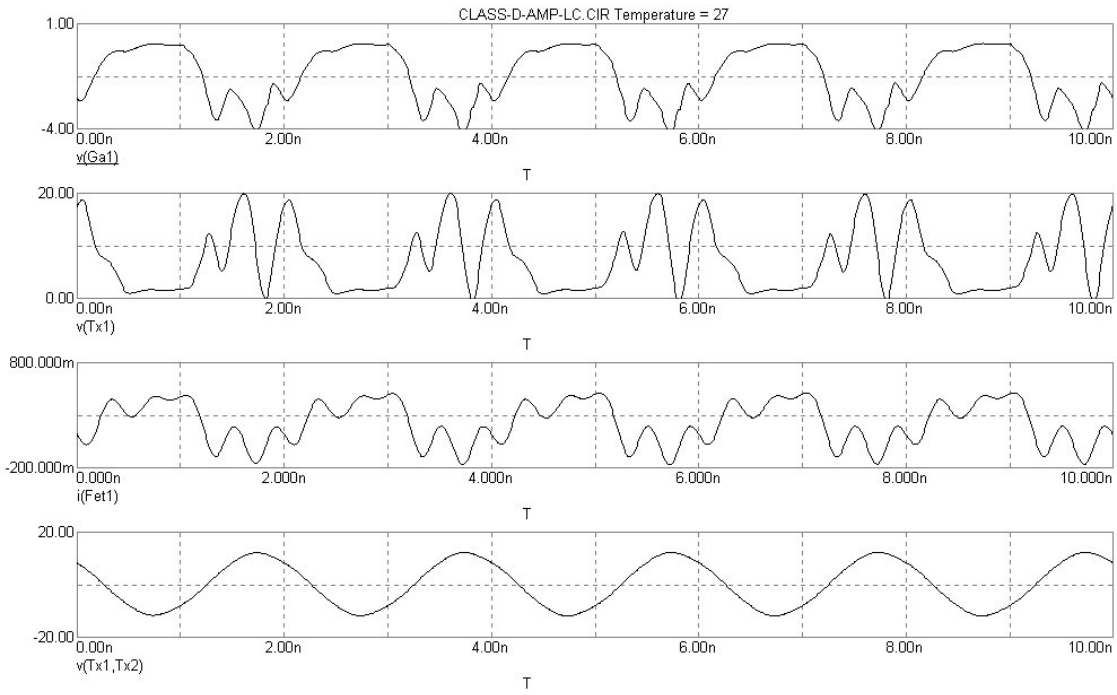

Figure 4.6 - Transient waveforms for voltage-switching Class-D PA of Figure 4.4 (load tuned to 500MHz by L3 and C4, Q = 10)

The current-switching (CS) Class-D amplifier is represented by the model in Figure 4.7. This is similar to the VS model except that the output FET drain bias is fed via the RF chokes L1 and L2 directly to the drains. C5 and C6 are dc blocking capacitors, coupling the signal voltage through a transmission-line balun to the load. The transmission line is modelled here with ideal components in the absence, at this stage, of a model for the broadside-coupled tapered stripline balun that has been designed into the prototype. Tuning of the CS amplifier is with a parallel-resonant circuit, L3-C7, having a nominal Q of 10, as in the VS case.

A first simulation was performed with the elements L3 and C7 disconnected, so that switching waveforms would be available for direct comparison with oscilloscope

waveforms captured from the prototype. The latter would not be immediately available with a tuned circuit in place as design and construction of a practical tuned circuit was considered to be a non-trivial project in itself.

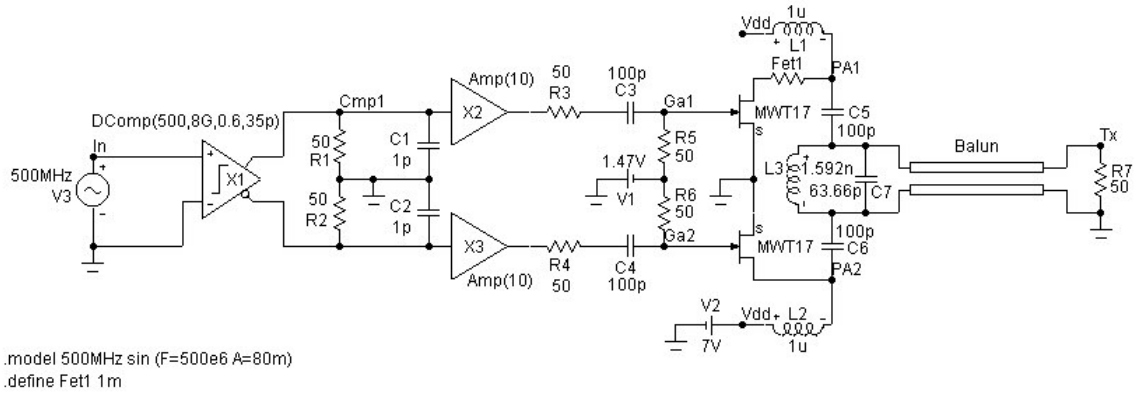

Figure 4.7 - Simulation model for current-switching Class-D PA

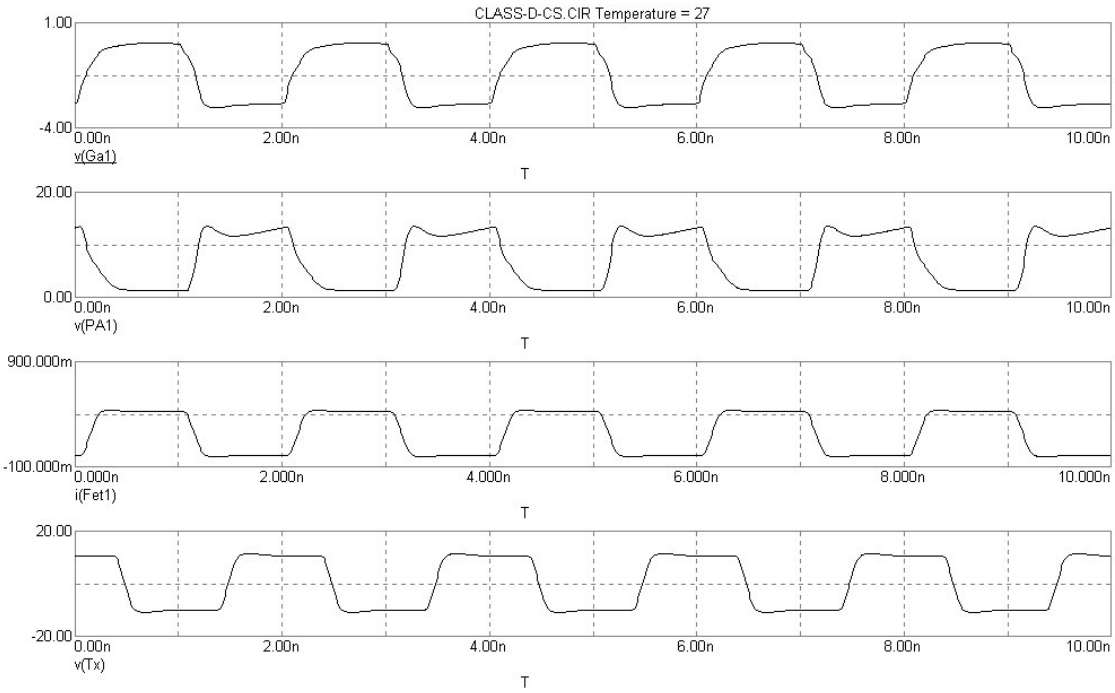

Figure 4.8 - Transient waveforms for current-switching Class-D PA of Figure 4.7 (untuned load, L3 and C7 omitted)

Transient waveform plots for the CS Class-D amplifier of Figure 4.7, without the output resonator, are shown in Figure 4.8. These waveforms exhibit no ringing because the terminated transmission line balun appears as a resistive load to the FETs. The effect of gate voltage risetime on the drain voltage swing is clearly evident in trace 2.

Figure 4.9 shows the waveforms for the same circuit with the resonator L3-C7 in circuit. The first, obvious effect is that the drain voltage (trace 2) approximates a half sinewave and the output is, as expected, sinusoidal. It is interesting to observe that the gate drive waveform (trace 1) exhibits sharper rise times, owing to the reduced drain-gate feedback with the slow-rising half-sine drain waveform, and the FET drain current has faster transitions. The output power, at 1.99W, is higher than for the VS topology but this causes an increased I^2R loss in the FETs, reducing the efficiency to 61.4%.

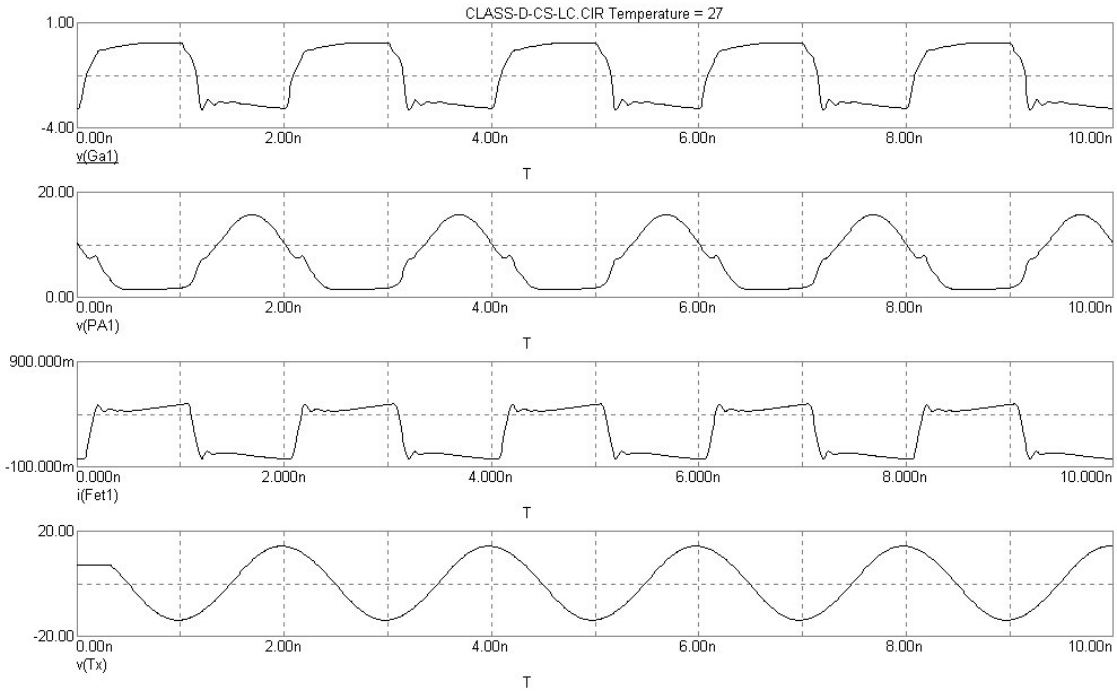

Figure 4.9 - Transient waveforms for current-switching Class-D PA of Figure 4.7 (load tuned to 500MHz by L3 and C7, Q = 10)

4.1.2.2 Practical Realisation of Class-D PA

The development of the simulation model of Figure 4.7 into a design for a practical working prototype is shown in Figure 4.10, for the signal path. The main difference is the inclusion of the output FET drain-current sensing and the control for the FET gate bias. Potentiometers for Q1 and Q2 bias are each set so that the corresponding FET is just starting to conduct with no carrier signal applied. A shutdown circuit is included to inhibit the +7V FET drain supply until the –5V gate bias supply has started up. This provision is essential for GaAs FETs to avoid the flow of destructive drain currents on power-up.

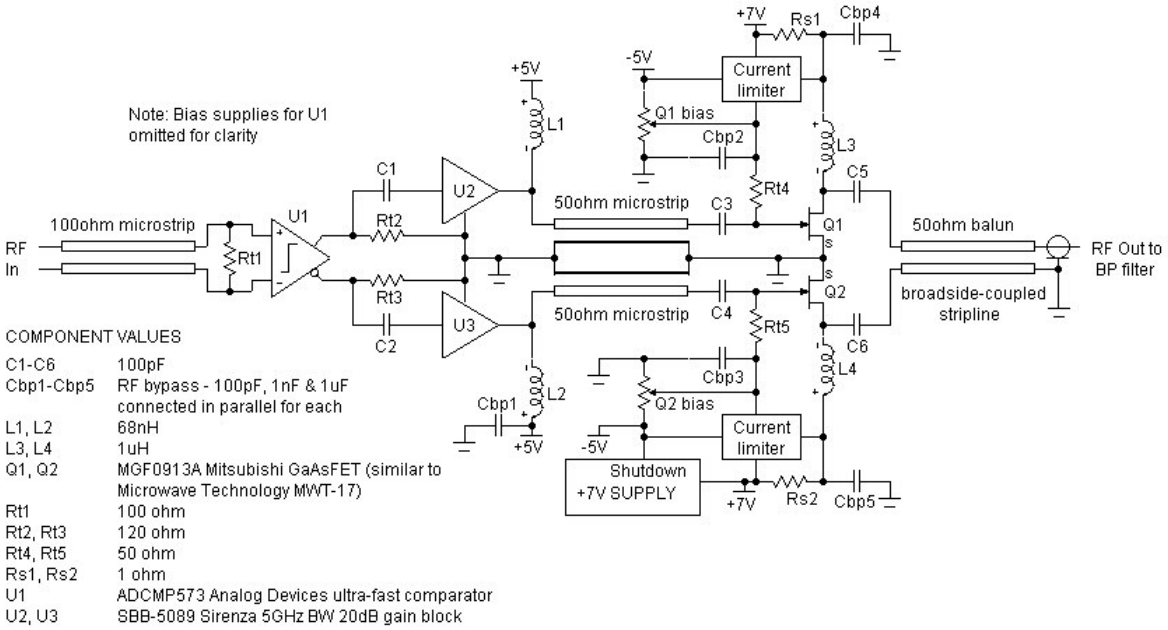

Figure 4.10 - Prototype Class-D PA circuit arrangement

4.1.2.3 Stripline Balun

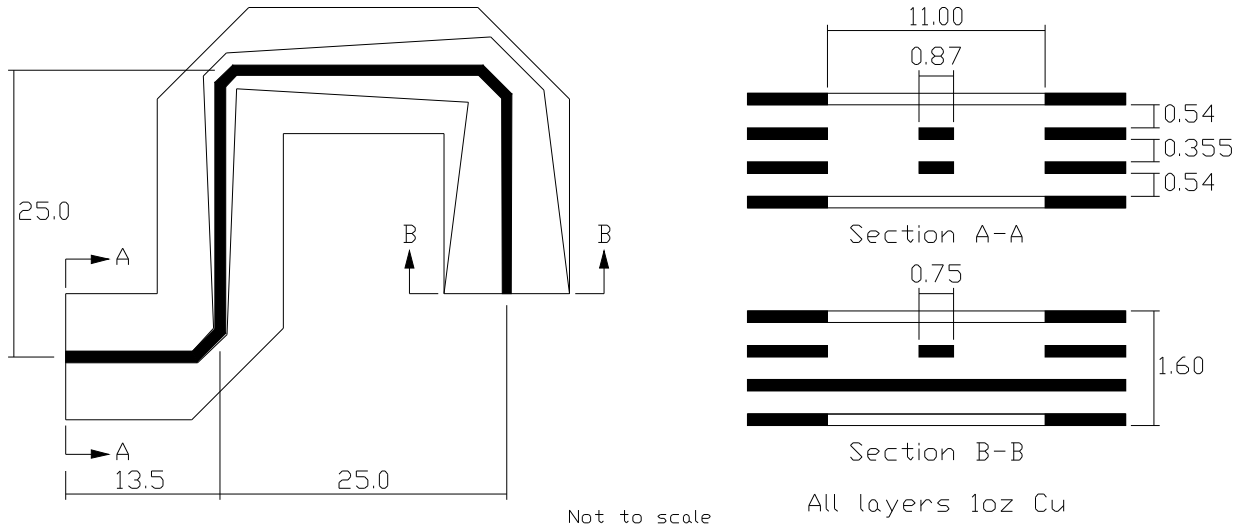

Figure 4.11 - Broadside-coupled tapered stripline balun

The performance of lumped-element transformers at UHF is limited by parasitic capacitance, leakage inductance and copper losses, in addition to the inductance and capacitance of connecting leads. Moreover, the power-handling capacity may be limited. A stripline type of balun has potentially better performance at UHF and microwave

frequencies than a lumped-element balun. The broadside-coupled tapered stripline concept is based on the original coaxial-line tapered-slot balun developed by Duncan and Minerva [41] which was characterised by its good balance and low VSWR over a wide frequency range. Disadvantages include the need for considerable circuit board area, at lower UHF bands, and the power loss from radiation. Figure 4.11 shows the outline dimensions of the balun designed for this prototype. A linear taper has been used for the low-side trace and the high-side trace is tapered very slightly to compensate and provide a 50Ω characteristic impedance at each end. This simplified approach was considered adequate for an initial trial, although it was recognised that the impedance would not have been very uniform along the length of the line and the folding of the line to reduce the required board area introduced sharp corners that would have some radiation loss.

4.1.3 HIGH-FREQUENCY LAYOUT CONSIDERATIONS

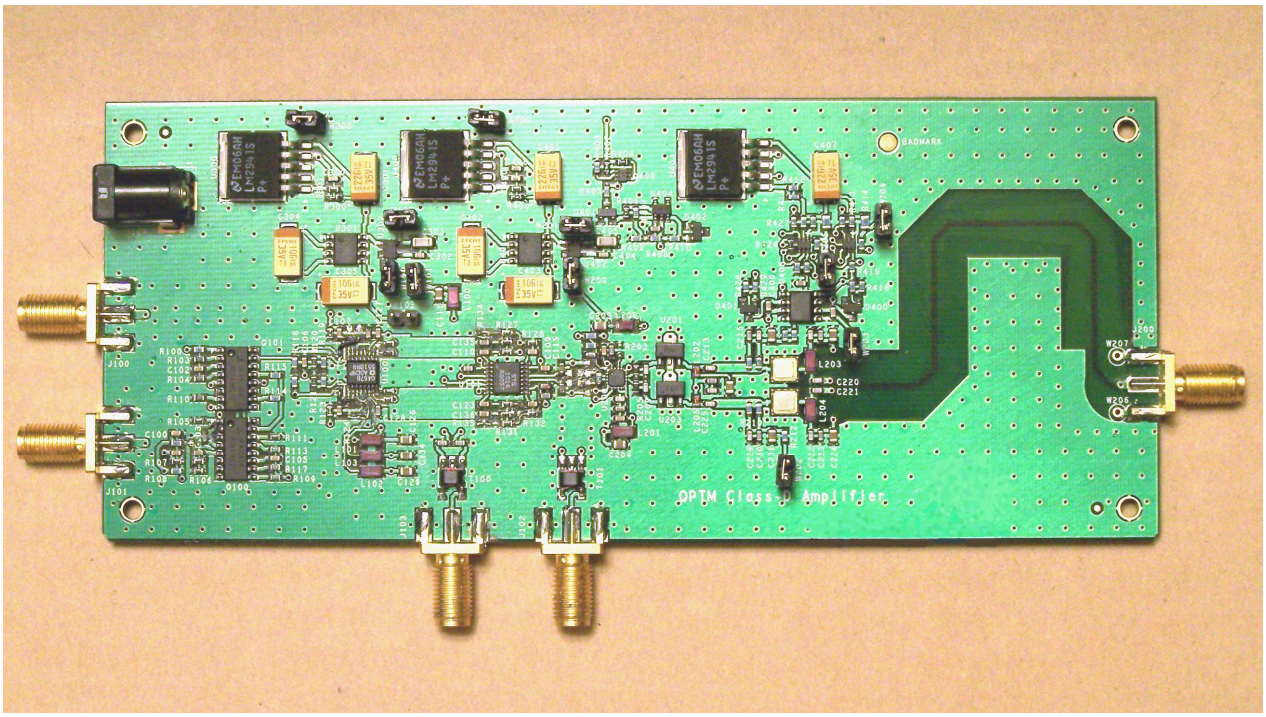

Figure 4.12 - Experimental QPTM and Class-D amplifier prototype

The photograph of a prototype system in Figure 4.12 shows the general layout of circuit blocks, with the power supply circuits at the top. The reference generator is at the left, the quadrature modulator is in the centre and the Class-D PA is at the right, feeding the serpentine broadside-coupled balun. (Some modification to the reference generator circuit is visible. This was to replace a slightly inferior dual comparator type with the current type ADCMP551). Design and construction of the experimental prototype system was undertaken using a four-layer printed-circuit stack-up, so that a combination of buried stripline and microstrip technology could be used

to couple test signals into and out of the circuit, safely crossing over similarly-constructed lines interconnecting the signal processing stages, an intermediate ground plane reducing mutual interference. The material used was FR4-grade epoxy-glass and 1oz copper laminate (see Figure 4.11). FR4 is not a high-frequency material but, in low-Q circuits such as this, performs adequately in the 400-500MHz frequency range. All of the RF transmission lines are balanced, differential lines to minimise cross-talk and feedback problems that might cause instability. Solid ground planes are used on all layers, heavily bonded by an array of vias, and each section of the circuit has its own regulated power supply with low-impedance RF bypass components close to each device, with extreme care being taken to keep ground return paths short and direct, even with transmission-line terminations. Shield cans have not been included in the prototype design, in order to provide access for measurements. However, they would be essential in a real application of the system, because the components would then be in closer proximity and there would also be the need to keep out external interfering signals.

The reference triangle-wave generator required particular care in layout, so as to achieve a balance in the pcb track capacitances. This proved to be extremely difficult because of the unbalanced location of the particular transistor terminals. In this type of circuit, minor asymmetry of duty cycle may be corrected by trimming the ratio of the current source resistors, R8 to R9 in Figure 4.1. However, capacitance from a timing node to ground or other parts of the circuit is difficult to compensate and may cause significant non-linearity. The dividers R4,R7 and R5,R6 do not affect duty cycle but are important for dc offset of the output, whilst frequency is controlled by R1, R2 and C1. No trimmers were provided, in case they may have resulted in additional parastics being introduced. The ideal, although totally impractical for this prototype, would have been to have the whole circuit integrated.

4.2 Performance Measurements

The prototype circuit board has been designed so that the QPTM and transmitter subsystems may be tested and operated quite separately. A test port has been included to facilitate this and it may be used either as an output for the QPTM circuit or an input for the transmitter circuit, according to the position of soldered links on the circuit board. Both the test and the local oscillator connections are single-ended but are immediately transformed to differential signals by baluns placed adjacent to each connector. All signal connectors are of the broadband SMA type.

4.2.1 QUADRATURE PHASE-TIME MODULATOR

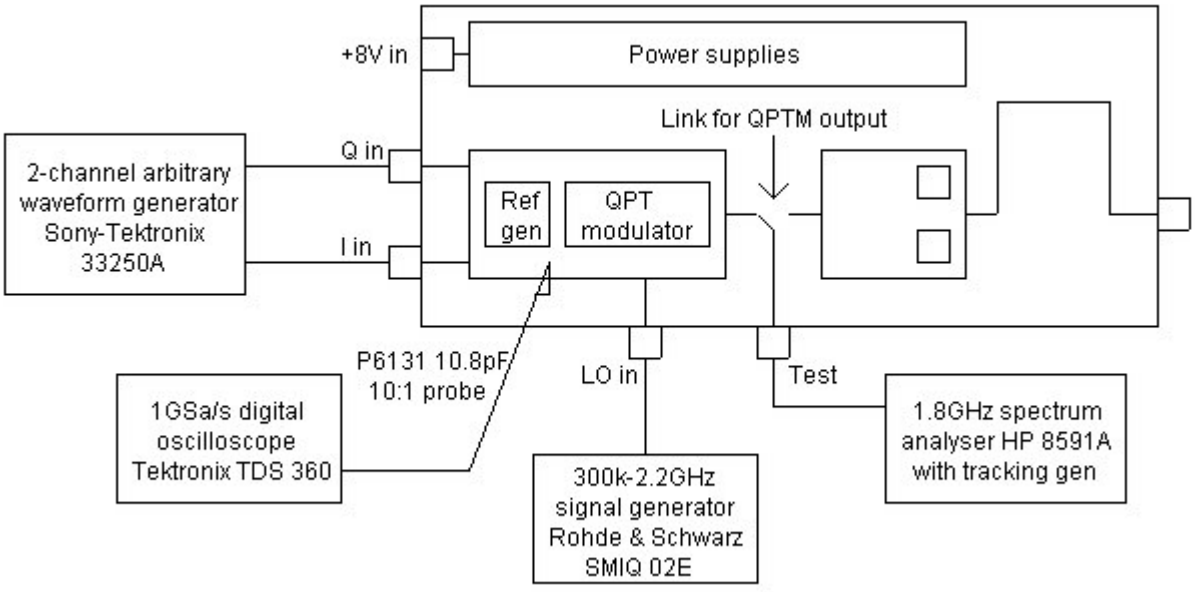

Figure 4.13 - QPTM measurement setup

The equipment setup used for testing the modulator subsystem is shown in Figure 4.13. For the reference generator, no external test signals are needed as the circuit is free-running. Of special interest here is the linearity of the triangular waveform as it appears at each PWM comparator input. The reference waveform, shown in Figure 4.14, was acquired by probing across a 100Ω terminating resistor. The probe capacitance thus created a 1.08ns time-constant at this node, slightly degrading the 1.75ns risetime of the oscilloscope used. However the major problem encountered in making this measurement was stray coupling of the comparator output switching signal into the oscilloscope probe, only a few millimetres away. The waveform obtained is a "best-effort" one but still not completely free of the effect, as may be seen by the small ripple on the slope of the waveform. A further observation is that the periods of each ramp of the triangle are not equal. This has no significant effect on the PWM process but results in the presence of low-level sidebands in the modulated RF carrier spectrum spaced at even-harmonics of the

reference frequency. As there was no immediate need, and it would have involved changing the circuit layout, it was decided to improve this only in a future development.

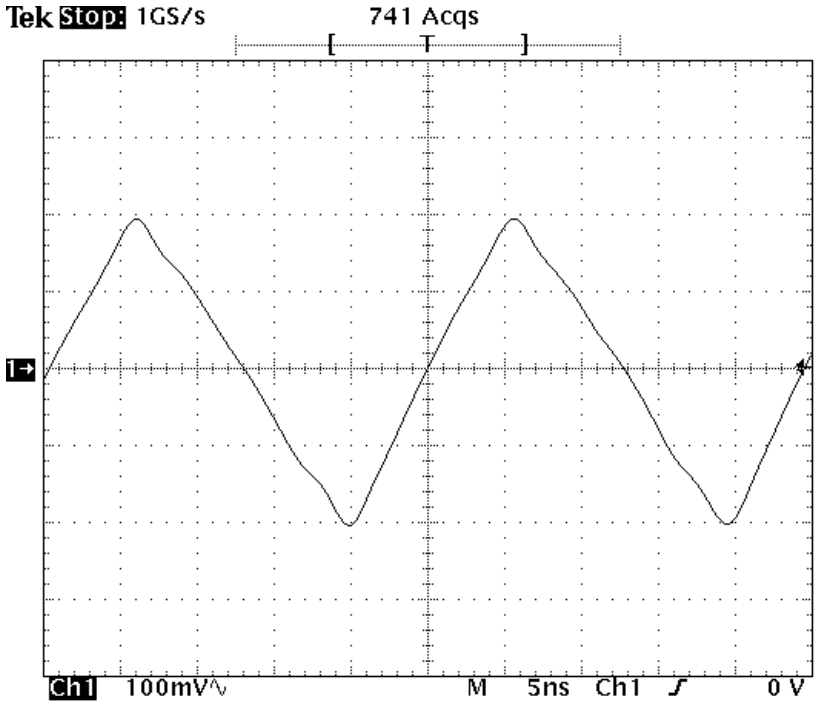

Figure 4.14 - 40MHz reference PWM triangle wave

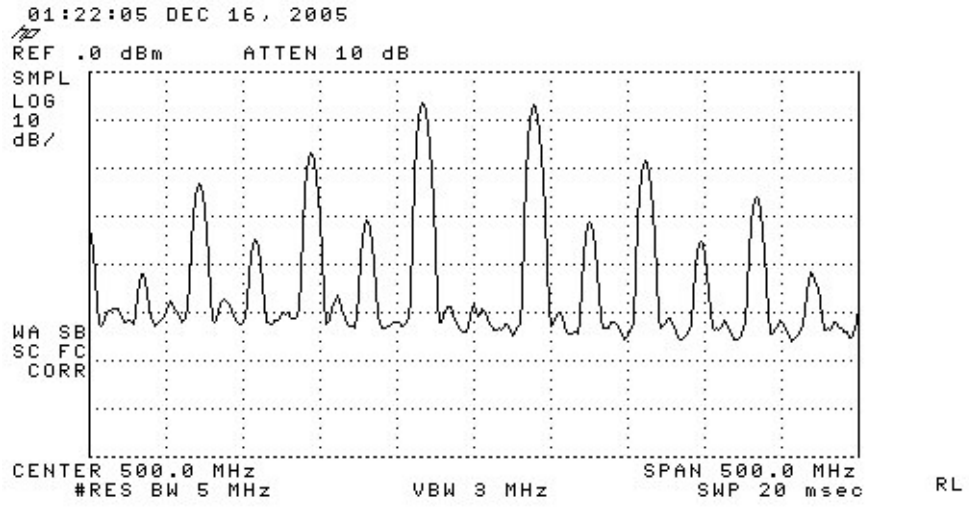

Figure 4.15 - Quadrature modulator output spectrum with no I-Q inputs

The object of subsequent modulator tests is to determine the linearity of the overall QPTM process, before feeding the signal to the transmitter. Figure 4.15 shows the spectrum of the

quadrature modulator output signal at the 'Test' socket, with no I or Q baseband input. The carrier frequency of 500MHz is suppressed. The intermediate lines spaced at even harmonics of the reference frequency from the carrier frequency are due to the triangle asymmetry discussed above.

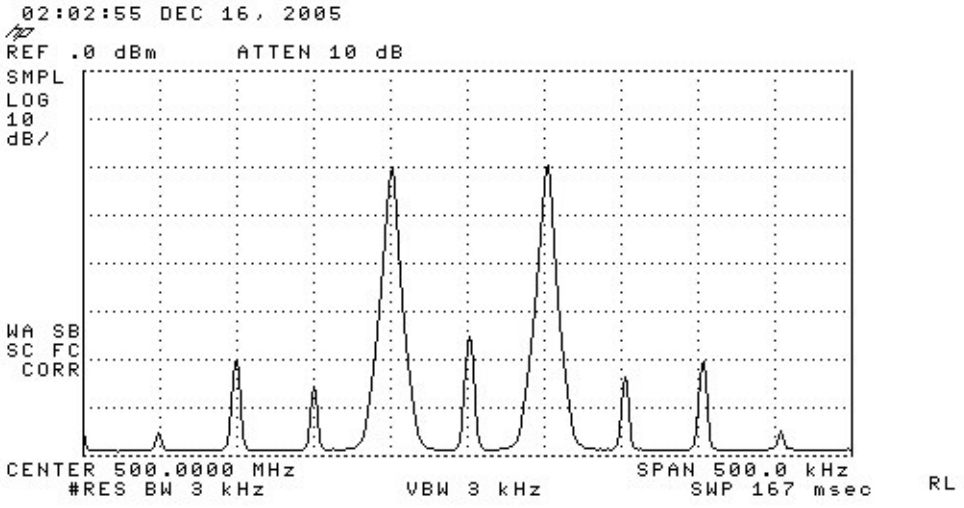

Figure 4.16 - QPTM spectrum with 50kHz 200mV I-ch input

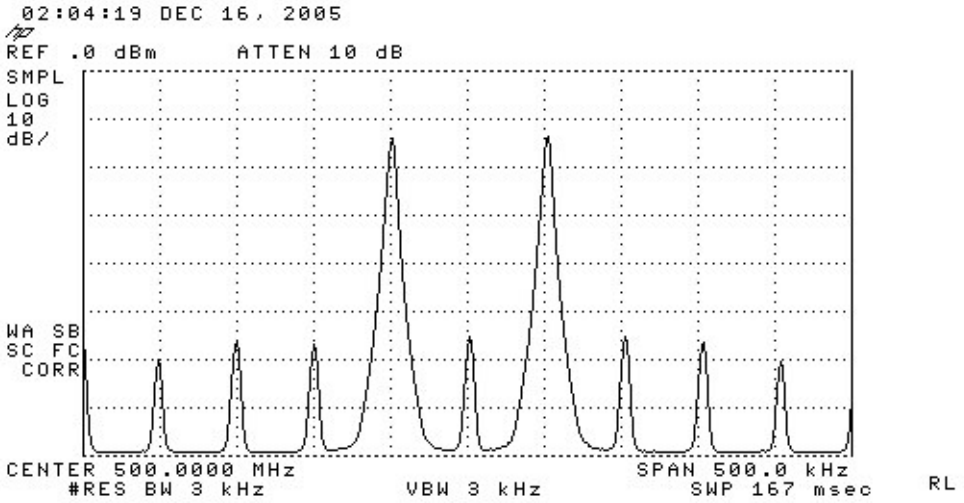

Figure 4.17 - QPTM spectrum with 50kHz 400mV I-ch input

Figures 4.16 and 4.17 show the close-in spectrum with a 500MHz carrier modulated by a single tone of 50kHz at two different levels, 200mV and 400mV respectively. There is a relative increase in even harmonic distortion but the components are still 40dB below the fundamental sidebands. This is an indication of triangle-wave linearity but not a measure of it, since the quadrature modulator is also involved in the process.

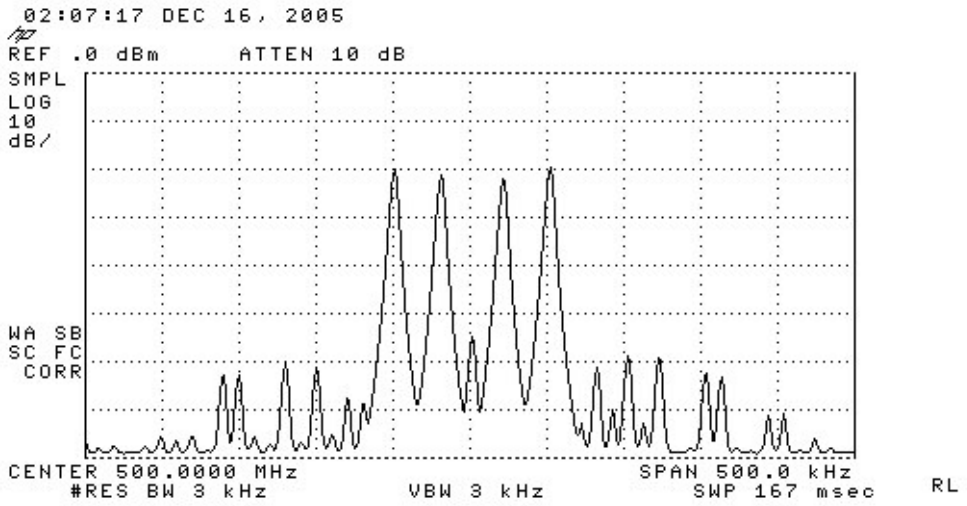

Figure 4.18 - QPTM spectrum with 50kHz I-ch and 20kHz Q-ch 200mV inputs

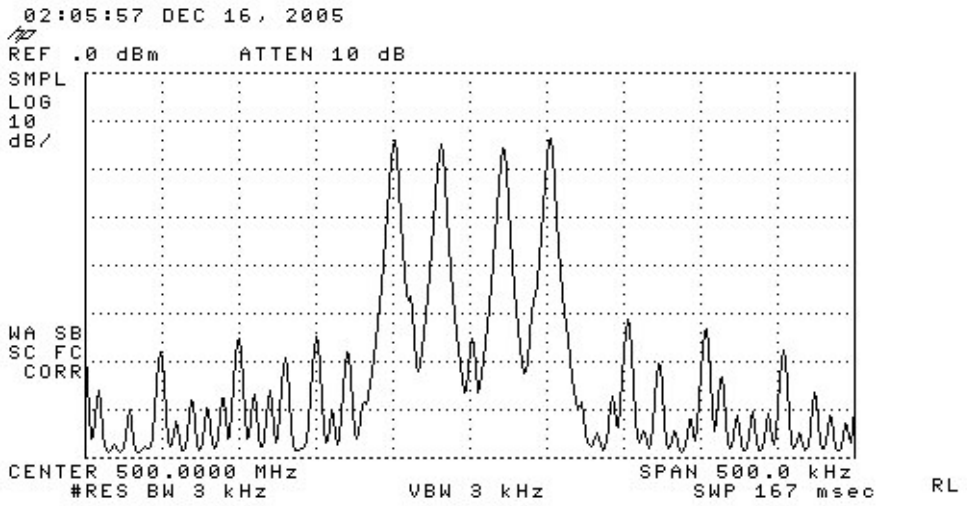

Figure 4.19 - QPTM spectrum with 50kHz I-ch and 20kHz Q-ch 400mV inputs

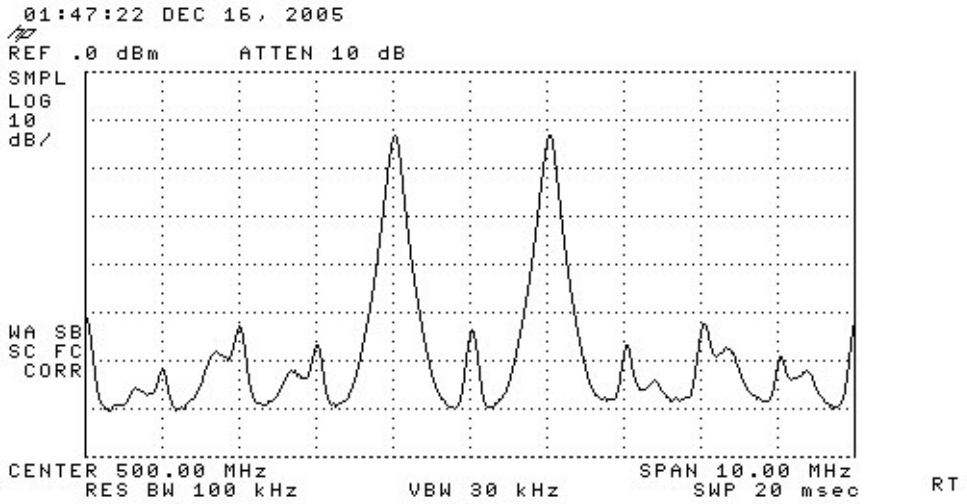

Figure 4.20 - QPTM spectrum with 1MHz 400mV I-ch input

Figures 4.18 and 4.19 show the close-in spectrum with a 500MHz carrier, two-tone modulated by 50kHz (I) and 20kHz (Q) signals at the two different levels used in the preceding test, 200mV and 400mV respectively. There is a relative increase in even harmonic distortion but the components in Figure 4.19 are now about 2dB higher than in the test for Figure 4.17. This is apparently due to the higher peak power of the two-tone input affecting the quadrature modulator summing stage. Figure 4.20 is a repeat of the test of Figure 4.17 but with the modulating signal frequency increased from 50kHz to 1MHz. The magnitude of the odd-harmonic distortion components is approximately similar, at 40dB below the fundamental sidebands, but the even-harmonic components are now 3 or 4dB less. These distortion figures are well above the arbitrary waveform generator distortion specification at 1MHz, which is stated as –62dB at the second harmonic and –52dB at the third, at 0dBm signal level. However, they are comparable with the direct quadrature modulator specification, which indicates sideband suppression of 44dB typically at 500MHz and 32dB in the worst case.

4.2.2 TRANSMITTER

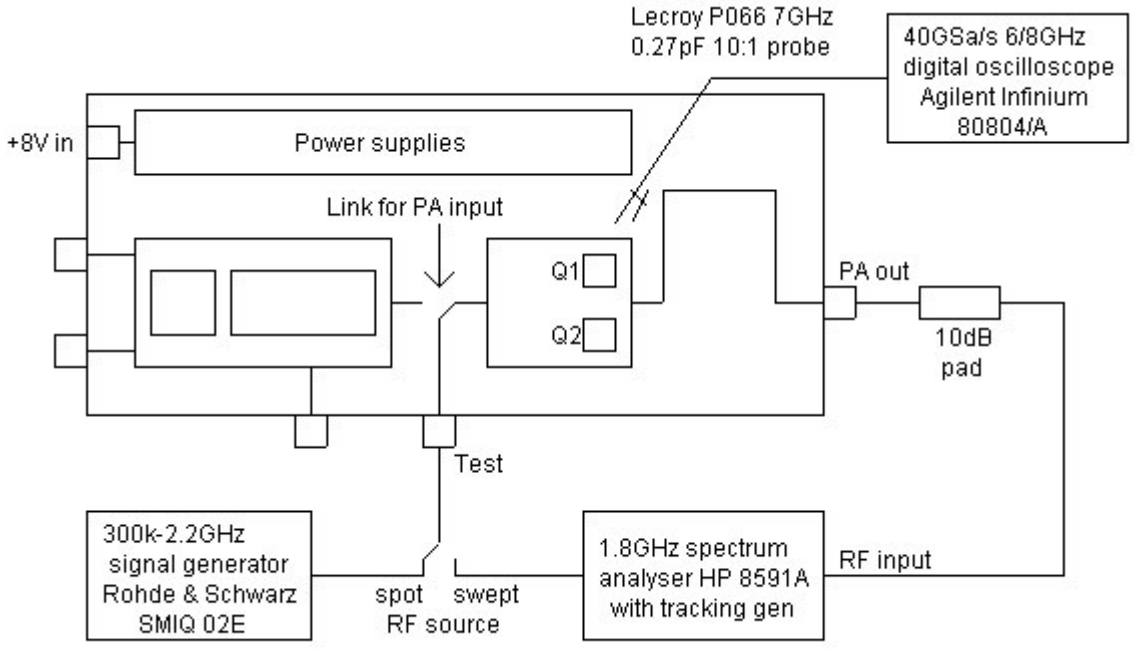

Figure 4.21 - Class-D PA measurement setup

Two complete prototypes were built, using an SMD reflow process. One of these was modified by the substitution of a discrete output transformer for the stripline balun, so that it could be used in VS mode (with differential output load), whilst the other was kept in original CS form. The setup in Figure 4.21 depicts the latter version – a signal is not available from the 'PA out' socket

in the differential adaptation. Tests of the PA subsystem were able to be performed by connecting the solder links at the PA input so that an RF signal could be injected via the 'Test' socket. This signal could be either a fixed carrier frequency from the signal generator or a swept signal from the tracking generator of the spectrum analyser, according to the test to be performed. For tests of the CS version, when the PA output was monitored by the spectrum analyser, a 10dB attenuator pad was included in series with the analyser input to protect it from the potentially damaging power levels. This pad was inserted at the PA output socket to provide the best possible termination match, both for the analyser cable and the PA output balun.

4.2.2.1 Voltage-switching PA

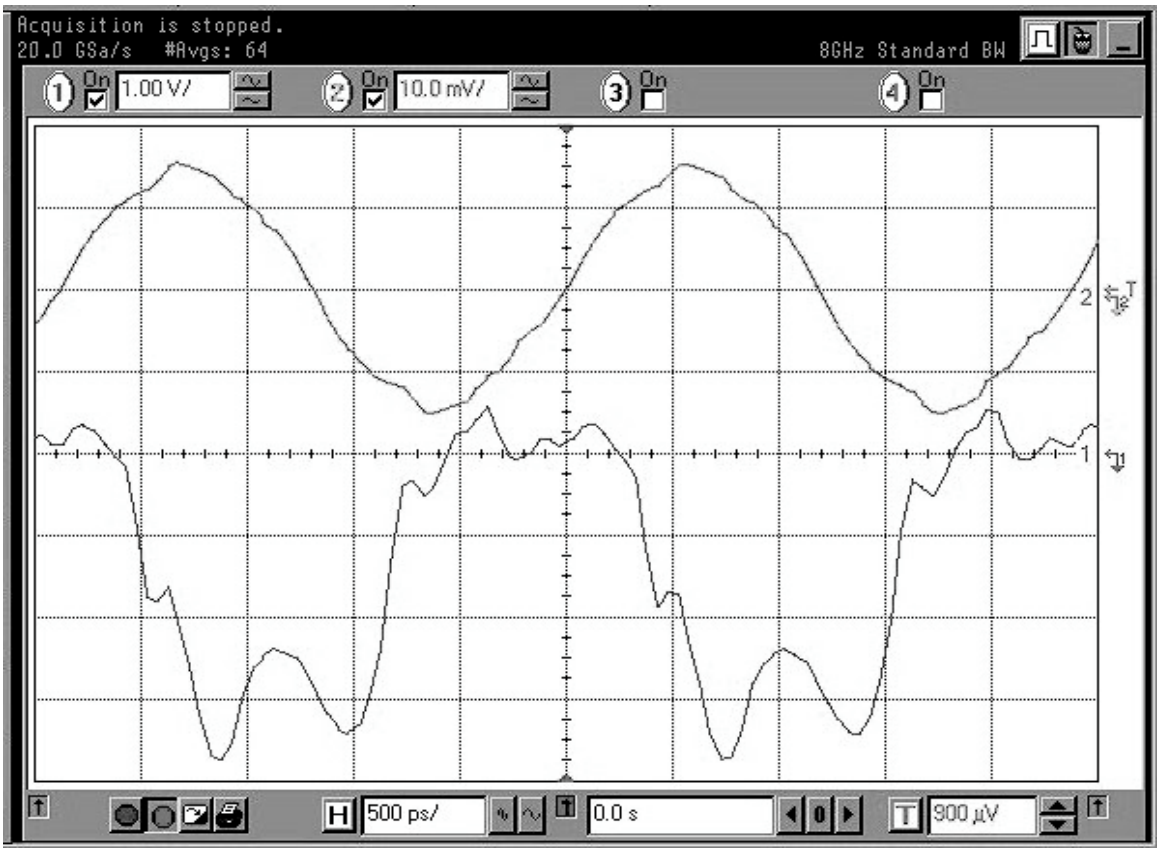

Figure 4.22 - FET Q1 Gate (trace1) and input waveforms in untuned VS mode

For the VS mode test, the prototype PA circuit has the same configuration as that shown in the simulation model of Figure 4.4, with the output tuned circuit eliminated, and the transient waveforms obtained are thus able to be compared with those of Figure 4.5. For both of the transient plots, the Q1 Gate waveform in Figure 4.22 and the Q1 Drain waveform in Figure 4.23, the input signal was used as a timing reference. An Agilent 8GHz bandwidth oscilloscope was used to obtain these plots, coupled through a single

LeCroy 10:1 passive probe having 0.27pF input capacitance, as this enabled the bandwidth of the measurement system to be maximised. This probe also featured a robust and convenient mechanical arrangement. The sinewave input reference signal was tapped off at the 'Test' socket connection point using a 50Ω resistive splitter. Using this method, it was unnecessary to match cable delays, as each waveform acquired had the same cable-delay offset from the reference.

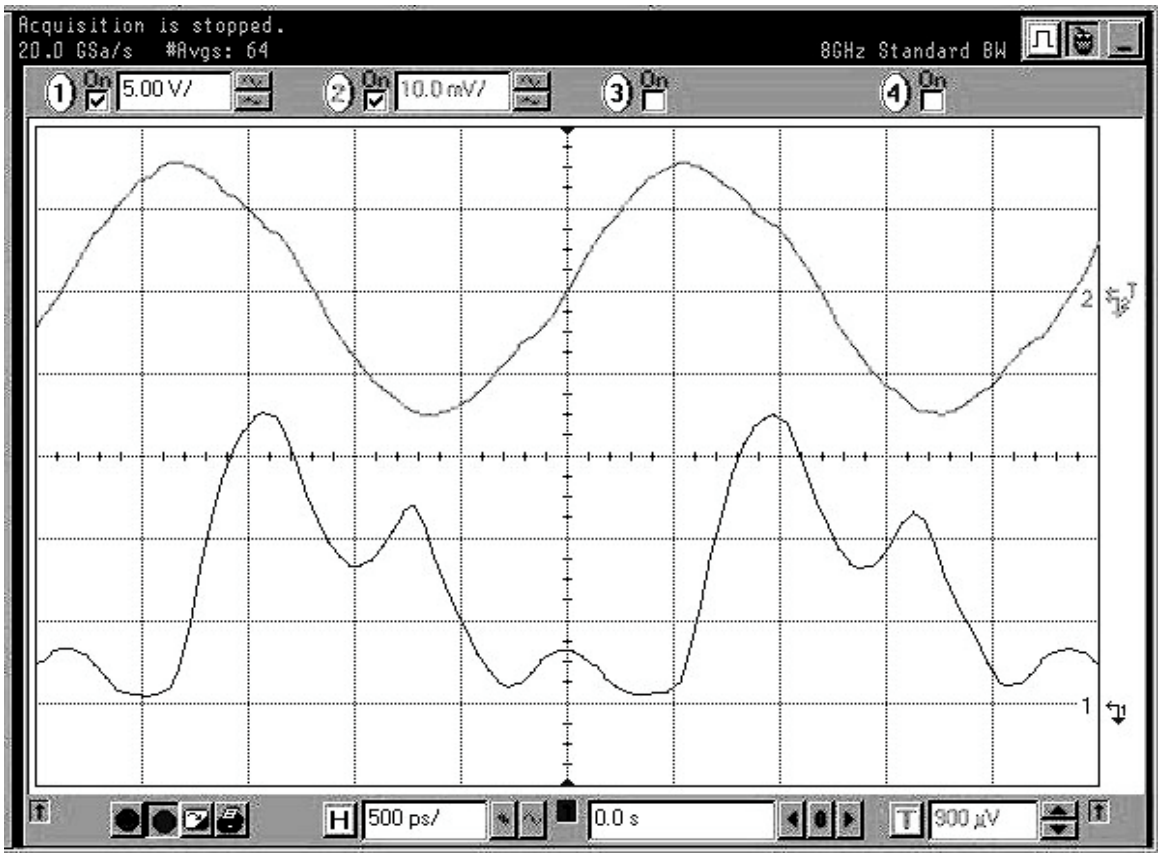

Figure 4.23 - FET Q1 Drain (trace1) and input waveforms in untuned VS mode

The Q1 Gate waveform in Figure 4.22 is similar to that in Figure 4.5 except that much higher harmonic levels are present when the FET is turned 'off'. This is apparently a function of the output, rather than the gate, circuit as similarly large harmonic excursions are evident on the Q1 Drain waveform of Figure 4.23. The reason for this is observed to be the parasitic inductance associated with the output transformer connecting leads, which range from about 2 to 6mm in length, and were not included in the simulation.

4.2.2.2 Tapered stripline balun

Testing of the broadside-coupled tapered stripline was most easily performed on a bare, unassembled circuit board. This enabled matching terminations to be constructed on the

board and signal take-off to be accomplished via a section of semi-rigid coaxial cable, soldered to the top ground-plane of the board. The arrangement is shown diagrammatically in Figure 4.24.

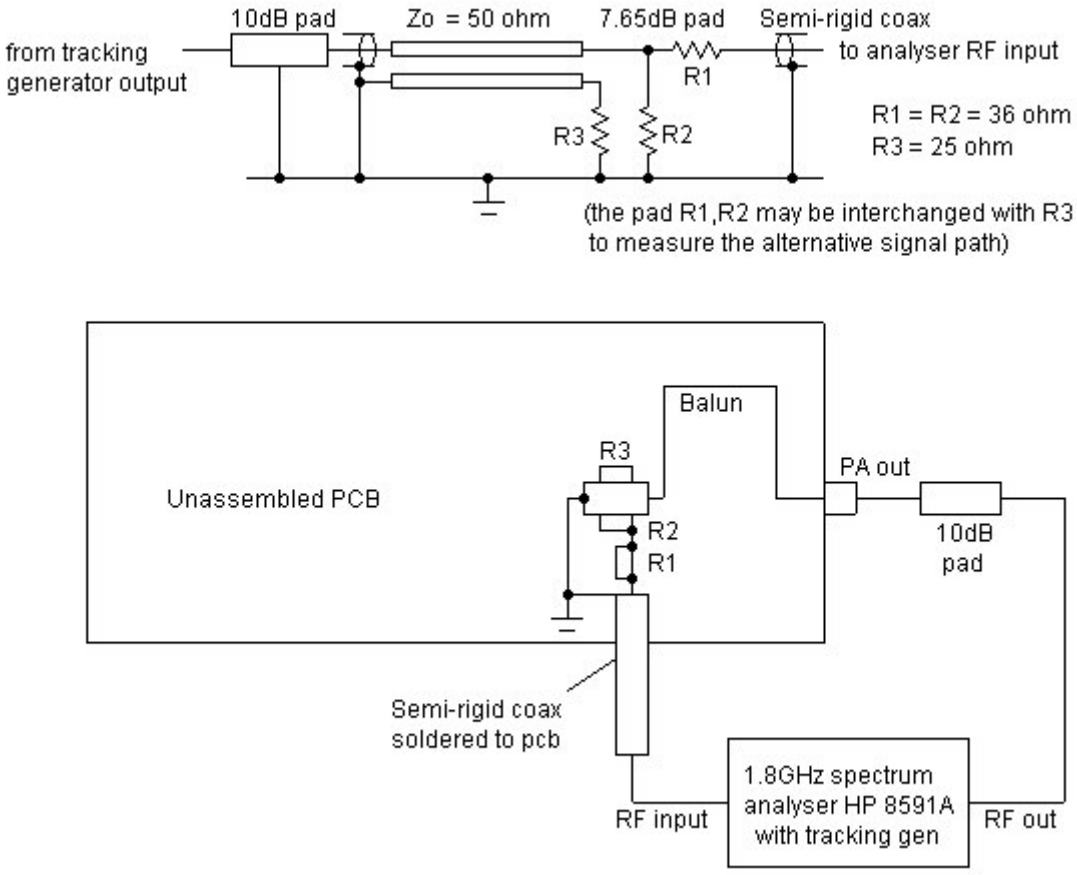

Figure 4.24 - Test setup for tapered-stripline balun

The frequency response sweeps of Figures 4.25 and 4.26 show the direct and coupled responses respectively, over the range from 0 to 1.8GHz. When analysing the curves, one should allow for about 22dB total insertion loss, comprising the 3dB power division, 17.65dB of resistive pad loss and cable and connector losses. The balun transmission loss is very small except for a notch in the direct path close to 960MHz of about 3dB and one in the coupled path at just over 1.3GHz of about 12dB. Good low-frequency performance extends to below 200MHz.

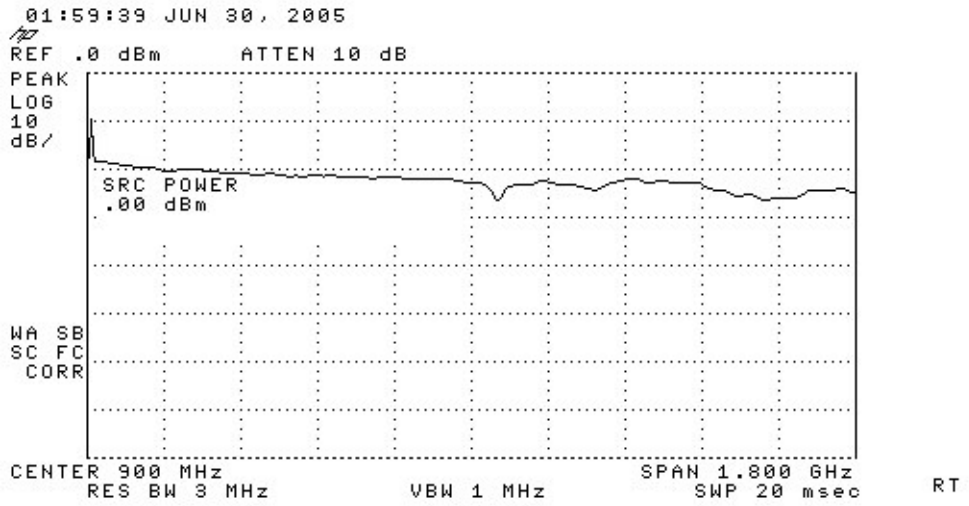

Figure 4.25 - Unbalanced input to direct line balun output via 17.65dB padding

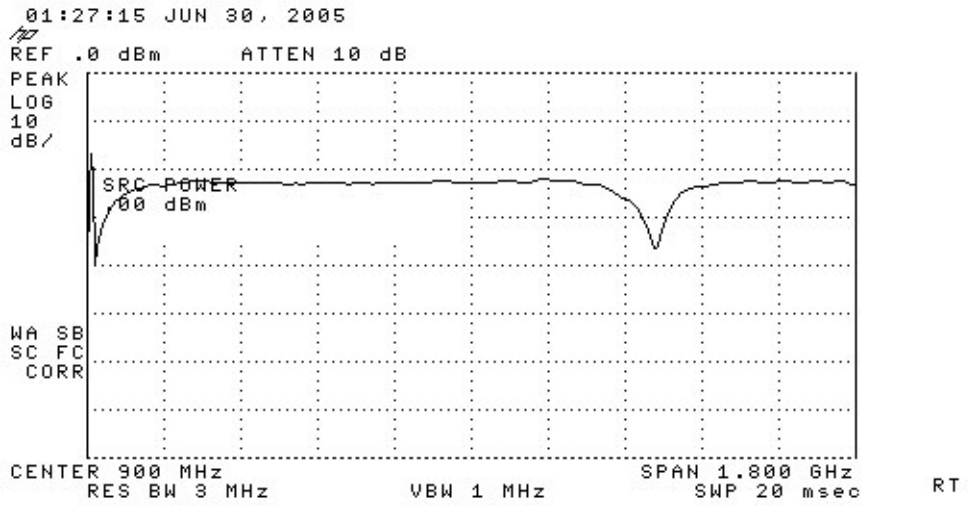

Figure 4.26 - Unbalanced input to coupled line balun output via 17.65dB padding

4.2.2.3 Current switching PA with stripline balun

The CS-mode circuit is similar to that in the simulation circuit of Figure 4.7 but with FET output circuit untuned. The amplifier was first set up as in Figure 4.21 for a swept response measurement. The resulting frequency response plot of Figure 4.27 shows the response of the balun to be flat within ±1.5dB over the range from 200MHz to 1.2GHz. The spectrum of Figure 4.28 is taken with a carrier of 460MHz and shows that the third harmonic is 10dB below the carrier level, consistent with a square-wave output signal. There is a second harmonic at –26dB and a fourth harmonic at –24dB with respect to the carrier level.

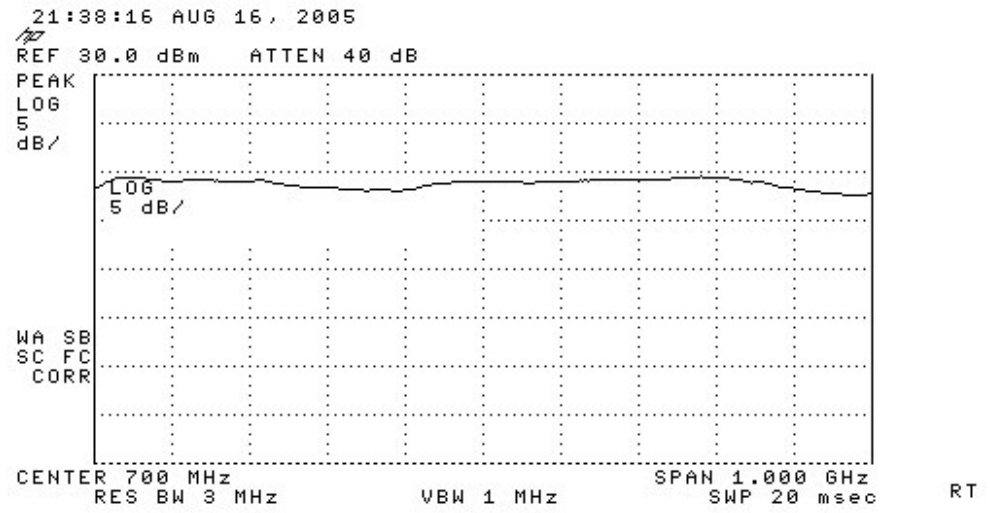

Figure 4.27 - Class-D PA frequency response with stripline balun and 10dB pad

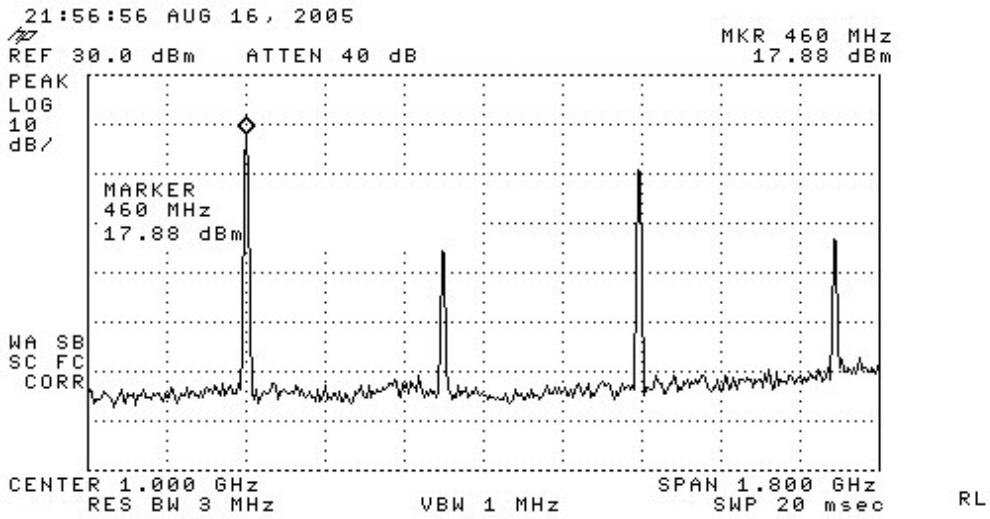

Figure 4.28 - Class-D PA output spectrum with stripline balun and 10dB pad

The FET Q1 Gate waveform in Figure 4.29 shows less ringing than in the VS case but does indicate very strong feedback from the drain during the output switching risetime. This results in a quite asymmetric gate drive. The effect was not nearly as exaggerated in the simulation plot of Figure 4.8, suggesting that there may be some parasitic contribution related to the device packaging or mounting. The output risetime apparent in Figure 4.30 is close to 100ps.

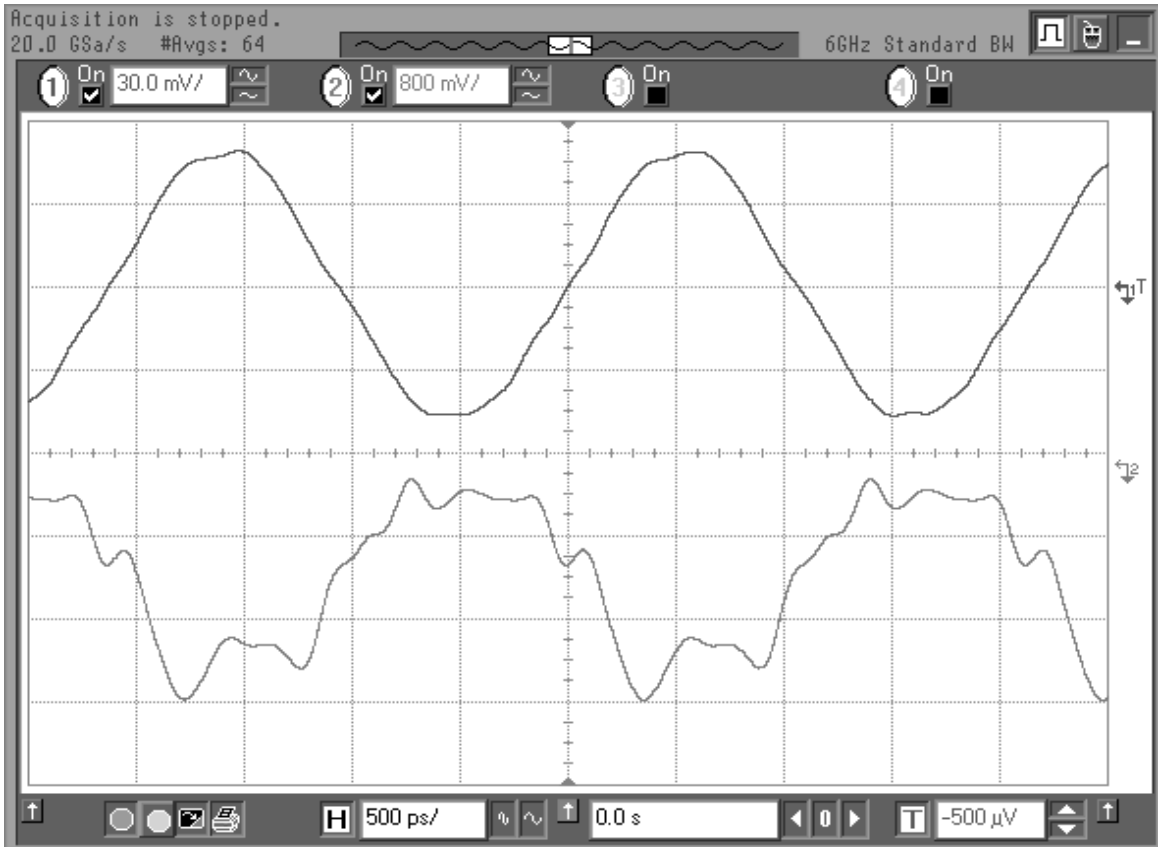

Figure 4.29 - FET Q1 Gate (trace2) and input waveforms in untuned CS mode

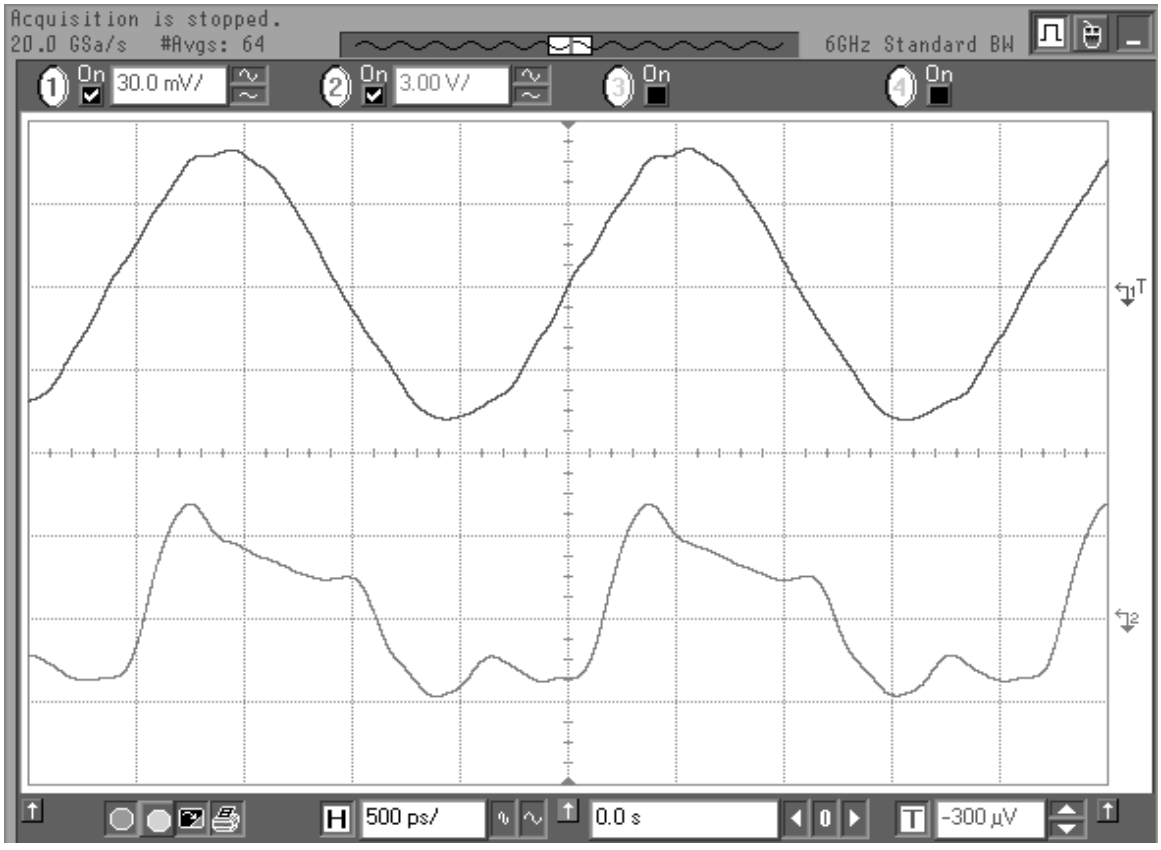

Figure 4.30 - FET Q1 Drain (trace2) and input waveforms in untuned CS mode

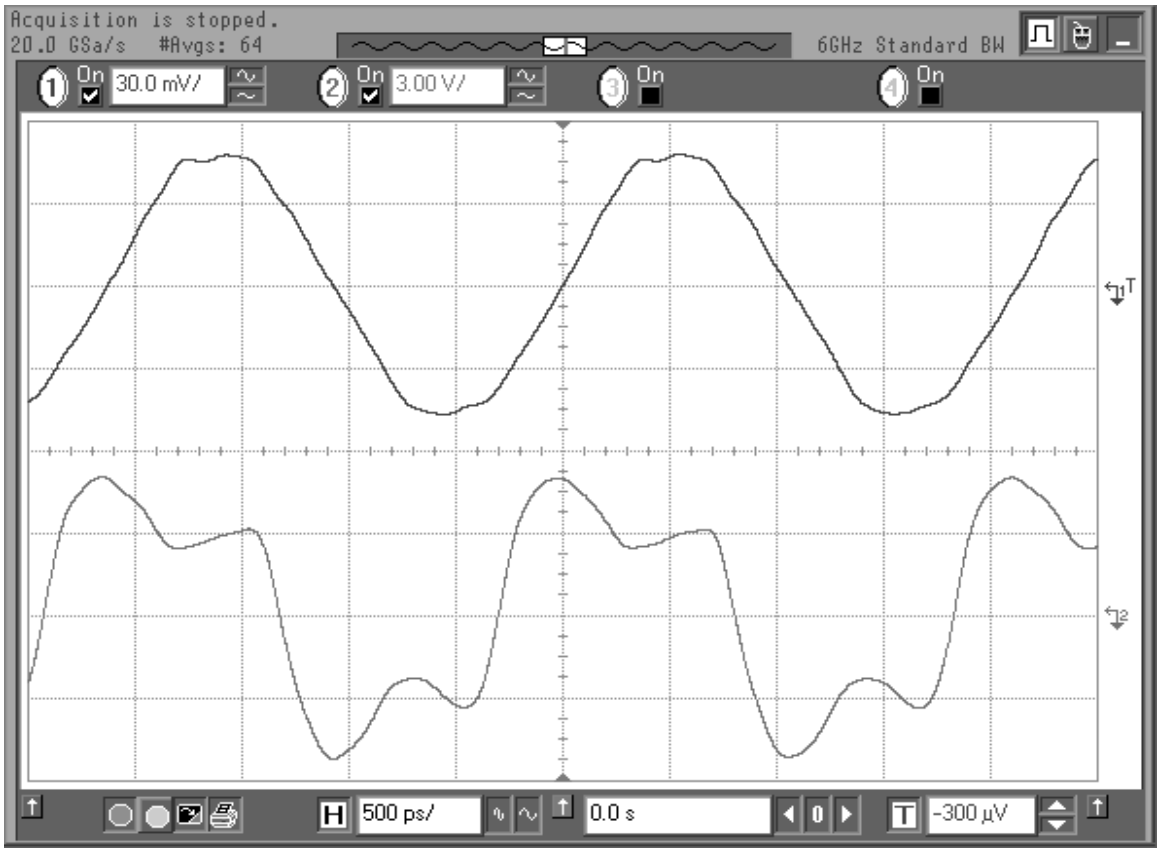

Figure 4.31 - Stripline balun output (trace 2) and input in untuned CS mode

Figure 4.31 shows the output waveform captured at the 'PA out' socket (trace 2). The shape, with strong third harmonic, is indicative of a rectangular wave that has been band-limited. This is to be expected because of the combination of switching risetime of the FET drain current and bandwidth of the output balun. The more rectangular waveform in the simulated plot of Figure 4.8 (lower trace) is the result of using the idealised, infinite-bandwidth transmission-line model. However, the test demonstrates correct functionality of the prototype system and consequently, with the future addition of a resonant 'tank' in the FET drain circuit, may be expected to perform substantially in accordance with the corresponding simulation in Figure 4.9. The measured efficiency of the untuned output stage was 57%.

4.2.2.4 Trial of Unfiltered Class-D with QPTM

Although the untuned PA could not be expected to perform efficiently as a true Class-D amplifier, it was nevertheless found useful to test the effect that the switching amplifier had on a QPTM signal spectrum. A plot of the spectrum obtained for two-tone modulation is presented in Figure 4.32 and this may be compared with that for the QPTM circuit by itself in Figure 4.19, obtained for the same input signals. As may be seen, the spurious harmonic components in Figure 4.32 are about 26dB below the signal level,

compared with about 40dB for the modulator alone. This result is consistent with the simulated Class-D distortion shown in Figure 3.7(a) for an SSB input and may be improved only with much greater PWM bandwidth.

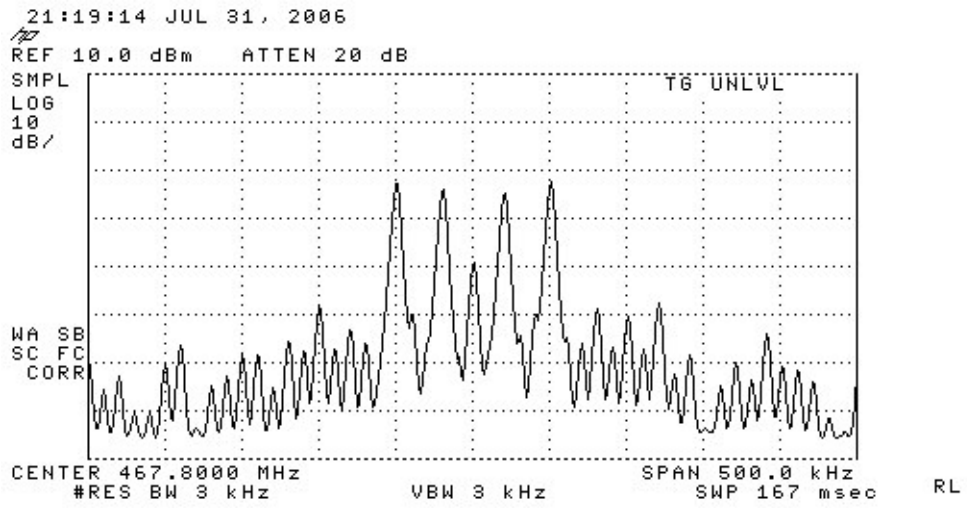

Figure 4.32 - QPTM spectrum at output of untuned switching PA 50kHz and 20kHz quadrature modulator inputs

4.3 Summary of QPTM Prototype

The experimental prototype has been designed in two basic subsystems, the QPTM subsystem and the PA subsystem, each with its own set of power supplies so that they could be tested and characterised separately without mutual interference. Ultimately, they could be interconnected to form a complete transmitter chain (with added filter). The reference triangle-wave generator was designed and simulated at transistor level and ultimately constructed using the corresponding microwave-bandwidth transistor arrays. Extreme care had to be taken in the layout of this section because of the array packaging limitations and associated parasitics. Latest-technology comparator ICs were used to obtain the necessary fast transition times and these also demanded particular care with layout. The direct quadrature modulator is a standard RF part, although the type was selected for its precision. Measured performance of the QPTM system fully matched expectations.

The PA subsystem was simulated in both a basic voltage-switching Class-D form, as a reference baseline, and as a current-switching type with a transmission-line balun output. The latter has advantages at high frequencies because of the slower risetime of FET drain voltage, with correspondingly-reduced feedback to the gate, and the use of a transmission-line transformer that could be integrated in the circuit board using stripline techniques. The broadside-coupled tapered-stripline transformer is neither very well-known nor adequately documented so it has been useful to build and characterise it, as it appears to be particularly advantageous for upper-

band UHF push-pull amplifiers. The circuit board layout was found to behave well. However, some difficulty was found when making certain probing measurements, indicating that a revised version with removable shields should be built. At the same time, advantage may be gained from the PA waveform data obtained to assist in the design of an output filter suitable for integration with the stripline balun. The waveforms were able to be correlated to a reasonable degree with the simulated waveforms, so that, by extending the simulation models to include stripline parameters and more parasitic elements, there is some confidence that a good output filter design may be achieved with a minimum of iterations. Future work in this area will enable end-to-end performance measurements to be achieved.

Chapter 5

Discussion, Conclusions and Further Work

5.1 Discussion of Results

5.1.1 BACKGROUND RESEARCH

5.1.1.1 PAPR Reduction

In order to determine reasonable target requirements for an improved transmitter system, it was necessary to set an approximate upper bound for the expected PAPR of the modulating signal. This would have been the case even if, by some technique, the signal were converted to a constant-envelope modulation prior to final amplification, because of implications for the converter or modulator linearity. In (1.2.1) we found that a 64-QAM single-carrier system had a PAPR of almost 3.7dB, without the overhead of any pulse shaping, whilst an *m*-PSK OFDM signal modulated by Golay complementary codes could achieve a PAPR of 3dB. We observed that, for OFDM signals that did not have uniform phase modulation or had adaptive modulation, clipping and filtering seemed to be the most attractive technique for controlling PAPR. Errors resulting from this process could be reduced by applying the Chen and Haimovich iterative reconstruction technique in the receiver [12]. For a 64-carrier OFDM signal clipped to 4dB PAPR, E_b/N_0 was degraded only 1dB compared with the unclipped system for similar PER. Thus we may conclude from the above that 4dB would represent a reasonable target upper bound for PAPR in an improved OFDM transmitter system, although a single-carrier system may require substantially more headroom to avoid adjacent channel interference.

5.1.1.2 Constant-Envelope Modulations

Two existing continuous-phase techniques have been found, the constant-envelope phase modulation technique by Tan and Stuber [23] and carrier pulse-width modulation, by Keyzer et al [24]. The former has the drawback of being incompatible with existing OFDM receivers and also requires complex receiver decoding. The latter requires very

high digital processing clock rates, typically eight times the RF carrier frequency, making its implementation for the UHF bands extremely difficult. There is some concern about the linearity achievable with the carrier pulse-width modulator if used for higher-order modulations than OQPSK.

5.1.1.3 PA Linearisation

In (1.5) we examined seven different classes of PA linearisation that, in the main, seem to have been developed for narrowband applications. Of these, only digital adaptive predistortion, which does not rely on "real-time" feedback loops, appears to be suitable for broadband OFDM systems because it avoids the loop gain-stability trade-offs. This technique could also be used with a Doherty amplifier, in either classical Class-B/Class-C or Class-F technology, to further improve efficiency. The technique of complex gain mapping, as presented by Mann in [25], is effective with linear PA systems, and may be further enhanced by Cartesian mapping to overcome quadrature modulator errors. However, the EER systems that are necessary to achieve high efficiency make use of non-linear PA stages so that a predistortion technique may not achieve sufficient correction by itself. Nevertheless, its use could reduce the loop gain required in the "real-time" feedback path of an EER system, allowing it to have a faster response time. Wideband envelope tracking is similar to EER but uses a linear PA, so that, although a fast response time is still necessary for the drain power supply, it is less critical than for EER, which relies on the drain supply for the amplitude part of the modulation. Higher levels of integration, giving better control of delay times, may make this a competitive solution in future.

5.1.2 QUADRATURE PHASE-TIME MODULATION

5.1.2.1 System Simulation

Simulation of the proposed QPTM system showed that it would be feasible to design a practical modulation system using available integrated circuit technology. Good agreement was obtained between the MicroCap and earlier Matlab simulation plots. The most significant problem identified was the presence of dominating sidebands related to the reference triangle-wave frequency. Such high out-of-band components tend to limit modulator dynamic range and place tight constraints on the PA output filter specification.

Examples of low-cost commercial coaxial filters may be found in [41] that would be suitable for use as output bandpass filters in typical mobile radio bands, for example in the

400-500MHz band. For the more recently allocated microwave bands, dielectric resonator filters appear to be an attractive solution [42], with advantages including high selectivity, low insertion loss and low cost. It is anticipated that a goal of future research and development may be to achieve spectral emission characteristics compatible with specifications similar to those in [43] and [44] for UHF and microwave applications respectively.

A possible solution to the reference spectrum problem, Suppressed-Carrier QPTM, has been proposed and briefly examined and simulated. This offers linearity benefits over the original QPTM proposal, as dynamic range is not limited by reference signal components and it does not require extremely-wide bandwidth PWM signals at the quadrature modulator inputs. In this respect, its full performance, neglecting modulator parasitics, should be realisable with present off-the-shelf parts. A drawback is that the modulated signal is no longer truly constant-envelope. However, the resulting signals, if combined prior to the PA stage, assume one of three envelope levels, including zero, and thus an efficient PA with suitable linearity correction would still be easier to design for this than for an infinitely-variable level amplitude-modulated signal. If the signals are combined after the PA stage, the PA design is simplified because, when active, it transmits a constant level, however the problem then is shifted to the design of a suitable combiner. This is different from the usual power combiner because the quadrature carrier phasing prevents application of the usual isolation techniques.

A third technique, that could potentially overcome all of the above problems, involves the combination of the suppressed-carrier quadrature-modulated signals by time-division multiplexing. This requires two quadrature-phased reference signals at the PWM stage but the generating circuits may be less demanding as the reference waveforms need only be linear over half the time range. Further investigation of the Suppressed-Carrier QPTM technique is outside the scope of the present project but is considered to be the most promising direction for future work.

5.1.2.2 PWM Reference

The reference generator was designed to have a free-running frequency of about 40MHz and an integral non-linearity of better than ±1% of full-scale over its working range. The non-linearity measured on the simulation plot of Figure 4.2 was 0.29% between 10 and 90% of the triangular waveform. The prototype reference waveform, shown in

Figure 4.14, was acquired by probing across a 100Ω terminating resistor. Some difficulty was experienced in measuring this because of stray coupling from the associated high-speed comparator output, only a few millimeters away. Although the triangle-wave generator appeared to operate as expected, the interference prevented a satisfactory measurement of linearity being made. Shielding between these sections of circuit would be helpful in any future version. The use of differential lines reduced cross-coupling of switching signals under normal operating conditions. It was also noted previously that the periods of each ramp of the triangle were unequal, giving rise to low-level sidebands in the RF spectrum, on even-harmonics of the reference frequency.

5.1.2.3 QPTM Linearity and Spectrum

The complete modulator comprised the reference generator, a dual high-speed comparator IC and a direct quadrature modulator IC. The layout of the PCB facilitated the testing of the subsystem as a single entity. Figure 4.15 shows the spectrum of the quadrature modulator output signal obtained at the 'Test' socket, with no I or Q baseband input. The carrier frequency of 500MHz is suppressed. The intermediate lines spaced at even harmonics of the reference frequency from the carrier frequency are due to the triangle asymmetry mentioned above.

Figures 4.16 to 4.20 show the spectra with different levels of single- and two-tone signals at the 'I' and 'Q' inputs. These indicate in-band distortion levels of about –40dB with respect to the modulation sidebands, a level that is comparable with the specification of the direct quadrature modulator IC. Since the in-band distortion is due to upper sideband components referenced to the quadrature modulator image frequency, at twice the carrier frequency, we may expect much lower levels of in-band distortion when the carrier frequency is much higher, as for the 5GHz bands, because of the diminishing PWM spectrum. The level of distortion is adequate for wireless LAN applications but would cause too much adjacent-channel interference for PMR or linking applications in the UHF bands where channels are relatively narrow. This could be improved by filtering out the image frequency components of the PWM signal before the quadrature modulation. Doing this has a negligible effect on the pulse energy or time-domain waveforms.

The output bandpass filter requirements for both of the application areas are quite practicable. If we first consider an application in the 5-5.7GHz bands, the standard spectral mask for IEEE 802.11a is as follows [44]:

Frequency Offset	Relative Level
-9MHz to +9MHz	0dBc
±11MHz	<=-20dBc
±20MHz	<=-28dBc
<-30MHz, >+30MHz	<=-40dBc

Channel spacing is 20MHz, so that the 9 to 11MHz region is the transition between channels. The OFDM signal has a –3dB bandwidth of 16.56MHz.

The bandpass filter could be implemented with a cavity filter, for example, a Telonic type TCG [41] with 2.5dB insertion loss for 3 elements, but an interesting and more efficient alternative has been found, using dielectric resonators. Such a filter is easily manufactured using printed circuit microstripline techniques and the very-high Q dielectric resonator discs. In a paper by Podcameni and Conrado [42], an example is given of a 3-element 50MHz BW, 1dB Chebyshev bandpass filter, operating at 8220MHz. This would appear to scale well to our application in, say, the 5.7GHz band. Practical bandwidths are quoted as from 2 to 0.3%, with insertion loss from 0.2 to 0.7dB per resonant element. In other words, we could expect about 1.5dB overall loss. It would appear that such a filter could be made tunable, a necessary feature for the European HiperLAN/2, which has an additional requirement for dynamic channel selection.

A potential rural linking application in the 403-520MHz band may be expected to comply substantially with the AS/NZS 4768 standard [43], using the maximum carrier spacing of 25kHz. Maximum rated output power is 1W for point-point and 5W for point-multipoint in Australia. The equivalent limits are 50W in New Zealand for UHF. Adjacent channel power (ACP) must be <=-70dB for 25kHz spacing (but not below –37dBm). Spurious emissions must be <=-30dBm. The –70dB ACP is probably achievable using a linear power amplifier. The usual back-off would not be necessary with QPTM.

The resonator loaded-Q factors required are relatively low, at 35-40, but the practical filter must have a symmetrical stop-band characteristic and low loss. For these reasons, helical filters, although small and low-cost, are not the most suitable. A cavity filter, such as a Telonic type TCF [41], provides the lowest loss, at 0.5dB total insertion loss for 3 elements. Less efficient alternatives are low-cost lumped-constant “tubular” bandpass filters. These are not as symmetrical in response but appear to be adequate. The lowest power (4W) Telonic type TBP has an insertion loss of 2dB at 400MHz.

5.1.2.4 PA Functionality

The behaviour of the switching-type PA at UHF is of special interest since much of the literature pertaining to such amplifiers has been found to be of a theoretical rather than practical nature. One also finds that related semiconductor data is not typically available for non-linear operating modes. The PA in this case was designed with GaAs FET devices that appeared to be well-suited for the task, because of their high bandwidth, low 'on' resistance and low feedback capacitance. However, one difficulty was found with the magnitude of gate drive required to fully switch the devices between 'on' and 'off' states. This amounted to a significant level of power from the driver stage because of the capacitive loading of the FET gate and, particularly, of the Miller-effect capacitance, even though this was small. In order to approximate the desired square-wave drive signal, the modulated RF carrier was first limited by an ultra-high-speed differential comparator, the two outputs of which were then fed via a pair of ultra-wideband 20dB gain blocks, each having 50Ω input and output ports, through 50Ω terminated lines to the respective FET gates. In a real product design, it is anticipated that the efficiency of the gate drive would be optimised by using, for example, a closely-coupled tuned-amplifier driver stage that might itself be a scaled-down Class-D or Class-F amplifier. However, the Class-D PA is at a disadvantage because of the need for a fast, high-level, square-wave gate drive to minimise output switching loss, whereas the Class-F amplifier is similar to the Class-B in that it will operate with a relatively low level, substantially linear, drive signal. The second major difficulty was found to be the correct tuning of the FET drains with the appropriate series- or parallel-resonant circuit, depending on whether the PA was in VS Class-D or CS Class-D operating configuration.

During simulation, we saw that the VS form, with a typical output transformer model, suffered from parasitic inductance. As a result, significant ringing was apparent on both the drain and the gate waveforms, the latter because of Miller feedback from the drain. The CS form did not show this because, on the one hand, an idealised transmission-line balun was substituted and, on the other, the use of a parallel-resonant drain 'tank' resulted in a half-sinusoidal waveform on each drain, the slow rise-time substantially reducing the Miller feedback effect.

In practice, it has only been possible so far to test the PA in untuned mode, and therefore not actually Class-D operation. The two prototypes, one VS and one CS, were each tested with 500MHz carrier signals and the waveforms captured at the gate and the drain nodes

using the 8GHz-bandwidth digital oscilloscope that had fortunately just become available. The results for the VS mode compare with those in the simulation but have much more pronounced ringing, due to parasitic circuit inductance. This shows the extreme difficulty of using a discrete transformer in a switching circuit of this type. The problem of feedback is clearly exacerbated by a fast rise-time drain signal.

Before testing the CS version, it was necessary to characterise the experimental broadside-coupled tapered stripline balun used in its output circuit. The spectrum analyser plots confirmed that this device had a –3dB bandwidth extending from about 160 to 1600MHz range when terminated resistively in 50Ω. It was intended that, ultimately, a suitable parallel-resonant circuit would be attached differentially at the FET drain nodes. However, this requires careful, detailed, design work that is beyond the scope of this project purely because of the time-scale. Figures 4.27 and 4.28 show the frequency response and transmitter spectrum respectively of the CS PA and stripline balun combination. The results appear to be entirely satisfactory. Figures 4.29 and 4.30 show the captured FET gate and drain waveforms. They have much less ringing evident than in the VS case but clearly show the Miller feedback effect during the very fast (100ps) turn-off transition of the FET. If the output were effectively tuned, this loading would substantially diminish and there would be correspondingly higher efficiency. Figure 4.31 shows the untuned, but band-limited, switching output from the stripline balun into a 50Ω load.

5.2 Conclusions

The QPTM system has been found to be realisable in practice with economical, off-the-shelf components in its basic constant-envelope form. The prototype QPTM module has already been shown to have a linearity performance comparable with that of the direct quadrature modulator used in its implementation, so that it may need little further work to integrate it with a linear amplifier in a practical system, with the addition of a commercial output filter. Owing to the very high modulator bandwidth needed to achieve the desired spurious harmonic levels of better than -40dB with respect to the signal, the switching–type PA does not appear to be the best match for QPTM. However, the near-constant envelope characteristic of the PA drive does offer the potential of very high efficiencies for linear amplifiers driven close to saturation. It is considered that the efficiency and linearity might be further improved in practice by using a suppressed-carrier form of QPTM, that has been simulated, as this would allow the output filter to have a wider bandwidth, with correspondingly-reduced insertion loss.

The design and construction has been accomplished of a prototype switching PA, that could be used as a test-bed for prototyping a Class-D, or even Class-F, amplifier. This amplifier embodies a push-pull GaAs FET output stage that has been integrated with an unusual broadside-coupled tapered stripline balun that has been demonstrated to have about 160MHz to 1.6GHz bandwidth. Switching waveforms for the PA output stage have been captured for the untuned test configuration and these will provide useful design input for future work. An output efficiency of over 60% has been shown by simulation to be feasible with an appropriately-designed output filter and balun Practical measurements on the prototype gave a figure of 57% without output tuning. We should expect this to be improved by incorporating PA tuning and a harmonic filter.

5.3 Suggestions for Further Work

5.3.1 QPTM SYSTEM

There is a need to investigate and quantify the effect of PA non-linearity on the production of in-band non-linear distortion products with various OFDM signal formats. This would provide data for use in optimisation of PA drive conditions.

The suppressed-carrier form of QPTM holds the promise of increasing PA efficiency and reducing output filter complexity and losses. However, research is required to determine the optimum quadrature combining system, along with the configuration of the PA and output filter functional entities, and to characterise the resulting system behaviour.

Future work is likely to require more precise work relating to harmonic reduction and this would be easier if the reference triangle frequency were locked, so that some new design work is envisaged in this area. The possible need for a two-phase reference, should a time-division multiplexing approach to combining be adopted, makes this requirement even more likely.

In the simulation work undertaken so far, models have been developed that are considered to provide a reasonable amount of realism. However, the inclusion of parasitic elements and variable parameters that might hinder, rather than aid, the interpretation of results has been avoided where possible. Such would include mismatch of devices, modulator phase and gain imbalance, gain compression in ‘linear’ gain blocks and asymmetric rise and fall times of switching devices. Once an appropriate system configuration has been clearly established and its principal characteristics defined, it will be important to introduce the other known performance-limiting characteristics to the simulations and practical measurement processes.

5.3.2 PA OPTIMISATION

The efficiency of the PA is likely to be a trade-off between drive power and FET 'on' resistance power loss. Furthermore, since we have found that hard limiting does introduce some intermodulation distortion of the QPTM signal, it would be preferable to operate the PA as close to linear conditions as efficiency considerations may permit in this application. For these reasons, it may be more beneficial to operate the PA under Class-F conditions than Class-D but that is yet to be determined.

The stripline balun has been found to operate well enough so far to be of interest in a future design. It is therefore considered important to fully characterise the structure, including the effects of bends, tapers, coupling and reactive or unequal terminations.

5.3.3 PROTOTYPE PCB REFINEMENT

The present prototype design has been shown to work well from the point of view of flexibility and ease of use during various tests. However, it would be appropriate to address some issues to facilitate the ongoing research that is envisaged. Firstly, the components in the QPTM chain should be slightly repositioned to allow the placement of stock-sized screening cans over individual sections. They should be retained by SMD clips, for easy removal of individual cans for measurements to be made. Secondly, alternative connection to the gate driver amplifiers should be added to facilitate linear or non-linear gate drive selection. Thirdly, a tuned-filter section should be designed into the PA stage, suitably integrated with the stripline balun and based on current findings and data.

References

[1] R. van Nee and R. Prasad, *OFDM for Wireless Multimedia Communications,* Artech House, London, 2000, pp. 138-150.

[2] WWRF/WG4/Subgroup on New Air Interfaces White Paper Version 1.4, Wireless World Research Forum, Oct. 25, 2002.
(Found at http://www.signal.uu.se/Research/PCCWIP/kaiser_1230.pdf.)

[3] J. A. Davis and J. Jedwab, *Peak-to-mean power control in OFDM, Golay complementary sequences and Reed-Muller codes,* HP Laboratories Bristol, UK,
Technical Note HPL-97-158, Dec. 1997.

[4] J. A. Davis, J. Jedwab and K.G. Paterson, *Codes, correlations and power control in OFDM,* HP Laboratories Bristol, UK, Technical Note HPL-98-199, Dec. 1998.

[5] M. G. Parker and C. Tellambura, *Generalised Rudin-Shapiro constructions,*
Elsevier Preprint, Reed-Elsevier Group, London, Jan. 4, 2001.

[6] B. M. Popović, "Efficient Golay correlator," *Electronics Letters,* Vol. 35, No. 17,
Aug. 19, 1999.

[7] K. G. Paterson and A. E. Jones, *Efficient decoding algorithms for generalised Reed-Muller codes,* HP Laboratories Bristol, UK, Technical Note HPL-98-195, Nov. 1998.

[8] H. Ochiai, and I. Hideki, "On decoding of block codes with peak-power reduction in OFDM systems," *IEEE Communications Letters,* Vol. 4, No. 7, Jul. 2000.

[9] V. P. G. Jimenez, et al, "Study and implementation of complementary Golay sequences for PAR reduction in OFDM signals," *Proc. IEEE Mediterranean Electrotechnical Conference MELE-CON 2002,* May 7-9, 2002, Cairo, Egypt.

[10] G. A. Awater, Lucent Technologies Inc., *Coding for the reduction of peak to average power ratio in multicarrier modulation systems,*
European patent app. no. EP 0 822 690 A2, filed Jul. 22, 1997.

[11] X. Li and L. J. Cimini, Jr., "Effects of clipping and filtering on the performance of OFDM," *IEEE Commun. Lett.,* vol.2, no.5, pp. 131-133, May 1998.

[12] H.Chen and A. Haimovich, "An iterative method to restore the performance of clipped and filtered OFDM signals," *IEEE International Conference on Communications, 2003*, vol. 5, pp. 3438-3442, May 11-15, 2003.

[13] R. W. Bauml, R. F. H. Fischer, and J. B. Huber, "Reducing the peak-to-average power ratio of multicarrier modulation by selected mapping," *Electron. Letters*, vol. 32, no. 22, pp. 2056–1257, Oct. 1996.

[14] N.Y. Ermolova and P. Vainikainen, "On the relationship between peak factor of a multicarrier signal and aperiodic autocorrelation of the generating sequence," *IEEE Communications Letters*, Vol. 7, No. 3, Mar. 2003.

[15] S. H. Muller and J. B. Huber, "OFDM with reduced peak-to-average power ratio by optimum combination of partial transmit sequences," *Electron. Letters*, vol. 33, no. 5, pp. 368–369, Feb. 1997.

[16] L. J. Cimini, Jr. and N. R. Sollenberger, "Peak-to-average power ratio reduction of an OFDM signal using partial transmit sequences," *IEEE Commun. Lett.,* vol.4, no.3, pp. 86-88, Mar. 2000.

[17] Y. H. You, W. G. Jeon, and J. H. Paik, "Investigation of peak-to-average power ratio in STBC-OFDM," *Electron. Letters,* vol. 39, no. 13, p. 1010, Jun. 26, 2003.

[18] E. Lawrey and C. J. Kikkert, "Peak to average power ratio reduction of OFDM signals using peak reduction carriers," *Fifth International Symposium on Signal Processing and its Applications, ISSPA '99,* pp. 737-740, Aug. 22-25, 1999, Brisbane, Australia.

[19] F. H. Raab, P. Asbeck, S. Cripps, P. B. Kennington, Z. B. Popović, N. Pothecary, J. F. Sevic and N. O. Sokal, "RF and microwave power amplifier and transmitter technologies – Part 5," *High Frequency Electronics*, Jan. 2004.

[20] F. H. Raab, P. Asbeck, S. Cripps, P. B. Kennington, Z. B. Popović, N. Pothecary, J. F. Sevic and N. O. Sokal, "Power amplifiers and transmitters for RF and microwave," *IEEE Trans. Microwave Theory Tech.*, vol. 50, no. 3, pp. 814-826, Mar. 2002.

[21] F. H. Raab, "An introduction to Class-F power amplifiers," *RF Design*, vol. 19, no. 5, pp. 79-84, May 1996.

[22] F. H. Raab, "Maximum efficiency and output of Class-F power amplifiers," *IEEE Trans. Microwave Theory Tech.*, vol. 49, no. 6, pp. 1162-1166, Jun. 2001.

[23] Jun Tan and G. L. Stuber, "Constant envelope multi-carrier modulation," *Proc. MILCOM 2002*, Vol. 1, pp. 607-611, Oct. 7-10, 2002.

[24] J. Keyzer, R. Uang, Y. Sugiyama, M. Iwamoto, I. Galton and P. M. Asbeck, *"Generation of RF pulsewidth modulated microwave signals using delta-sigma modulation,"* IEEE MTT-S International Microwave Symposium Digest, vol.1, pp.397-400, Jun. 2-7, 2002.

[25] S. I. Mann, *A Hybrid Linearisation Technique for Hand-portable Radio Transmitters,* Ph.D. Thesis, University of Bristol, UK, Sep. 2002.

[26] F. H. Raab, "Intermodulation distortion in Kahn-technique transmitters," *IEEE Trans. Microwave Theory Tech.*, vol. 44, no. 12, pp. 2273-2278, Dec. 1996.

[27] K. Chiba, T. Nojima and S. Tomisato, "*Linearised saturation amplifier with bidirectional control (LSA-BC) for digital mobile radio*," IEEE Globecom 1990, vol. 3, pp. 1958-1962.

[28] M. J. Koch and R. E. Fisher, "*A high efficiency 835 MHz linear power amplifier for digital cellular telephony*," IEEE VTC, vol. 1, pp. 17-18, May 1989.

[29] M. D. Weiss, F. H. Raab and Z. Popović, "Linearity of *X*-band Class-F power amplifiers in high-efficiency transmitters," *IEEE Trans. Microwave Theory Tech.*, vol. 49, no. 6, pp. 1174-1179, Jun. 2001.

[30] T. J. Fergus, "EDGE modulation – how linearization improves amplifier performance," *RF Design*, pp. 18-30, Oct. 2002.

[31] B. Sahu and G. A. Rincón-Mora, A high-efficiency linear RF power amplifier with a power-tracking dynamically adaptive buck-boost supply," *IEEE Trans. Microwave Theory Tech.*, vol. 52, no. 1, pp. 112-120, Jan. 2004.

[32] F. Wang, A. H. Yang, D. F. Kimball, L. E. Larson and P. M. Asbeck, "Design of wide-bandwidth envelope-tracking power amplifiers for OFDM applications," *IEEE Trans. Microwave Theory Tech.*, vol. 53, no. 4, pp. 1244-1255, Apr. 2005.

[33] W. H. Doherty, "A new high efficiency power amplifier for modulated waves," *Proc. IRE,* vol. 24, no. 9, pp. 1163-1182, Sep. 1936.

[34] "The Doherty Amplifier," Bell Telephone Laboratories Western Electric, 12 pp., ca. 1942, (Found at http://www.hallikainen.org/history/equipment/westernelectric/doherty.pdf, 10 Sep. 2006.)

[35] R. J. McMorrow, D. M. Upton and P. R. Maloney, *"The microwave Doherty amplifier,"* IEEE MTT-S International Microwave Symposium Digest, no. TH3E-7, pp.1653-1656, 1994.

[36] Y. Suzuki, T. Hirota and T. Nojima, *"Highly efficient feed-forward amplifier using a Class-F Doherty amplifier,"* IEEE MTT-S International Microwave Symposium Digest, no. TU3B-3, pp.77-80, 2003.

[37] Y. Zhao, M. Iwamoto, L. E. Larson and P. M. Asbeck, *"Doherty amplifier with DSP control to improve performance in CDMA operation,"* IEEE MTT-S International Microwave Symposium Digest, no. WE3A-1, pp.687-690, 2003.

[38] H. S. Black, *Modulation Theory*, Bell Telephone Laboratories Series, D. van Nostrand Co. Inc., New York, 1953.

[39] MATLAB® Student Version 6.0.0.42a, Rel. 12 with Simulink®, The MathWorks, Inc., Prentice Hall, Inc., NJ, USA.

[40] Micro-Cap 6™ Version 6.2.6, Spectrum Software, Inc., Sunnyvale, CA, USA.

[41] "Telonic Fixed Frequency Filters – Engineers' Design Handbook," Telonic/Berkeley, Laguna Beach, CA, USA, 2004.

[42] A. Podcameni and L. F. M. Conrado, "Design of microwave oscillators and filters using transmission-mode dielectric resonators coupled to microstrip lines," *IEEE Trans. Microwave Theory Tech.,* vol. MTT-33, pp.1329-1332, Dec. 1985.

[43] Australia/New Zealand Standard AS/NZS 4768.1:2003, "Digital radio equipment operating in land mobile and fixed services bands in the frequency range 29.7 MHz to 1GHz, Part 1: Radiofrequency requirements."

[44] IEEE Std 802.11a – 1999, "Supplement to IEEE standard for information technology – Telecommunications and information exchange between systems - Local and metropolitan area networks – Specific requirements - Part 11: Wireless LAN Medium Access Control (MAC) and Physical Layer (PHY) specifications - High-speed Physical Layer in the 5GHz Band."

[45] "MWT-17 500MHz-12GHz High Linearity, Low Noise GaAS FET," MicroWave Technology Inc. (Found at http://www.mwtinc.com/cat/fets/htm/new-html/MwT-17_3.htm.)

[46] A. B. Williams and F. J. Taylor, *Electronic filter design handbook*, 3rd Ed., McGraw-Hill, Inc., NY, USA, 1995.

[47] M. Albulet, *RF power amplifiers*, Noble Publishing Associates, NC, USA, 2001.

[48] P. L. D. Abrie, *Design of RF and microwave amplifiers and oscillators*, Artech House, Inc., MA, USA, 1999.

[49] J. W. Duncan and V. P. Minerva, "*100:1 bandwidth balun transformer,"* Proc. IRE, vol. 48, pp. 156-164, Feb. 1960.

Appendix 1 – Spectra of Pulse-Modulation Systems

The following method of spectral analysis was attributed by Black [29] to J. G. Kreer, Jr. and presented as a means of characterising the various forms of pulse modulation (pp.282-285 of [29]). We have changed some variable names in order to identify them more clearly in the current context.

According to this method, a pulse-modulated wave may be expressed as a series of modulated sinusoidal waves, modulated in phase or amplitude or both. This is based on an assumption that each period function is repeated indefinitely and may be expanded in a Fourier series. The Fourier series coefficients are then allowed to vary from period to period according to the modulating signal.

Consider a system in which a train of rectangular pulses, when unmodulated, has an amplitude of unity, repetition period of T and pulse duration t_0. The cyclic pulse frequency f_r is then $1/T$ and the corresponding fundamental angular frequency ω_r is $2\pi/T$. Let the leading edge be modulated with modulation factor k_1, the trailing edge with factor k_2 and the amplitude with factor k_3. The resulting modulated wave may then be defined as:

$$\left.\begin{aligned} &p(t) = 0, \quad \left(n - \frac{1}{2}\right)T \le t \le nT - \frac{t_0}{2} + k_1 x_1(t_{n1}) \\ &p(t) = 1 + k_3 x_3(t_{n3}), \quad nT - \frac{t_0}{2} + k_1 x_1(t_{n1}) \le t \le nT + \frac{t_0}{2} + k_2 x_2(t_{n2}) \\ &p(t) = 0, \quad nT + \frac{t_0}{2} + k_2 x_2(t_{n2}) \le t \le \left(n + \frac{1}{2}\right)T \end{aligned}\right| \qquad \text{(A1.1)}$$

where $x_1(t)$, $x_2(t)$ and $x_3(t)$ are independent modulating waves, $n = 0, \pm1, \pm2, \ldots$, and t_{n1}, t_{n2} and t_{n3} denote the respective times in the nth period that $x_1(t)$, $x_2(t)$ and $x_3(t)$ were sampled. For our present application we may set $x_1(t) = x_2(t) = x_3(t) = x(t)$ and $t_{n1} = t_{n2} = t_{n3} = t_n$.

It is assumed that the modulated wave may be represented as

$$p(t) = a_0(n) + \sum_{m=1}^{\infty} [a_m(n)\cos m\omega_r t + b_m(n)\sin m\omega_r t] \tag{A1.2}$$

where $a_m(n)$ and $b_m(n)$ are constants over any one period T but may vary from period to period.

Then:

$$\begin{aligned} a_0(n) &= \frac{1}{T}\int_c^d [1 + k_3 x(t_n)]dt \\ &= \frac{1 + k_3 x(t_n)}{T}[t_0 + (k_2 - k_1)x(t_n)], \end{aligned} \tag{A1.3}$$

where $c = nT - \frac{t_0}{2} + k_1 x(t_n)$ and $d = nT + \frac{t_0}{2} + k_2 x(t_n)$

$$\begin{aligned} a_m(n) &= \frac{2}{T}\int_c^d [1 + k_3 x(t_n)]\cos m\omega_r t \; dt \\ &= \frac{2[1 + k_3 x(t_n)]}{m\pi}\sin m\omega_r\left[\frac{t_0}{2} + \frac{k_2 - k_1}{2}x(t_n)\right]\cos m\omega_r\left[\frac{k_1 + k_2}{2}x(t_n)\right] \end{aligned} \tag{A1.4}$$

$$\begin{aligned} b_m(n) &= \frac{2}{T}\int_c^d [1 + k_3 x(t_n)]\sin m\omega_r t \; dt \\ &= \frac{2[1 + k_3 x(t_n)]}{m\pi}\sin m\omega_r\left[\frac{t_0}{2} + \frac{k_2 - k_1}{2}x(t_n)\right]\sin m\omega_r\left[\frac{k_1 + k_2}{2}x(t_n)\right] \end{aligned} \tag{A1.5}$$

Substituting (A1.3), (A1.4) and (A1.5) in (A1.2) gives:

$$\begin{aligned} p(t) = {} & \frac{t_0}{T} + \frac{k_2 - k_1 + k_3 t_0}{T}x(t_n) + \frac{k_3(k_2 - k_1)}{T}x^2(t_n) \\ & + \sum_{m=1}^{\infty} 2\left[\frac{1 + k_3 x(t_n)}{m\pi}\right]\sin m\omega_r\left[\frac{t_0}{2} + \frac{k_2 - k_1}{2}x(t_n)\right]\cos\left[m\omega_r t - m\omega_r\frac{k_1 + k_2}{2}x(t_n)\right] \end{aligned} \tag{A1.6}$$

By substituting regular sample times Tn for t_n, (A1.6) may also be applied to uniform sampling. The first three terms in (A1.6) represent an amplitude-modulated zero-frequency carrier, whilst the remainder comprises a set of harmonics of ω_r that are each amplitude- and phase-modulated. Hence, the factors (k_2 - k_1) and k_3 contribute only amplitude modulation and (k_1 + k_2) contributes only phase modulation. When k_3 = 0 we have pulse-width modulation that is proportional to the

term (k_2 - k_1). In the PWM system being modelled, natural sampling is used and the reference is a symmetrical triangle wave, so that $k_1 = -k_2$. Then (k_2 - k_1) = $2k_2 = k$, $k_3 = 0$, $t_0 = T/2$ and (A1.6) reduces to

$$p(t) = \frac{1}{2} + \frac{k}{T} x(t_n) + \sum_{m=1}^{\infty} \left[\frac{2}{m\pi} \right] \sin m\pi \left[\frac{1}{2} + \frac{k}{T} x(t_n) \right] \cos m\omega_r t \qquad \text{(A1.7)}$$

The first term is a dc component that will be eliminated and the second term represents a series of samples of the baseband signal. The last term represents a series of amplitude-modulated harmonics of the reference wave.

Appendix 2 – Simulation Macromodels

The macromodels (macros) described in this appendix provide a compact and convenient way of representing the relevant behavioural characteristics of functional blocks in the system being simulated. They are intended for use with the Micro-Cap 6 ™ (MC6) circuit analysis program [30] but may be adapted to other SPICE-based simulation software.

A2.1 TRI.MAC

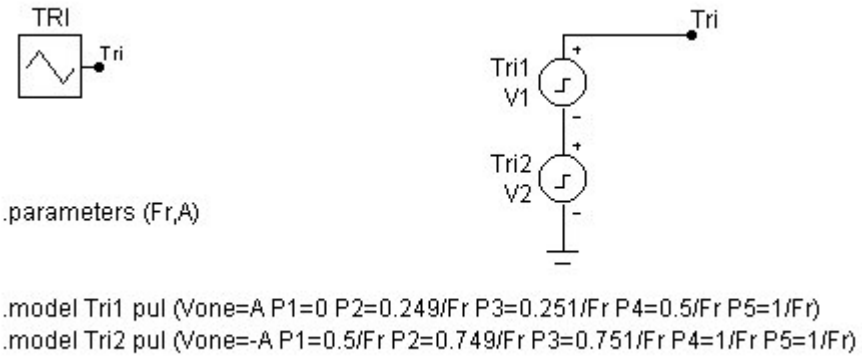

Figure A.1 - Tri macro

The standard pulse model in MC6 generates a two-level pulse with specified rise and fall slopes. These enable a triangle wave to be defined. However, it is more convenient to start the waveform at zero, rather than one of the peak values, to minimise the disturbance to initial analysis conditions. The requisite three specified levels are achieved by summing two pulse sources. The parameters that may be passed to the macro are triangle reference frequency Fr and amplitude A.

A2.2 COMP.MAC - COMPARATOR

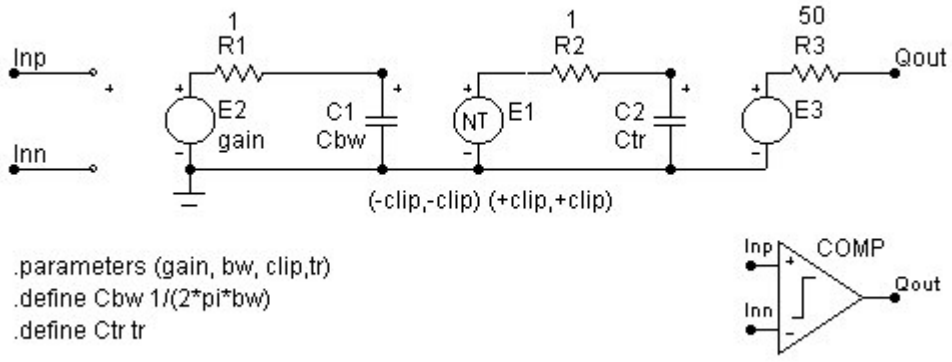

Figure A.2 - Comp macro

The comparator model in Figure A.2 is based on a limiter implemented with a non-linear table voltage-dependent source (E1). This function has two limiting values (+clip and –clip) with linear gain in between (unity, in this case). A differential input amplifier (E2) comprises a voltage-controlled voltage source (VCVS), with programmable gain, followed by a low-pass network (R1, C1) that is programmed with the equivalent input bandwidth (bw) of the comparator. The limiter stage is followed by a second low-pass network (R2, C2) programmed with the output risetime (tr) and buffered by a VCVS (E3) with unity gain and 50Ω output resistance.

A2.3 DCOMP.MAC – DIFFERENTIAL OUTPUT COMPARATOR

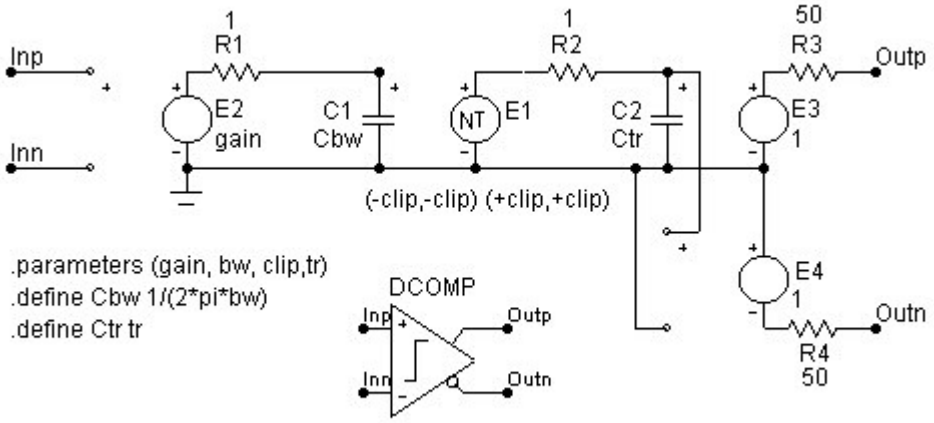

Figure A.3 - DComp macro

The differential-output comparator DComp in Figure A.3 is identical to the Comp macro in Figure A.2 except that a complementary output buffer (E4), similar to (E3), has been added.

A2.4 Q-MOD.MAC – QUADRATURE MODULATOR

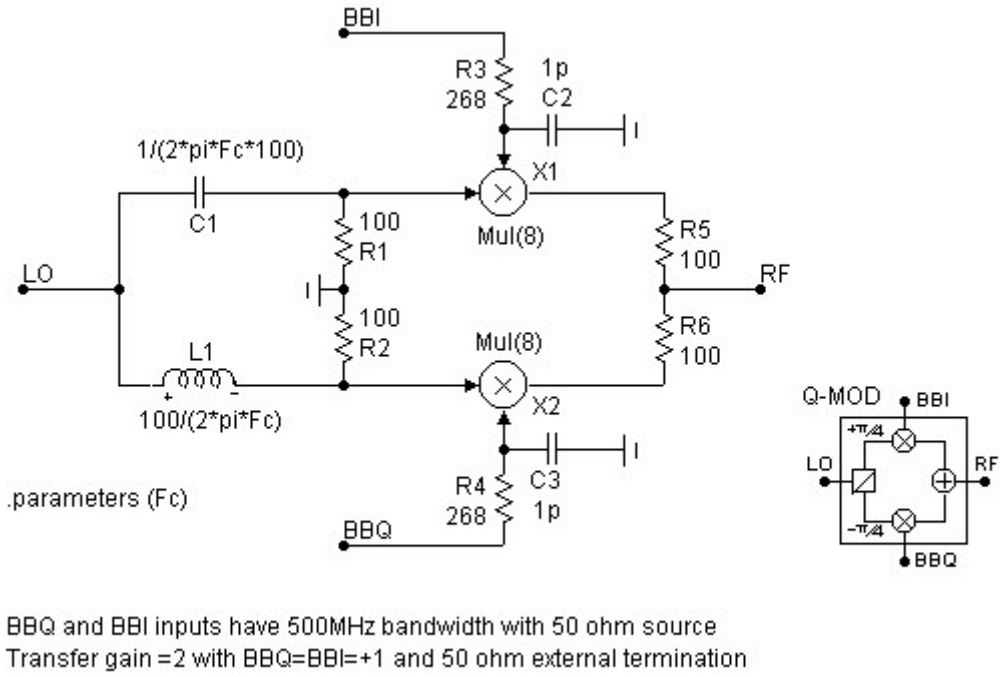

Figure A.4 - Q-Mod macro

The Q-Mod macro in Figure A.4 has been designed to simulate a typical direct quadrature modulator IC, type STQ-1016 from Sirenza Microdevices. For simplicity, however, inputs and outputs are single-ended and frequency-dependent reactor values are used in the input phase shifters that generate quadrature versions of the carrier signal (with frequency Fc). The bandwidth limit of the modulating inputs is fixed at 500MHz (R3, C2 and R4, C3). The values assume 50Ω sources.

A2.5 Q-MOD2.MAC – 2 OUTPUT QUADRATURE MODULATOR

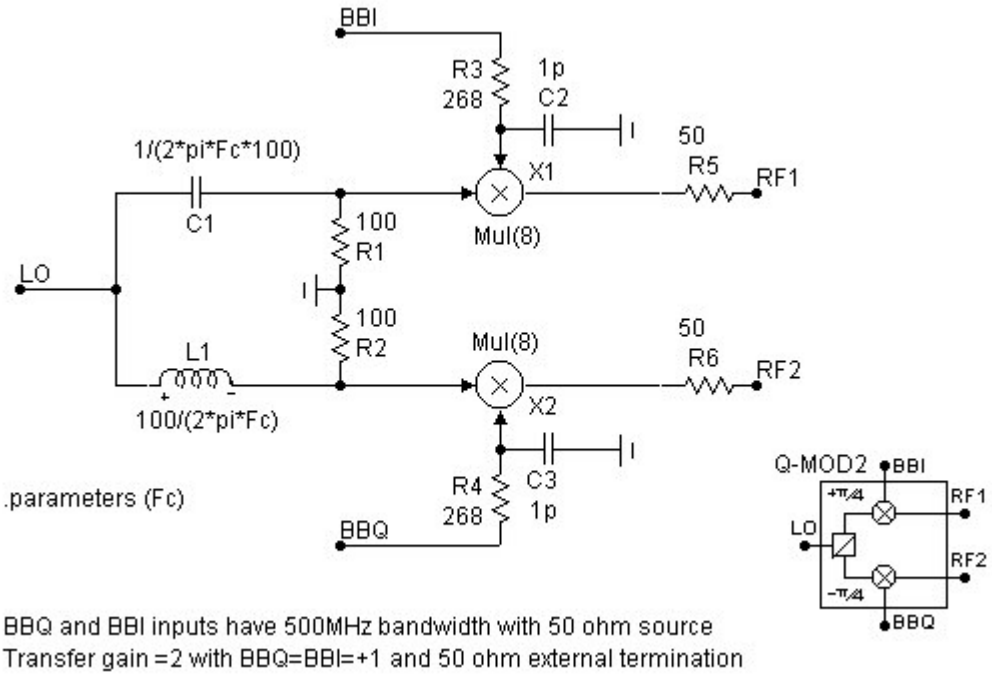

Figure A.5 - Q-Mod2 macro

The Q-Mod2 macro in Figure A.5 is the same as the Q-Mod macro in Figure A.4 except that the quadrature products are output separately instead of being summed.

A2.6 LINEAR.MAC – LINEAR PA

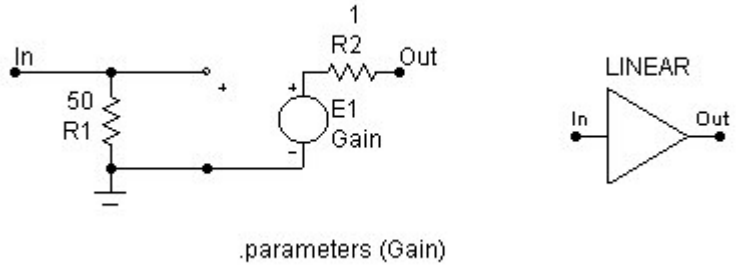

Figure A.6 - Linear macro

The Linear macro in Figure A.6 represents an ideal PA with neither non-linearity nor limiting. The output resistance is low for simulation compatibility with the switching PA macro, described below, so that the same filter macro may be used with either. In any case, it would depend, in practice, on the circuit design approach used for the PA.

A2.7 RF-D.MAC – SWITCHING PA

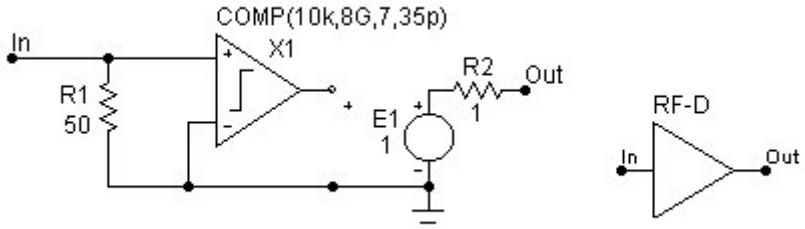

Figure A.7 - RF-D macro

The RF-D macro in Figure A.7 makes use of the previously-described comparator macro (Comp) to approximate the gain and bandwidth characteristics of a realisable 400MHz-band Class-D amplifier and driver chain. *Note that this only represents a classical Class-D when a series-tuned circuit is connected in-line with the load.* The balanced-output GaAs FET stage has been represented here as a single VCVS stage with the 1Ω output resistor R2 representing the drain 'on' resistance of each FET.

A2.8 500M-CHB.MAC – 20MHz BW 0.1dB CHEBYSHEV BPF

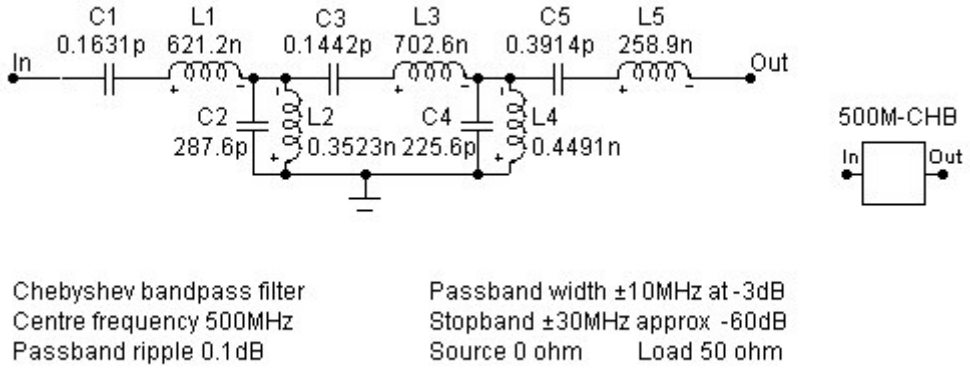

Figure A.8 - 500M-Chb macro

The 500M-Chb macro in Figure A.8 is a lossless, idealised approximation to an order-10 Chebyshev bandpass filter with 0.1dB passband ripple. This filter is analogous to a Telonic type TBC filter [31] that was found from manufacturer's data to be suitable for the application, assuming the specification of appropriate impedances. The element values used in the macro were calculated by impedance and frequency transformation from normalised values given in Table 11-28, p.11-29 of [35], for zero source and 50Ω termination resistances. The values are suitable for simulation only and various circuit transformations would be employed in practice to achieve realisable network element values.

Figure A.9 shows plots of the amplitude and group delay versus frequency for the 500M-Chb macro. In our system applications, we are constraining the modulation bandwidths to within half of the filter passband width, thereby keeping delay spread within about 15ns. The response of this filter to the PWM reference frequency components ±40MHz from the carrier is below –70dB. However, a practical implementation of the filter would be somewhat worse than this, because of element losses, and the passband would not be flat, for the same reason.

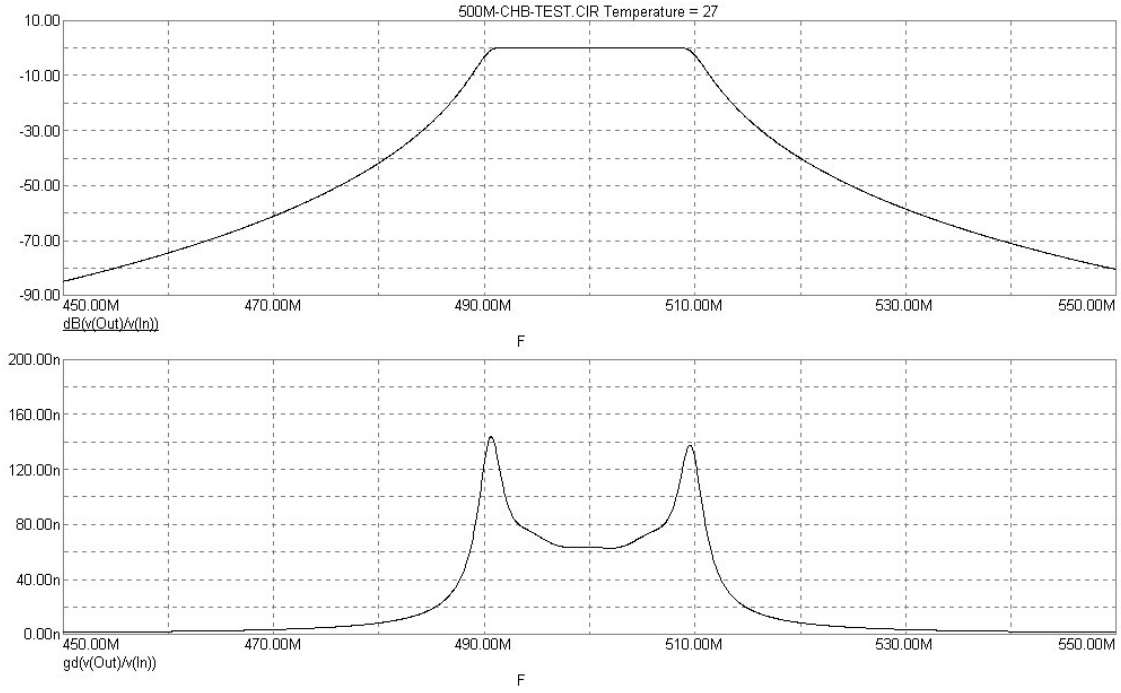

Figure A.9 - 500M-Chb frequency response

A2.9 500M-CHB2.MAC – COMBINER AND 20MHz BW BPF

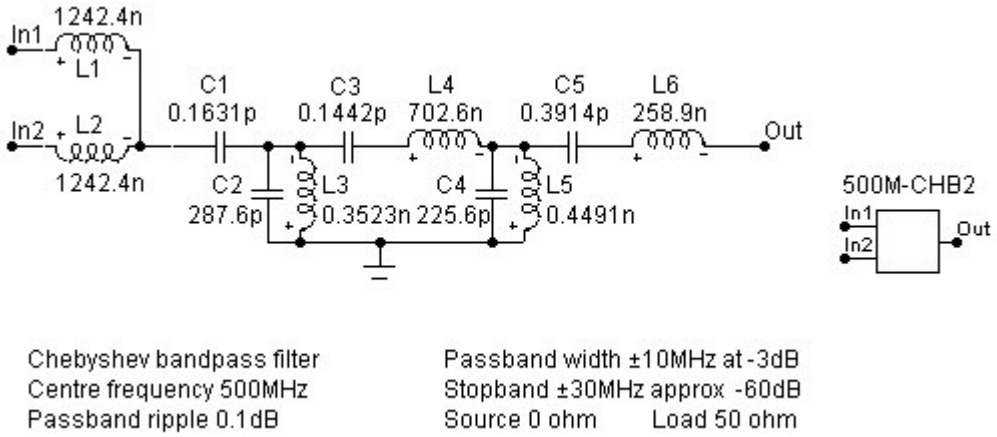

Figure A.10 - 500M-Chb2 macro

For simulation purposes, it has been found convenient to form a power combiner by dividing one of the first stage elements of the bandpass filter in Figure A.10 into two equal-valued components (L1, L2), their parallel value being the same as that of L1 in Figure A.8. The filter characteristics of the macro 500M-Chb2 are thus identical to those of 500M-Chb and a suitable load impedance is presented to each Class-D amplifier driving the filter network.

A2.10 MWT17.MAC – GaAs MESFET WITH PACKAGE PARASITICS

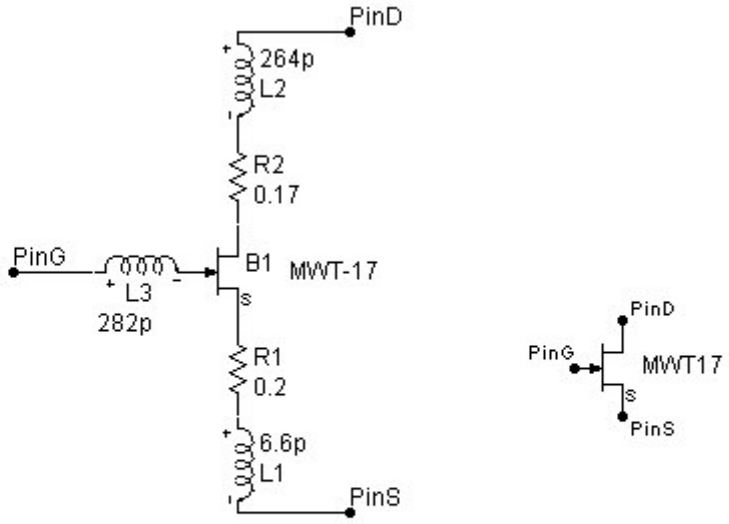

.MODEL MWT-17 GASFET (LEVEL=3 VTO=-1.473 ALPHA=1.358 BETA=0.295 GAMMA=0.086
DELTA=0.042 Q=1.403 IS=8e-12 N=1.22 VBI=0.8 CGD=0.263p CGS=4.256p CDS=0.707p)

Figure A.11 - MWT17 macro

The transient model in Figure A.11 has been constructed from MwT-17 model data supplied by MicroWave Technology Inc. [35] by adding package data to the Triquint device model.

A2.11 RF-PP-XFMR.MAC – PUSH-PULL OUTPUT TRANSFORMER

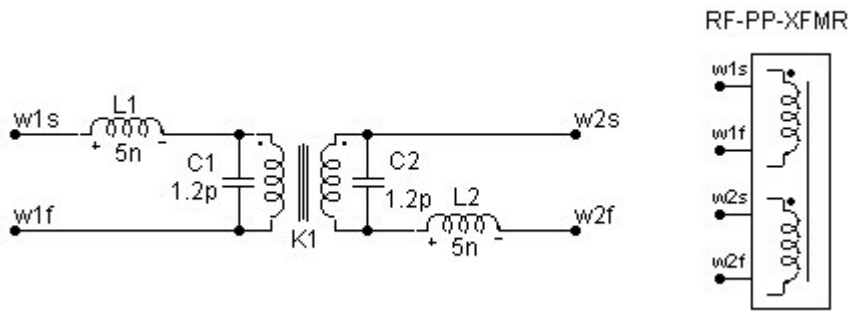

Figure A.12 - RF-PP-Xfmr macro

A convenient output transformer for initial tests on a Class-D amplifier has been implemented with a small, 1:1 ratio RF transformer, reconfigured as a centre-tapped inductor. Element values for the resulting RF-PP-Xfmr macro in Figure A.12 were derived by matching the curve of frequency response given in the datasheet for the (custom) Toko 617DB-1653 balun. In the equivalent circuit of Figure A.13, L3 determined the lower cut-off frequency, whilst the combination of leakage inductance (L1, L2) and winding shunt capacitance (C1) determined the upper cut-off frequency and the slight resonant peak. The resulting response curve is shown in Figure A.14. In the macro of Figure A.12, an ideal transformer has been substituted for L3, with coupling coefficient K =1 and mutual inductance M = L3, a reasonable approximation since the winding is bifilar. However, since the zero-voltage points will be on opposite phases of the bifilar windings in this application, the self capacitance is effectively doubled and C2 is added, equal to C1. This reduces the bandwidth of the transformer to 2.2GHz.

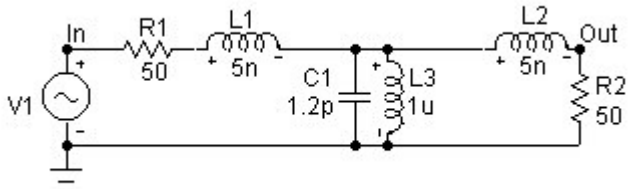

Figure A.13 - Toko 617DB-1653 transformer 'T' equivalent circuit

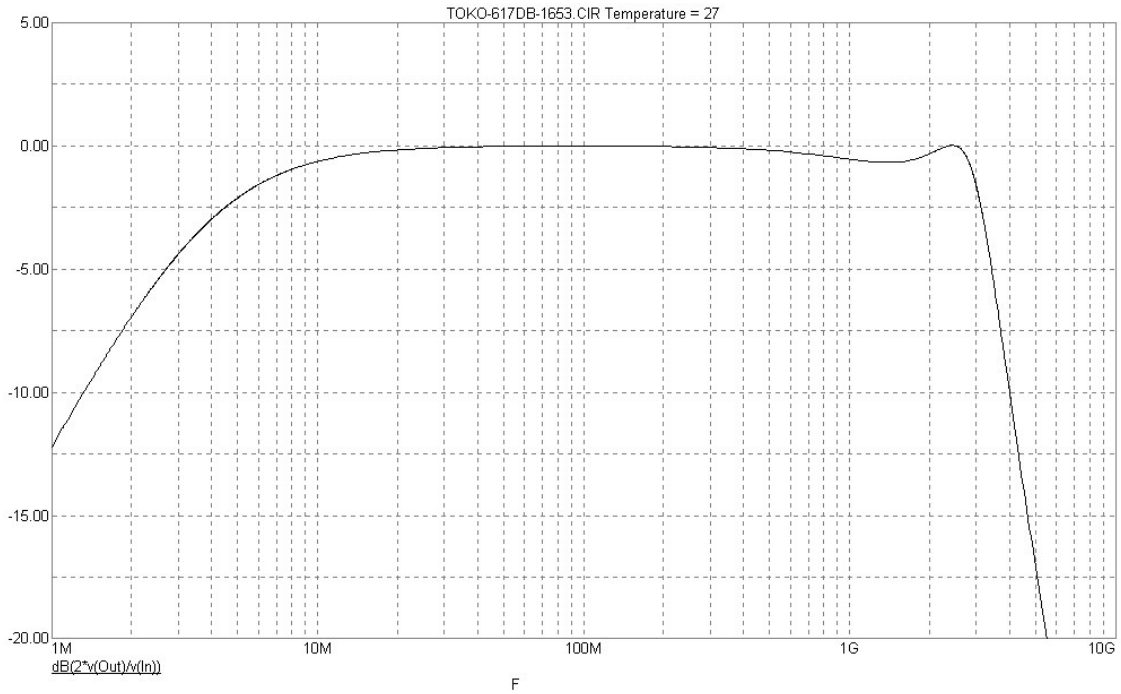

Figure A.14 - Toko 617DB-1653 equivalent circuit frequency response